UNIVERSITAT ROVIRA I VIRGILI
NUMERICAL AND EXPERIMENTAL STUDY OF FLOW AND WALL MASS TRANSFER RATES IN CAPILLARY DRIVEN FLOWS IN MICROFLUIDIC CHANNELS
Salvatore Cito
ISBN:978-84-693-0720-5/DL: T-425-2010

NUMERICAL AND EXPERIMENTAL STUDY OF FLOW AND WALL MASS TRANSFER RATES IN CAPILLARY DRIVEN FLOWS IN MICROFLUIDIC CHANNELS.

by
Salvatore Cito

A Thesis Submitted to the Doctoral Programme in Chemical, Environmental and Process Engineering, in Partial Fulfilment of the Requirements for the degree of DOCTOR OF PHILOSOPHY
Major Subject: Mechanical & Chemical Engineering

Supervised by
Dr. Jordi Pallarès Curto
and
Dr. Ioanis Katakis

UNIVERSITAT ROVIRA I VIRGILI

Tarragona 2009

UNIVERSITAT ROVIRA I VIRGILI
NUMERICAL AND EXPERIMENTAL STUDY OF FLOW AND WALL MASS TRANSFER RATES IN CAPILLARY DRIVEN FLOWS IN MICROFLUIDIC CHANNELS
Salvatore Cito
ISBN:978-84-693-0720-5/DL: T-425-2010

UNIVERSITAT ROVIRA I VIRGILI
NUMERICAL AND EXPERIMENTAL STUDY OF FLOW AND WALL MASS TRANSFER RATES IN CAPILLARY DRIVEN FLOWS IN MICROFLUIDIC CHANNELS
Salvatore Cito
ISBN:978-84-693-0720-5/DL: T-425-2010

CONTENTS

UNIVERSITAT ROVIRA I VIRGILI
NUMERICAL AND EXPERIMENTAL STUDY OF FLOW AND WALL MASS TRANSFER RATES IN CAPILLARY DRIVEN FLOWS IN MICROFLUIDIC CHANNELS
Salvatore Cito
ISBN:978-84-693-0720-5/DL: T-425-2010

UNIVERSITAT ROVIRA I VIRGILI
NUMERICAL AND EXPERIMENTAL STUDY OF FLOW AND WALL MASS TRANSFER RATES IN CAPILLARY DRIVEN FLOWS IN MICROFLUIDIC CHANNELS
Salvatore Cito
ISBN:978-84-693-0720-5/DL: T-425-2010

UNIVERSITAT ROVIRA I VIRGILI
NUMERICAL AND EXPERIMENTAL STUDY OF FLOW AND WALL MASS TRANSFER RATES IN CAPILLARY DRIVEN FLOWS IN MICROFLUIDIC CHANNELS
Salvatore Cito
ISBN:978-84-693-0720-5/DL: T-425-2010

UNIVERSITAT ROVIRA I VIRGILI
NUMERICAL AND EXPERIMENTAL STUDY OF FLOW AND WALL MASS TRANSFER RATES IN CAPILLARY DRIVEN FLOWS IN MICROFLUIDIC CHANNELS
Salvatore Cito
ISBN:978-84-693-0720-5/DL: T-425-2010

ABSTRACT

Micro-channels are believed to open up the prospect of precise control of fluid flow and chemical reactions. The high surface to volume ratio of micro size channels allows efficient mass transfer rates and it can be used in multifunctional Microsystems.

A passive pumping for lab-on-a-chip using surface tension only is the most effective method because the effect of surface tension on a flow is significant in micro-scale. The movement of the triple point at a meniscus is driven by surface tension, resisted by viscous stress, and balanced by inertial force.

The capillary effect can be used to pump fluids in micro-channels and the flow generated can dissolve chemicals previously deposited on the walls of the channel.

In previous studies, the meniscus motion has been predicted theoretically with one-dimensional model. However, three-dimensional flow field around the meniscus and the effect of cross-sectional shapes on the flow and wall mass transfer have not assessed yet.

In this work, numerical and experimental approaches have been developed to investigate the wall mass transfer rate generated by capillary driven flows (CD-Flow). The numerical approach to CD-Flow is based on the resolution of the Navier-Stokes equations for the two phase flow with a free surface between the two fluids. The experimental set up considered to study CD-Flow of blood, deals with fast flow of turbid fluid, occurring in micro-channels. The study of wall mass transfer rate in CD-Flow, can be done numerically by solving the mass transfer equation in a CD-Flow field and experimentally by using a micro-channel with reactive walls (i.e. electrodes) in which the fluid flowing inside has to produce a fast heterogeneous reaction with the micro-channel walls.

The purpose of this work is to analyze the wall mass transfer rates generated by a CD-Flow in a micro-channel. The results have implications in the optimization and design of devices for biological assays.

UNIVERSITAT ROVIRA I VIRGILI
NUMERICAL AND EXPERIMENTAL STUDY OF FLOW AND WALL MASS TRANSFER RATES IN CAPILLARY DRIVEN FLOWS IN MICROFLUIDIC CHANNELS
Salvatore Cito
ISBN:978-84-693-0720-5/DL: T-425-2010

Spectral-domain Doppler optical coherence tomography (SDDOCT) has been used to visualize and analyze the surface tension-driven blood flow in PDMS (Polydimethylsiloxane) and glass made micro-channels.

The challenge of fabricating Microsystems for wall mass transfer analysis has been investigated.

Microsystems are commonly manufactured by photolithographic or injection molding techniques in a variety of realizations and on almost any material. A perennial problem of Microsystems manufacturing is the difficulty to obtain hybrid devices that incorporate distinct materials with different functionalities. In most of the cases, cumbersome prototyping and the high investment needed for manufacturing are additional problems that add to the cost of the final product. Such drawbacks are true for lab-on-a-chip but also for certain microreactor applications. Most importantly, in many commercial applications where an intermediate product between full fluidics control and a "strip" is needed, such restraints prohibit feasibility of reduction to practice.

Screen-printing on the other hand is a low cost technique that has been used for years in mass producing of two dimensional low cost reproductions of a mask pattern for circuits and art incorporates prototyping in production and it allows the use of an almost limitless variety of materials as "inks". In this work it is demonstrated that taking advantage of the deposited ink's three dimensional nature, screen-printing can be used as a versatile and low cost technique for the fabrication of micro-channels. Micro-channels with dimensions of the order of 100 μm were fabricated that and they can be readily incorporate functionalities through the choice of the materials used to create the microstructure. Different variables have been investigated through a factorial experimental design as important process parameters that affect the resolution and the printed thickness of the resulting micro-channels that incorporate electroactive elements. Such technique has been implemented to produce the micro-channel used to investigate wall mass transfer rate in micro-channels using confocal microscopy.

UNIVERSITAT ROVIRA I VIRGILI
NUMERICAL AND EXPERIMENTAL STUDY OF FLOW AND WALL MASS TRANSFER RATES IN CAPILLARY DRIVEN FLOWS IN MICROFLUIDIC CHANNELS
Salvatore Cito
ISBN:978-84-693-0720-5/DL: T-425-2010

We performed simulations of the capillary-driven flow in two-dimensional rectangular and circular micro-channels by solving numerically the governing momentum and mass transfer equations with a second order accuracy finite volume code.

The effect of the Reynolds number, of the contact angle and of the channel geometry on the time evolution of the local and averaged wall mass transfer rates are reported and analyzed. The flow field behind the meniscus showed to have two recirculations that enhance the wall mass transfer rates close to the triple point. The correlation for Sherwood number, Reynolds number, contact angle and time is reported. This correlation can be a useful tool for design purposes of microfluidic devices that work with fast heterogeneous reaction and have capillary driven flow as passive pumping system. The numerical results have been confirmed by the experimental results.

UNIVERSITAT ROVIRA I VIRGILI
NUMERICAL AND EXPERIMENTAL STUDY OF FLOW AND WALL MASS TRANSFER RATES IN CAPILLARY DRIVEN FLOWS IN MICROFLUIDIC CHANNELS
Salvatore Cito
ISBN:978-84-693-0720-5/DL: T-425-2010

UNIVERSITAT ROVIRA I VIRGILI
NUMERICAL AND EXPERIMENTAL STUDY OF FLOW AND WALL MASS TRANSFER RATES IN CAPILLARY DRIVEN FLOWS IN MICROFLUIDIC CHANNELS
Salvatore Cito
ISBN:978-84-693-0720-5/DL: T-425-2010

RESUMEN

La perspectiva del uso de micro-canales para el control preciso del flujo y de las reacciones químicas está ampliamente aceptada. La alta relación de aspecto entre la superficie y volumen del micro-canal permite ratios eficientes de transferencia de masa y puede ser aprovechada en microsistemas multifuncionales.

Considerando que el efecto de las tensiones superficiales en la micro-escala es significativo, el bombeo pasivo basado en el uso de la tensión superficial para los Lab-on-a-chip resulta ser el método más eficaz.

El movimiento del punto triple en un menisco aumenta por tensión superficial y disminuye por la resistencia de esfuerzo viscoso y por la fuerza inercial. El efecto del flujo por capilaridad puede ser utilizado para bombear los fluidos en micro-canales y el flujo generado puede disolver los productos químicos previamente depositados en las paredes del canal.

En estudios anteriores, el movimiento del menisco ha sido predicho teóricamente con un modelo uni-dimensional. Sin embargo, el campo de flujo tridimensional en todo el menisco y el efecto de las formas de la sección transversal sobre el flujo y la transferencia de masa de la pared no se han evaluado todavía.

En este trabajo, el enfoque numérico y experimental ha sido desarrollado para investigar la transferencia de masa en la pared en un campo dinámico de un flujo impulsado por capilaridad (CD-Flow: capillary driven flow).

La aproximación numérica se basa en la resolución de las ecuaciones de Navier-Stokes en flujos bifásicos con una superficie libre entre los dos fluidos.

El trabajo experimental necesario para el estudio del flujo de la sangre, implica el uso de fluidos turbios que se mueven a velocidades relativamente altas dentro de los micro-canales.

UNIVERSITAT ROVIRA I VIRGILI
NUMERICAL AND EXPERIMENTAL STUDY OF FLOW AND WALL MASS TRANSFER RATES IN CAPILLARY DRIVEN FLOWS IN MICROFLUIDIC CHANNELS
Salvatore Cito
ISBN:978-84-693-0720-5/DL: T-425-2010

El estudio de la transferencia de masa en una pared en el campo dinámico para un flujo impulsado por capilaridad, se enfoca desde un punto de vista numérico, resolviendo la ecuación de transferencia de masa y experimentalmente usando micro-canales con pared reactiva (en este caso, electrodos) en la que el líquido circula por el interior produciéndose una reacción heterogénea rápida en las paredes del micro-canal.

El propósito de este trabajo es analizar la transferencia de masa en la pared en un campo dinámico de un flujo impulsado por capilaridad. Los resultados permitirán mejorar el diseño y optimizar los dispositivos para ensayos biológicos.

La tomografía de coherencia óptica con anemometría por efecto Doppler se ha utilizado para visualizar y analizar el campo fluido-dinámico de un flujo de sangre impulsado por capilaridad en micro-canales fabricado con PDMS (Polydimethylsiloxane) y vidrio.

En este trabajo nos hemos enfrentado al desafio que representa la fabricación de microsistemas para la análisis de transferencia de masa en una pared.

Los microsistemas se fabrican en la mayoría de los casos por fotolitografía o técnicas de moldeado por inyección en una amplia variedad de tipos y sobre casi cualquier material. Un problema actualmente aún por solventar en la fabricación de microsistemas es la dificultad para obtener dispositivos híbridos que incorporen materiales distintos con diferentes funcionalidades.

En la mayoría de los casos la creación de dispositivos híbridos es un proceso complejo que exige grandes inversiones en el proceso de fabricación aumentando así el coste del producto final. Estos inconvenientes se dan tanto en los casos de Lab-on-a-chip, como en aplicaciones específicas de micro-reactores. Y aún más importante es el hecho de que en muchas aplicaciones comerciales además del pleno control sobre la microfluidica, es necesaria la presencia de un elemento de detección/reacción al estilo de una tira reactiva, (también conocida comúnmente como "strip". Estos requisitos hacen que en la práctica, la viabilidad de la fabricación a micro-escala sea difícil.

La serigrafía por otra parte es una técnica económica que se ha utilizado durante años en la producción masiva de patrones de máscaras para los circuitos bidimensionales

UNIVERSITAT ROVIRA I VIRGILI
NUMERICAL AND EXPERIMENTAL STUDY OF FLOW AND WALL MASS TRANSFER RATES IN CAPILLARY DRIVEN FLOWS IN MICROFLUIDIC CHANNELS
Salvatore Cito
ISBN:978-84-693-0720-5/DL: T-425-2010

de bajo coste. La tecnología actual permite la creación de prototipos en la producción y permite el uso de una variedad casi ilimitada de materiales para usarse como"tintas".

En este trabajo se demuestra que aprovechando la naturaleza tridimensional de las estructuras formadas por la tinta depositada mediante serigrafía se pueden fabricar micro-canales híbridos de forma económica y versátil.

Distintos micro-canales con dimensiones del orden de 100 μm han sido fabricados mediante un procedimiento relativamente simple y se ha demostrado la facilidad con la que se pueden incorporar funcionalidades a través de la elección de los materiales utilizados para crear la microestructura.

Las diferentes variables del estudio han sido investigadas a través de un método experimental factorial basado en los parámetros más importantes del proceso que afectan a la resolución y al espesor de impresión de los micro-canales con una atención especial a las partes que incorporan elementos electroactivos. Esta técnica se ha aplicado para producir los micro-canales usados para el estudio de la transferencia de masa en la pared de un micro-canal y para la visualización del fenómeno de transferencia de masa utilizando la microscopía confocal.

Hemos realizado simulaciones del campo dinámico de un flujo impulsado por capilaridad en un micro-canal con sección transversal rectangular y cilíndrica, resolviendo numéricamente las ecuaciones de conservación de momento y masa. Las ecuaciones han sido resueltas usando una discretización con una precisión de segundo orden mediante un una herramienta de CFD basada en el método de volúmenes finitos.

Se presenta y analiza el efecto del número de Reynolds, del ángulo de contacto y de la geometría del canal en la evolución temporal de los ratio promedio de transferencias de masa en la pared en un campo fluido-dinámico de un flujo impulsado por capilaridad en un micro-canal. El campo fluido-dinámico detrás de los meniscos demostró tener dos recirculaciones que mejoran los rateos promedio de transferencia de masa en la pared cerca del punto triple. Se incluye la correlación para el número de Sherwood, el número de Reynolds, ángulo de contacto y el tiempo.

UNIVERSITAT ROVIRA I VIRGILI
NUMERICAL AND EXPERIMENTAL STUDY OF FLOW AND WALL MASS TRANSFER RATES IN CAPILLARY DRIVEN FLOWS IN MICROFLUIDIC CHANNELS
Salvatore Cito
ISBN:978-84-693-0720-5/DL: T-425-2010

La correlación puede ser una herramienta útil en el diseño de dispositivos microfluídicos que trabajen con una reacción rápida y heterogénea y usen el bombeo pasivo impulsado por el flujo capilar. Los resultados numéricos han sido confirmados por los resultados experimentales.

UNIVERSITAT ROVIRA I VIRGILI
NUMERICAL AND EXPERIMENTAL STUDY OF FLOW AND WALL MASS TRANSFER RATES IN CAPILLARY DRIVEN FLOWS IN MICROFLUIDIC CHANNELS
Salvatore Cito
ISBN:978-84-693-0720-5/DL: T-425-2010

ACKNOWLEDGMENT

The Accomplishment of this interdisciplinary thesis was made possible thanks to the cooperation established between the BBG group and the Ecommfit group, respectively part of the Chemical and Mechanical department of the Escola Tècnica d'Enginyeria Química of the University Rovira i Virgili.

This is to acknowledge that I am very grateful to Dr Ioanis Katakis and Dr Jordi Pallarès for their valuable guidance, which facilitated the completion of this work.

I am also thankful to the rest of the members of ECOMMFIT group and BBG group for their support and collaboration, especially to Dr. Alexandre Fabregat, Dr Gabriel Usera, Guillaume Novelli, and Manuel Martínez for their unconditional support in solving CFD problems, to Dr Pablo Lozano and Diego Bejarano for their assistance with the screen-printing technique, to Obai Younis, Roland Blanch, Elkin Florez Ojeda, Silvana Varela and Reis Gavernet for sharing with me everyday problems encountered during the period of my PhD.

The interdisciplinary nature of this thesis has given me the opportunity to collaborate with the University of California Irvine (UCI) and the University of Leeds (CFD centre). Through these experiences I have had the honour of working with people of great value as Rodrigo Martinez-Duarte, Dr Ahn-Yan, Dr. Horacio Kido Dr. Marc Madou, Dr. Lin Ma, Dr. Derek Ingham and Dr. Mohamed Pourkashanian, and I thank them for the immense scientific feedback they gave me.

A doctoral thesis is a unique experience in which a few moments of success alternate with many moments of frustration, for that I would never be able to accomplish this task without the moral support of my friends to whom I thank for the beautiful moments spent together in Tarragona.

Finally, I would like to thank Nuria and Eddus for their unconditional love and selfless support that they gave me everyday.

UNIVERSITAT ROVIRA I VIRGILI
NUMERICAL AND EXPERIMENTAL STUDY OF FLOW AND WALL MASS TRANSFER RATES IN CAPILLARY DRIVEN FLOWS IN MICROFLUIDIC CHANNELS
Salvatore Cito
ISBN:978-84-693-0720-5/DL: T-425-2010

UNIVERSITAT ROVIRA I VIRGILI
NUMERICAL AND EXPERIMENTAL STUDY OF FLOW AND WALL MASS TRANSFER RATES IN CAPILLARY DRIVEN FLOWS IN MICROFLUIDIC CHANNELS
Salvatore Cito
ISBN:978-84-693-0720-5/DL: T-425-2010

LIST OF FIGURES

UNIVERSITAT ROVIRA I VIRGILI
NUMERICAL AND EXPERIMENTAL STUDY OF FLOW AND WALL MASS TRANSFER RATES IN CAPILLARY DRIVEN FLOWS IN MICROFLUIDIC CHANNELS
Salvatore Cito
ISBN:978-84-693-0720-5/DL: T-425-2010

UNIVERSITAT ROVIRA I VIRGILI
NUMERICAL AND EXPERIMENTAL STUDY OF FLOW AND WALL MASS TRANSFER RATES IN CAPILLARY DRIVEN FLOWS IN MICROFLUIDIC CHANNELS
Salvatore Cito
ISBN:978-84-693-0720-5/DL: T-425-2010

UNIVERSITAT ROVIRA I VIRGILI
NUMERICAL AND EXPERIMENTAL STUDY OF FLOW AND WALL MASS TRANSFER RATES IN CAPILLARY DRIVEN FLOWS IN MICROFLUIDIC CHANNELS
Salvatore Cito
ISBN:978-84-693-0720-5/DL: T-425-2010

LIST OF TABLES

UNIVERSITAT ROVIRA I VIRGILI
NUMERICAL AND EXPERIMENTAL STUDY OF FLOW AND WALL MASS TRANSFER RATES IN CAPILLARY DRIVEN FLOWS IN MICROFLUIDIC CHANNELS
Salvatore Cito
ISBN:978-84-693-0720-5/DL: T-425-2010

UNIVERSITAT ROVIRA I VIRGILI
NUMERICAL AND EXPERIMENTAL STUDY OF FLOW AND WALL MASS TRANSFER RATES IN CAPILLARY DRIVEN FLOWS IN MICROFLUIDIC CHANNELS
Salvatore Cito
ISBN:978-84-693-0720-5/DL: T-425-2010

Chapter 1

Background and objectives

1.1 Introduction

Microfluidics has emerged in the beginning of the 1980s and is used in the development of inkjet printheads, DNA chips, lab-on-a-chip technology, micro-propulsion, and micro-thermal technologies [1]. The advent of microfluidic devices has brought people in the need for a better understanding of the flows in capillary micro-channels, and in the last decade a consistent part of the academies and industries are facing the challenge of developing cheap and efficient microfluidic devices for several applications [2].

In order to induce the flows in the micro-channels, conventional pressure-driven methods are inadequate because they require an active pumping mechanism and in some application turn out to have a high pumping pressure. Novel passive pumping mechanisms that take the advantage of high surface–volume ratio have been tried, including surface-tension-driven method, droplet and bubble based thermocapillary [3], viscosity-temperature dependent valveless micropump, electroosmosis [4], electrowetting [5], electrohydro-dynamic effect etc. Among them, the surface-tension-driven method is suitable for handheld, disposable, and on-site diagnostic applications which usually utilize biological liquid like blood [6].

Another very important issue to consider in the development a microfluidic devices is that due to their relatively low Reynolds number the flow is laminar [2]. This, in terms

UNIVERSITAT ROVIRA I VIRGILI
NUMERICAL AND EXPERIMENTAL STUDY OF FLOW AND WALL MASS TRANSFER RATES IN CAPILLARY DRIVEN FLOWS IN MICROFLUIDIC CHANNELS
Salvatore Cito
ISBN:978-84-693-0720-5/DL: T-425-2010

of mass transfer rates, means that microfluidic devices are very bad mixers, compared with large scale systems operating in turbulent flow regimes [7] .

Then the pump system and the mixing associated with such devices is often a challenging element in the scale down process of the whole micro-system [2, 7, 8]. The use of capillary driven flow (CD-Flow) instead of a micro-pump can drastically reduce the cost and the complexity of microfluidic devices [9]. In this sense, the study of the effect of the meniscus on wall mass transfer rates in a CD-Flow can help to improve the efficiency of mixing [10] in microfluidic devices.

Microfluidic devices are commonly fabricated by photolithography, dry and wet etching and hot embossing [11]. Such methods allow the incorporation of functional elements such as sensors and actuators, valves and passive or active elements with different degrees of complexity and cost depending on; if the final realization is done on plastic or silicon. Work in the clean room is often required. For such methods prototyping has a long iteration cycle and it is feasible but laborious to produce hybrid devices especially incorporating sensors and active elements. For many applications the cost of these methods can be considerably high and a careful study of production volumes has to be undertaken before the product development. For many products, the low resolution required for the microfluidic elements (in the order of hundred microns) does not warrant the expense of high resolution techniques.

Screen-printing is a lower resolution thick film technology that can be applied to plastic substrates as well as glass or silicon. This technique has been used mainly in the microelectronics industry for fabrication of printed circuit boards in two dimensions. In order for screen-printing to be used as a Microsystems fabrication technique all that is needed is to realize the 3-D nature of the ink deposit. Seen as a layer-by-layer 3-D element fabrication method, the flexibility of the technique lies in that almost any substrate can be used. Different commercially available inks can be functionalized by adding different catalysts or enzymes. The possibility of printing different layers with various inks allows an unlimited variety of designs and the incorporation of different active elements. These advantages as well as the low cost and fast prototyping cycle

UNIVERSITAT ROVIRA I VIRGILI
NUMERICAL AND EXPERIMENTAL STUDY OF FLOW AND WALL MASS TRANSFER RATES IN CAPILLARY DRIVEN FLOWS IN MICROFLUIDIC CHANNELS
Salvatore Cito
ISBN:978-84-693-0720-5/DL: T-425-2010

make this technique ideal as a manufacturing approach for microfluidic elements. Screen-printing is used already in fields such as clinical, environmental or industrial analysis [12], and in fuel [13] and solar cells [14] In these applications screen printed inks are limited to be used as the reactive element and little has been reported. The use of screen-printing technique in the biosensors manufacturing area has reported microfluidic devices based on the production of micro-channels combined with electrodes [15]. These devices show a similar architectural concept as the one presented in this work but with a difference: the reported microfluidic device is composed of well-differentiated structural (fluidics) and functional parts (electrodes).

1.2 Background

When a micro-channel comes in contact with a blood droplet (see Figure 1), surface tension draws it into the micro-channel and sets the blood into motion. At the common line of intersection of the blood–gas interface and the solid wall of the micro-channel, the surface tension forces originating from blood-gas, blood-solid, and gas-solid interactions stay in local equilibrium by establishing a certain contact angle. Maintenance of this state of equilibrium pulls the blood toward the meniscus bounded by the common line which moves along the blood motion as well. It, however, is not straightforward to determine the surface tension forces or the contact angle in this situation with a moving common line. The contact angle would rather evolve dynamically due to the interrelation between the surface tension forces and the meniscus speed. Pioneering attempts to understand the surface-tension-driven flows for practical applications have been made by Lucas and Washburn [16]. By assuming a steady-state flow, they obtained a solution for, so-called, the Lucas–Washburn equation. The solution states that the meniscus position is governed by the square root of time.

UNIVERSITAT ROVIRA I VIRGILI
NUMERICAL AND EXPERIMENTAL STUDY OF FLOW AND WALL MASS TRANSFER RATES IN CAPILLARY DRIVEN FLOWS IN MICROFLUIDIC CHANNELS
Salvatore Cito
ISBN:978-84-693-0720-5/DL: T-425-2010

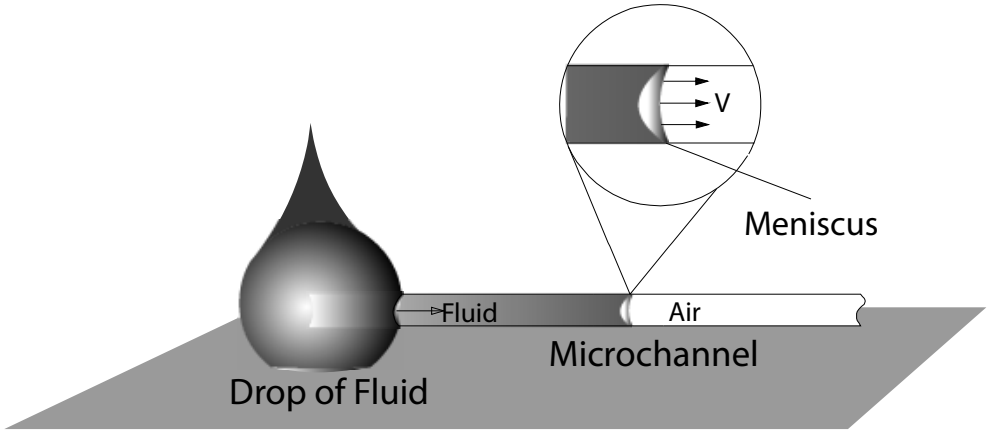

Figure 1: Schematic of a micro-channel drawing fluid from a droplet using capillary forces. The micro-channel can have either circular or rectangular cross section; the velocity of the meniscus is showed.

More recently Joos and Brake [17] and Van Remoortere and Joos [18] showed the effect of the dynamic contact angle in the velocity of the meniscus and extended the theoretical solution of Washburn-Lucas equation [16]. Fahraus and Lindqvist [19] have noticed that a drop of blood flowing in a capillary tube has a higher concentration of corpuscles behind the meniscus than in the bulk. This first interesting effect has been confirmed by Karnis [20] who studied the behaviour of particles in a fluid that is flowing in capillary tube. Karnis [20] observed that there is an accumulation of particles just behind the meniscus and Kung et al [6] showed the effect of the blood red cells in the overall viscosity of blood and in the velocity of the meniscus. Sheng and Zhou [21] and Zhou and Sheng [22] found the correlation between the macroscopic velocity of the meniscus and the effect on it of microscopic parameters like contact line and frictional forces.

One of the mathematical unsolved issues of capillary driven flow is the singularity present at the triple point. The triple point, known as well as contact line, is the border between the liquid, the air and the wall (see Figure 2). Even if the CD-Flow is well known, numerical simulations of the flow behind the meniscus are scarce in the literature [23-25].

UNIVERSITAT ROVIRA I VIRGILI
NUMERICAL AND EXPERIMENTAL STUDY OF FLOW AND WALL MASS TRANSFER RATES IN CAPILLARY DRIVEN FLOWS IN MICROFLUIDIC CHANNELS
Salvatore Cito
ISBN:978-84-693-0720-5/DL: T-425-2010

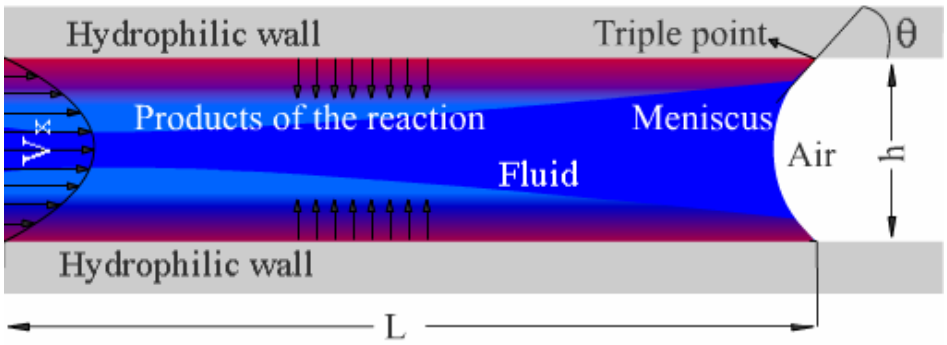

Figure 2: Schematic of capillary driven flow in the hydrophilic and reactive micro-channel with circular or rectangular cross section. Diffusion-convection mass transfer of the product reaction in the fluid from the wall to the bulk is over lighted.

To solve numerically the CD-Flow with the help of computational fluid dynamics (CFD), special consideration with respect to the boundary condition has to be done and the problem of the triple point has to be properly faced to obtain a consistent velocity of the meniscus. In the CD-Flow the contact angle may change dynamically, the consideration of the dynamic contact angle in a CFD simulation introduces a pronounced mesh dependency of the solution. Such problem has been successfully faced by Schönfeld [26], using a macroscopic slip range combined with a localized body force. An alternative approach to overcome the calculation of the shape of the meniscus, and consequently the boundary condition at the triple point, is to assume a fixed shape of the interface [27, 28].

One of the class of devices that better exploit capillary driven flow are bio-sensors and since most of the biosensors deal with bio-fluids like blood, the understanding of capillary driven flow of blood is a very important issue. One of the main challenges of blood flow study is that it is a turbid flow and consequently it has to be investigated using an experimental set up able to work with turbid flow. The more traditional and well established experimental system implemented in the study of fluid flow, like PIV (Particle image Velocimetry) deals with transparent flow like water or air [29] . To deal

UNIVERSITAT ROVIRA I VIRGILI
NUMERICAL AND EXPERIMENTAL STUDY OF FLOW AND WALL MASS TRANSFER RATES IN CAPILLARY DRIVEN FLOWS IN MICROFLUIDIC CHANNELS
Salvatore Cito
ISBN:978-84-693-0720-5/DL: T-425-2010

with turbid flow is necessary to implement techniques implemented in oncology like ODT (optical Doppler tomography) that can work with turbid flow like blood [30].

Most of the microfluidic biosensors measure concentration of a product generated by surface reactions and dissolved in the working fluid [10]. Then the study of the efficiency of wall mass transfer rates is fundamental in the development of a microfluidic device. To achieve such goal an hybrid 3D Microsystems with reactive walls and optically transparent ceiling for reaction visualization and wall mass transfer rate analysis is needed. A Microsystems with such property can be realized using high aspect ratio C-MEMS [31] or screen-printing technique[32].

1.3 Objective

The overall objective of this work is to develop a mathematical model and an experimental set up able to describe, the dissolution, mass transfer and fluid dynamic field of a capillary driven flow occurring in a micro-channel, in which fast heterogeneous electrochemical reactions occur on the wall of the electrode forming the micro-channel. The generic example of application of such a model is the design of minimally invasive biomedical diagnostic devices in which a small amount of blood sample, enters a capillary, dissolves the bio-molecule, which reacts specifically with some of the sample's components producing an electrochemically active product that is then detected in an integrated electrode at the wall of the capillary.

The physical model used is rather generic, so it can be easily used to optimize the design of biosensors using capillary driven flow.

In fact this kind of biosensor is under development in the BBG (Bioengineering and Bioelectrochemistry Group) laboratory of the University Rovira i Virgili to design a generic screen printed biosensor for massive production.

To achieve the objectives the following steps has been taken:

UNIVERSITAT ROVIRA I VIRGILI
NUMERICAL AND EXPERIMENTAL STUDY OF FLOW AND WALL MASS TRANSFER RATES IN CAPILLARY DRIVEN FLOWS IN MICROFLUIDIC CHANNELS
Salvatore Cito
ISBN:978-84-693-0720-5/DL: T-425-2010

- An extended version of Lucas-Washburn equation able to give the velocity of the meniscus of non-Newtonian fluid has been formulated.
- The flow of bovine blood in glass made micro-channels has been recorded using a commercial video camera to measure the average axial velocity of the meniscus in the micro-channels. The non-Newtonian behaviour of blood has been investigated and the experimental results have been compared with the extended version of Lucas-Washburn equations.
- Optical Doppler tomography (ODT) has been implemented, to measure the radial velocity of fluid under capillary driven flow in glass and PDMS made micro-channels.
- A mathematical model based on the numerical resolution of Navier-Stokes equation has been developed to reproduce the dynamic field of CD-Flow in micro-channels for Newtonian and non-Newtonian fluids. The numerical results have been validated by comparison with experimental results.
- A mathematical model based on the numerical resolution of the mass transfer equation have been implemented to predict the wall mass transfer rate in capillary driven flow.
- Optical detection of screen printed micro-channel has been optimized to predict pH gradient of concentration of a fluid under electrochemical reaction on the wall. This has been done using confocal microscopy.
- A parametrical study by means of CFD calculations of several cases has been done and a correlation able to predict the wall mass transfer rate in CD-Flow has been developed.

UNIVERSITAT ROVIRA I VIRGILI
NUMERICAL AND EXPERIMENTAL STUDY OF FLOW AND WALL MASS TRANSFER RATES IN CAPILLARY DRIVEN FLOWS IN MICROFLUIDIC CHANNELS
Salvatore Cito
ISBN:978-84-693-0720-5/DL: T-425-2010

UNIVERSITAT ROVIRA I VIRGILI
NUMERICAL AND EXPERIMENTAL STUDY OF FLOW AND WALL MASS TRANSFER RATES IN CAPILLARY DRIVEN FLOWS IN MICROFLUIDIC CHANNELS
Salvatore Cito
ISBN:978-84-693-0720-5/DL: T-425-2010

Chapter 2

CFD of capillary driven flow

2.1 Fluid dynamics in microfluidics

Fluid dynamics is a science that describes the motion of liquids and gases and the interaction between them. It is an interdisciplinary field that deals with much of science and engineering, and has implications in transportation, manufacturing, medicine, biology, energy and the environment.

Predicting the aerodynamic performance of airplanes, cars, and ships, the flow of blood in the human body, the behaviour of microfluidic devices, the cooling of electronic components, or the hazards of weather and climate, all require a detailed understanding of fluid dynamics.

Fluid dynamics is one of the most challenging and exciting fields of scientific activity and the quest for deeper understanding of it has inspired numerous advances in applied mathematics, computational science and experimental techniques.

A central problem is that the governing equations (the Navier-Stokes equations) have no general analytical solution, and computational solutions are challenging. Fluid dynamics is exciting and fruitful today in part because newly available diagnostic methods for experiments like Optical coherence tomography and parallel computers, for simulations and analysis, allow deep insight in several phenomena still unexplored like the micro scale fluid dynamics.

Like in macro-scale, also in micro scale the Navier-Stokes equation are used to solve the fluid dynamic field, with the only difference that in macro scale inertial forces are

UNIVERSITAT ROVIRA I VIRGILI
NUMERICAL AND EXPERIMENTAL STUDY OF FLOW AND WALL MASS TRANSFER RATES IN CAPILLARY DRIVEN FLOWS IN MICROFLUIDIC CHANNELS
Salvatore Cito
ISBN:978-84-693-0720-5/DL: T-425-2010

dominant. If we scale down to micro scale, the main role is played by surface forces, and. viscous forces.

2.1.1 Navier-Stokes equations in microfluidics

If we assume that fluid has a continue state of mater, then the flow can be mathematically described using the Navier-Stokes equations [28].

Navier-Stokes equations are non linear partial differential equations obtained from the conservation law of mass (see Equation (2.1)) and momentum (see Equation (2.2)).

$$\frac{\partial \rho}{\partial t} + \nabla \cdot \left(\rho \vec{v}\right) = S_m \tag{2.1}$$

$$\frac{\partial \left(\rho \vec{v}\right)}{\partial t} + \nabla \cdot \left(\rho \vec{v} \vec{v}\right) = -\nabla p + \nabla \cdot \left(\bar{\bar{\tau}}\right) + \rho \vec{g} + \vec{F} \tag{2.2}$$

Where ρ is the density of the fluid, $\vec{v}$ velocity vector of the flow, S_m is a source term, p is the static pressure, $\rho \vec{g}$ are the gravitational body force, $\vec{F}$ is the external body forces and $\bar{\bar{\tau}}$ is the shear stress tensor.

In most of the incompressible fluids the shear stress $\bar{\bar{\tau}}$ can be considered proportional to the rate of deformation tensor $\overline{\overline{D}}$.

$$\bar{\bar{\tau}} = \mu \cdot \overline{\overline{D}} \tag{2.3}$$

Where $\overline{\overline{D}}$ is defined by

$$\overline{\overline{D}} = \left(\frac{\partial u_j}{\partial x_i} + \frac{\partial u_i}{\partial x_j} \right) \tag{2.4}$$

and μ is the viscosity. If μ is independent of $\overline{\overline{D}}$ the fluid is called Newtonian.

UNIVERSITAT ROVIRA I VIRGILI
NUMERICAL AND EXPERIMENTAL STUDY OF FLOW AND WALL MASS TRANSFER RATES IN CAPILLARY DRIVEN FLOWS IN MICROFLUIDIC CHANNELS
Salvatore Cito
ISBN:978-84-693-0720-5/DL: T-425-2010

Non-Newtonian fluids are those fluids in which the viscosity is dependent of $\overline{\overline{D}}$. For some of the non-Newtonian fluids the shear stress can similarly be written using a non-Newtonian apparent viscosity η as showed in Equation (2.5).

$$\overline{\overline{\tau}} = \eta(\overline{\overline{D}}) \cdot \overline{\overline{D}} \tag{2.5}$$

A simple model that takes into account the non-Newtonian behaviour of a fluid is the power model. In the power law the apparent viscosity η is function only of the shear rate $\overline{\overline{\dot{\gamma}}}$ (see Equation (2.6).

$$\eta = k \cdot \left(\overline{\overline{\dot{\gamma}}}\right)^{n-1} \tag{2.6}$$

Where $\overline{\overline{\dot{\gamma}}}$ is related to the second invariant of $\overline{\overline{D}}$ and is defined as

$$\overline{\overline{\dot{\gamma}}} = \sqrt{\frac{1}{2}\overline{\overline{D}} : \overline{\overline{D}}} \tag{2.7}$$

In Equation (2.76) k is a consistency index and it is defined as the average viscosity of fluid, and n is a measure of the deviation of the fluid from the Newtonian behaviour.

For:

n=1 the fluid behaves as Newtonian,

n>1 the fluid has dilatants behaviour and it is defined as a shear-thickening fluid,

n<1 the fluid has a pseudo-plastic behaviour and it is defined as a shear-thinning fluid.

Blood is considered to be a shear-thinning fluid, n<1 [33, 34]

The Reynolds number *Re,* defines the ratio between inertial and viscous forces

$$\mathrm{Re} = \frac{\rho V L}{\mu} \tag{2.8}$$

and the Bond number Bo defines the ratio between body and surface tension forces.

UNIVERSITAT ROVIRA I VIRGILI
NUMERICAL AND EXPERIMENTAL STUDY OF FLOW AND WALL MASS TRANSFER RATES IN CAPILLARY DRIVEN FLOWS IN MICROFLUIDIC CHANNELS
Salvatore Cito
ISBN:978-84-693-0720-5/DL: T-425-2010

$$Bo = \frac{\rho g L^2}{\sigma} \tag{2.9}$$

Where V is a reference velocity L is the characteristic length scale and σ is the surface tension coeficient.

Re and *Bo* are important non-dimensional numbers that help to understand the role of the forces in microfluidics:

In microfluidics:

- The Reynolds number is small. So it is reasonable to assume that the viscous forces are dominant and the flow is laminar.
- The Bond number is small. This indicate that the surface forces are dominant and the body force like the gravitational force can be neglected while surface forces like surface tension play a fundamental role.

2.2 Physics of capillary driven flow

2.2.1 Introduction

The coexistence of a group of molecules with similar properties defines a state of matter. The states of matter as we know in nature are solid or fluid. Liquid is a fluid that has the property to form a certain surface at the boundary of its bulk and this surface is called free surface. The free surface of a liquid is not constrained by a container.

The attractive intermolecular forces between like molecules are called cohesive forces, and the attractive forces between unlike molecules are called adhesive forces.

Surface tension is caused by the cohesive forces existing between surface liquid molecules. The liquid molecule in the bulk of a liquid cohere between each others in all directions, while the molecule in the surface of the liquid cohere only with the molecule in the bulk and the neighbours in the surface, than cohesive force of surface molecules is distributed among less molecules, that why surface molecules cohere more strongly then

UNIVERSITAT ROVIRA I VIRGILI
NUMERICAL AND EXPERIMENTAL STUDY OF FLOW AND WALL MASS TRANSFER RATES IN CAPILLARY DRIVEN FLOWS IN MICROFLUIDIC CHANNELS
Salvatore Cito
ISBN:978-84-693-0720-5/DL: T-425-2010

the bulk molecule, forming a thin film where the penetration force is higher than in the bulk of the fluid (see Figure 3). This is one of the reasons why some insects can walk on the surface of a lake. Surface tension is a property of the liquid that can be found experimentally and it changes its value with temperature and with the molecular concentration of the liquid.

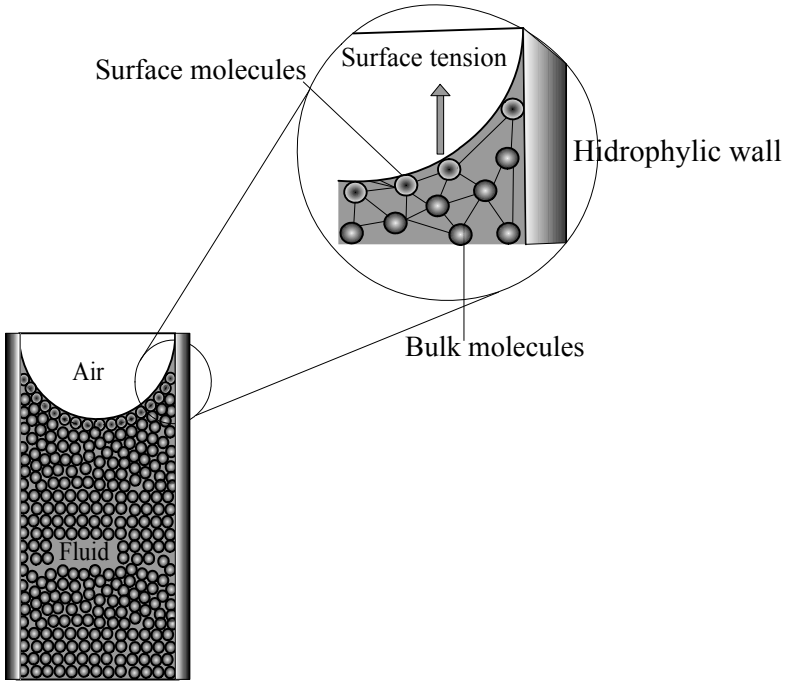

Figure 3: Schematic representation of two fluids in a container with evidence of cohesive forces of surface particle which generate a meniscus between the two fluids as consequence of surface tension.

If we consider a liquid in a reservoir with hydrophilic walls, the adhesion between liquid molecules and the hydrophilic wall will cause an outward force of the liquid that defines the wetting characteristic of the liquid. At the same time the surface tension will try to hold the surface intact. The equilibrium between adhesive forces and cohesive force in the free surface of the liquid will depend on the wettability property of the surface, and the free surface will take the form that minimizes the surface energy. The surface so generated is called meniscus. The angle formed between the meniscus and the

UNIVERSITAT ROVIRA I VIRGILI
NUMERICAL AND EXPERIMENTAL STUDY OF FLOW AND WALL MASS TRANSFER RATES IN CAPILLARY DRIVEN FLOWS IN MICROFLUIDIC CHANNELS
Salvatore Cito
ISBN:978-84-693-0720-5/DL: T-425-2010

solid wall is called contact angle θ. The contact angle is specific for any given system and it gives important information about the wettability of a surface with a liquid.

If the contact angle is larger than 90° the surface is hydrophobic, while if the contact angle is smaller than 90° the surface is hydrophilic.

If the reservoir considered has a sufficiently small diameter to form a micro-channel, and the walls are hydrophilic, a capillary driven flow can be initiated and the flow of the fluid will spontaneously occur.

2.2.2 Young-Laplace equation

The surface tension causes a capillary pressure difference across the interface between two fluids (see Figure 4).

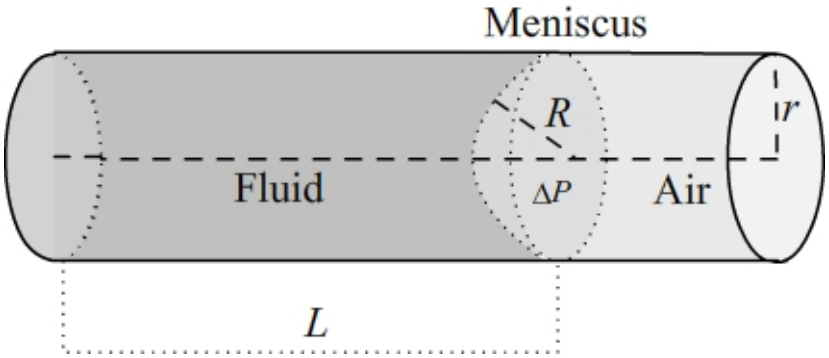

Figure 4: Schematic of CD-Flow with hemispheric meniscus with radius R in circular cross section micro-channel with radius r.

If we assume that the interface *S,* between two immiscible fluids (meniscus) at rest is a zero thickness surface, then the capillary pressure can be seen as a statement of normal stresses balance on the meniscus.

$$\Delta P = \sigma \nabla \cdot \hat{n} \tag{2.10}$$

The equation that describes capillary pressure was formulated by Thomas Young and Pierre-Simon Laplace and from them took the name Young-Laplace equation.

UNIVERSITAT ROVIRA I VIRGILI
NUMERICAL AND EXPERIMENTAL STUDY OF FLOW AND WALL MASS TRANSFER RATES IN CAPILLARY DRIVEN FLOWS IN MICROFLUIDIC CHANNELS
Salvatore Cito
ISBN:978-84-693-0720-5/DL: T-425-2010

The unit normal surface $\hat{n}$ defined in 3D is related to the mean curvature M with:

$$M = \frac{1}{2}\nabla \cdot \hat{n} \tag{2.11}$$

Then

$$\Delta P = 2\sigma M \tag{2.12}$$

Since the mean curvature M is the average curvature and can be defined with:

$$M = \frac{1}{2}(k_1 + k_2) \tag{2.13}$$

Where k_1 and k_2 are the maximum and minimum curvatures of surface S.

$$k_1 = \frac{1}{R_1} \tag{2.14}$$

$$k_2 = \frac{1}{R_2} \tag{2.15}$$

Where R_1 and R_2 are the radii of the minimum and maximum principal osculating circle of the principle curves of surface S (see Figure 5) .

Substituting Equation (2.13) into Equation (2.12) we obtain the following formulation for the Young-Laplace equation.

UNIVERSITAT ROVIRA I VIRGILI
NUMERICAL AND EXPERIMENTAL STUDY OF FLOW AND WALL MASS TRANSFER RATES IN CAPILLARY DRIVEN FLOWS IN MICROFLUIDIC CHANNELS
Salvatore Cito
ISBN:978-84-693-0720-5/DL: T-425-2010

$$\Delta P = -\sigma\left(\frac{1}{R_1}+\frac{1}{R_2}\right) \tag{2.16}$$

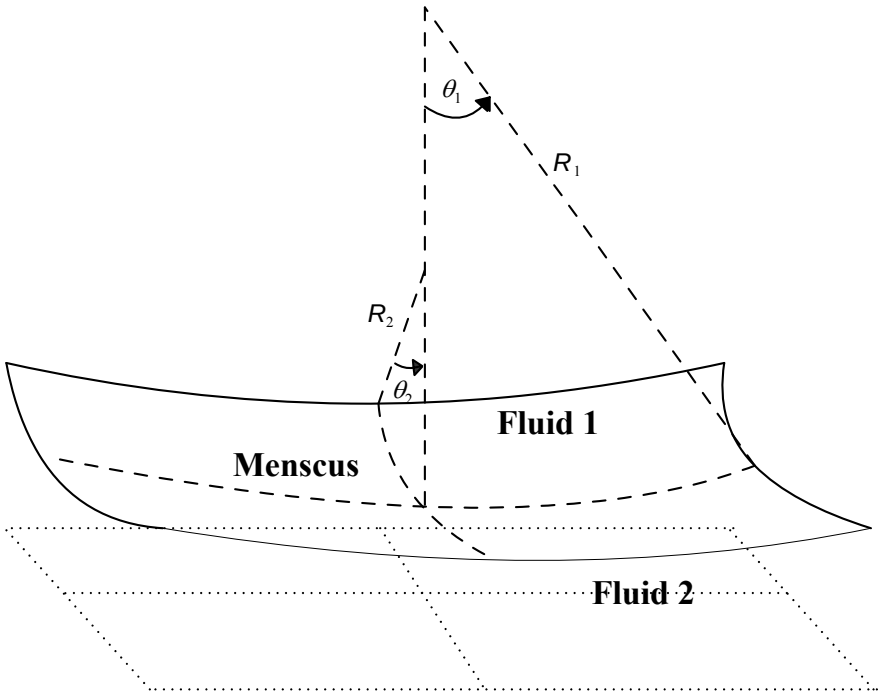

Figure 5: Schematic of the minimum and maximum principal osculating circle radius of the principle curves of a generic surface S.

2.2.3 Capillary pressure in a micro-channel

In a micro-channel of circular cross section with radius r (see Figure 4) filled with two immiscible fluids, the meniscus can be approximated as a portion of a sphere with radius R, and the pressure difference across the meniscus is:

$$\Delta P = -\frac{2\sigma}{R} \tag{2.17}$$

The radius R of the meniscus will depend only on the contact angle θ and the radius of the channel r:

UNIVERSITAT ROVIRA I VIRGILI
NUMERICAL AND EXPERIMENTAL STUDY OF FLOW AND WALL MASS TRANSFER RATES IN CAPILLARY DRIVEN FLOWS IN MICROFLUIDIC CHANNELS
Salvatore Cito
ISBN:978-84-693-0720-5/DL: T-425-2010

$$r = \frac{R}{\cos(\theta)} \tag{2.18}$$

Substituting Equation (2.18) in Equation (2.17) we obtain:

$$\Delta P = -\frac{2\sigma\cos(\theta)}{r} \tag{2.19}$$

2.2.4 Capillary driven flow

As we have seen in the previous treatment, a capillary pressure is present in the interface between two fluids confined in a micro-channel. Such value of pressure can work as intrinsic pumping force for the fluids and draw one of the fluids in the micro-channel at the expenses of the other fluid. Such kind of flow can be called capillary driven flow (CD-Flow) and its dynamics can be mathematically expressed using the Navier-Stokes equations.

Although analytical solutions of Navier Stoke equations for CD-Flow are not available, several authors have developed an approximation that gives the velocity of the meniscus under simplified conditions. The firsts to face such problem were Lucas and Washburn [16]. These authors have found an equation that gives the position of the meniscus L as a function of the time t when the two fluids considered have Newtonian behaviour.

$$L = \sqrt{\frac{r\sigma\cos(\theta)}{2\mu}t} \tag{2.20}$$

Equation (2.20) assumes that the fluid is Newtonian with constant physical properties and that the flow is incompressible, steady and laminar. The velocity of the meniscus which is assumed spherical with constant radius of curvature is:

UNIVERSITAT ROVIRA I VIRGILI
NUMERICAL AND EXPERIMENTAL STUDY OF FLOW AND WALL MASS TRANSFER RATES IN CAPILLARY DRIVEN FLOWS IN MICROFLUIDIC CHANNELS
Salvatore Cito
ISBN:978-84-693-0720-5/DL: T-425-2010

$$V_m = \frac{dL}{dt} = \sqrt{\frac{r\sigma\cos(\theta)}{8\mu \cdot t}} \tag{2.21}$$

A generalized equation of the Lucas-Washburn equation has been used in this work for non-Newtonian fluids that follow the power law for viscosity (See Equation (2.6)).

$$L = \left[\left(\frac{n+1}{3n+1} \right) \left(\frac{\sigma\cos(\theta)}{rk} \right)^{\frac{1}{n}} r^{\frac{n+1}{n}} t \right]^{\frac{n}{n+1}} \tag{2.22}$$

For n=1 the fluid is Newtonian and the well known Lucas-Washburn can be obtained from Equation (2.22)

In this case the velocity of the meniscus is:

$$V_m = \frac{dL}{dt} = \frac{n}{n+1} \frac{\left[\left(\frac{n+1}{3n+1} \right) \left(\frac{\sigma\cos(\theta)}{rk} \right)^{\frac{1}{n}} r^{\frac{n+1}{n}} \right]^{\frac{n}{n+1}}}{\sqrt[n+1]{t}} \tag{2.23}$$

2.3 CFD approach to capillary driven flow

2.3.1 Introduction

Computational fluid dynamics (CFD) is a tool that uses numerical methods to solve partial differential equations like Navier Stokes equations and Fick's Law. CFD has been used in this work to study CD-Flow and the mass transfer phenomena generated by a CD-Flow.

The choice of the language in which a CFD code is written has several implication and needs to be carefully evaluated.

Most of the CFD codes are written in FORTRAN or in C++. The main differences between FORTRAN and C++ languages are:

UNIVERSITAT ROVIRA I VIRGILI
NUMERICAL AND EXPERIMENTAL STUDY OF FLOW AND WALL MASS TRANSFER RATES IN CAPILLARY DRIVEN FLOWS IN MICROFLUIDIC CHANNELS
Salvatore Cito
ISBN:978-84-693-0720-5/DL: T-425-2010

FORTRAN77 and FORTRAN90 deal very well with mathematical arrays that make it very versatile for the implementation of complex numerical methods like FVM (Finite Volume Methods), while C and C++ need to be provided with a class of libraries that has the ability to allocate arrays of objects of elementary types such as ‘int’ or ‘float’.

C and C++ don’t have an array syntax that can be implemented to make mathematical array operations, and the libraries that can be implemented to make array operation of the array defined are not as efficient as the ones intrinsically implemented in FORTRAN.

C++ deals very well with object oriented philosophy of programming. This makes a C++ code very versatile for multiple uses and enhances its modularity in a multipurpose code.

These are some the reasons behind the choice of C based codes and FORTRAN based codes.

Most of the in-house CFD codes (like 3DINAMICS an in-house CFD FORTRAN code developed in the ECOMMFIT Laboratory) designed for specific physical cases, which require benchmark validation of basic fluid flow are developed in FORTRAN. While most of the commercial CFD codes (like Fluent), and open-source codes for multipurpose and complex physics (like Openfoam), are developed in C and C++.

For the reasons aforementioned, to solve CD-Flow we have used the commercial code Fluent that is a C based CFD code with the flexibility to use user defined subroutine implemented in C to introduce no standard boundary conditions.

CD-Flow is a complex unsteady fluid dynamics problem that deals with free surfaces and incorporates not standard boundary condition.

UNIVERSITAT ROVIRA I VIRGILI
NUMERICAL AND EXPERIMENTAL STUDY OF FLOW AND WALL MASS TRANSFER RATES IN CAPILLARY DRIVEN FLOWS IN MICROFLUIDIC CHANNELS
Salvatore Cito
ISBN:978-84-693-0720-5/DL: T-425-2010

2.3.2 Finite volume method

In the literature there are several numerical methods able to discretize partial differential equation like Navier Stokes equations. The most common are:

- Finite element Method FEM
- Finite differential method FDM
- Finite volume method FVM

All the aforementioned methods can be used to solve numerically partial differential equations successfully, but according to the complexity of the phenomena, the importance of coherently describe the conservation laws evocated by the equation itself and the computational capability available, is better to implement one method or another.

In the case of fluids the equation to be solved are the Navier Stokes equations, and the methods that more coherently maintains the conservation of all variable is the FVM. That's why most of the CFD codes are based on FVM.

In the finite volume method the discretization of the governing equations can be illustrated just considering the integral for of a steady conservation equation for transport of a scalar quantity ϕ in a control volume Ω:

$$\oint \rho\phi\vec{v}\cdot d\vec{A} = \oint \Gamma_\phi \nabla\phi \cdot d\vec{A} + \int_\Omega S_\phi d\Omega \tag{2.24}$$

Where:

ρ = density

$\vec{v}$ = velocity vector

$\vec{A}$ = surface area vector

Γ_ϕ = diffusion coefficient for ϕ

$\nabla\phi$ = gradient of ϕ

S_ϕ = source term of ϕ per unit volume

UNIVERSITAT ROVIRA I VIRGILI
NUMERICAL AND EXPERIMENTAL STUDY OF FLOW AND WALL MASS TRANSFER RATES IN CAPILLARY DRIVEN FLOWS IN MICROFLUIDIC CHANNELS
Salvatore Cito
ISBN:978-84-693-0720-5/DL: T-425-2010

Equation (2.24) can be discretized to give an algebraic formulation valid in each control volume of the computational domain. If the problem is steady then the space discretization of the Equation (2.24) on a given cell can be done with:

$$\sum \rho_f \vec{v}_f \phi_f \cdot \vec{A}_f = \sum \Gamma_\phi \nabla \phi_f \cdot \vec{A}_f + S_\phi V \tag{2.25}$$

The discretized transport equation contains the unknown scalar ϕ at the cell centre as well as the unknown values in surrounding neighbours cells, and this equation is non-linear with respect to these variables. A linearized discretized transport equation can be written using the following formulation:

$$a_p \phi = \sum_{nb} a_{nb} \phi_{nb} + b \tag{2.26}$$

Where the subscript *nb* refers to neighbours cells, and a_P and a_{nb} are the linearized coefficient for ϕ and ϕ_{nb}.

To solve the linear system obtained combining Equation (2.25) to Equation (2.26) for each cell of the computational mesh (see Figure 6), a matrix with sparse coefficient can be established, and the solution of such system gives the values of the scalar ϕ in the centre of the cell.

Fluent solves this linear system using a point implicit (Gauss-Seidel) linear equation solver in conjunction with a multigrid method fully described in the Fluent manual [35].

The values of the scalar ϕ_f on the faces of the cell are required in the convection terms of Equation (2.24) and they are obtained interpolating the scalar ϕ from the cell centre values of the cell. This means that the accuracy of the solution depends on how properly is predicted the value of ϕ_f in the face of the cells. In this work a second order Upwind Scheme has been used for every unknown of the equation solved.

Upwind, means that the face value ϕ_f is derived from quantities in the cell upstream (or upwind), relative to the direction of the normal velocity.

UNIVERSITAT ROVIRA I VIRGILI
NUMERICAL AND EXPERIMENTAL STUDY OF FLOW AND WALL MASS TRANSFER RATES IN CAPILLARY DRIVEN FLOWS IN MICROFLUIDIC CHANNELS
Salvatore Cito
ISBN:978-84-693-0720-5/DL: T-425-2010

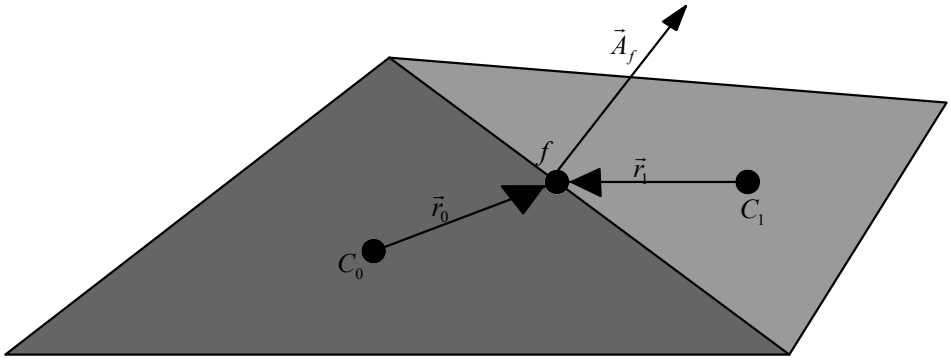

Figure 6: Schematic of Control volume used for the discretization of scalar transport equation.

A first order accuracy scheme is based on the assumption that the cell centred value of ϕ is the average cell-average value and hold throughout the entire cell, then; if a first order upwind scheme is implemented, the value ϕ_f is set equal to the cell centre value of ϕ in the upstream cell. In the second order upwind scheme higher order of accuracy for ϕ_f is achieved using a Taylor series expansion of the cell-centred solution ϕ . Thus the face value ϕ_f is computed using the following expression:

$$\phi_f = \phi + \nabla\phi \cdot \vec{r} \tag{2.27}$$

Where $\vec{r}$ is the displacement vector from the upstream cell centroid to the face centroid.

This formulation requires the determination of the gradient $\nabla\phi$ that can be calculated using the Green Gauss theorem.

Green Gauss theorem establishes that the gradient in the cell centre c_0 is given by:

$$\nabla\phi\big|_{c_0} = \frac{1}{V_\Omega}\sum_f \bar{\phi}_f \vec{A}_f \tag{2.28}$$

Where the summation is over all the faces enclosing the cell, and $\bar{\phi}_f$ can be calculated either with a cell based formulation or a node based formulation.

UNIVERSITAT ROVIRA I VIRGILI
NUMERICAL AND EXPERIMENTAL STUDY OF FLOW AND WALL MASS TRANSFER RATES IN CAPILLARY DRIVEN FLOWS IN MICROFLUIDIC CHANNELS
Salvatore Cito
ISBN:978-84-693-0720-5/DL: T-425-2010

The Green Gauss cell-based formulation of gradient is obtained from the arithmetic average of the values at neighbours' cell centres:

$$\bar{\phi}_f = \frac{\phi_{c_0} + \phi_{c_0}}{2} \tag{2.29}$$

The Green-Gauss cell-based formulation is obtained from the arithmetic average of the all nodal values N_f on the face.

$$\bar{\phi}_f = \frac{1}{N_f} \sum_{n}^{N_f} \bar{\phi}_n \tag{2.30}$$

Where nodal value $\bar{\phi}_n$ is obtained from the weighted average of the cell values surrounding the nodes. This method proposed by Holmes and Connel [35] reconstruct exact values of a linear function at a node from surrounding cell centred values on arbitrary unstructured meshes by solving a constrained minimization problem, preserving a second order spatial accuracy. The Green Gauss node based has been used in this work for his accuracy, even in highly skewed cells, even those is computationally more expensive than the cell based gradient scheme.

2.3.3 Time discretization

Capillary driven flow and mass transfer phenomena occurring in capillary driven fluid dynamics field are unsteady phenomena, and even if we assume that the fluid dynamic field reaches a quasi-steady condition after a certain time, it is interesting to see how the wall mass transfer rate evolves with time.

The time evolution of mass transfer phenomena in CD-Flow can be calculated by solving numerically the corresponding mass transfer equation.

This equation with an additional term that establishes the variation of the scalar ϕ with time can be written as:

UNIVERSITAT ROVIRA I VIRGILI
NUMERICAL AND EXPERIMENTAL STUDY OF FLOW AND WALL MASS TRANSFER RATES IN CAPILLARY DRIVEN FLOWS IN MICROFLUIDIC CHANNELS
Salvatore Cito
ISBN:978-84-693-0720-5/DL: T-425-2010

$$\int_{\Omega} \frac{\partial \rho \phi}{\partial t} + \oint \rho \phi \vec{v} \cdot d\vec{A} = \oint \Gamma_{\phi} \nabla \phi \cdot d\vec{A} + \int_{\Omega} S_{\phi} d\Omega \tag{2.31}$$

Since the fluid considered is incompressible we can write a generic expression for time evolution of the scalar ϕ,

$$\frac{\partial \phi}{\partial t} = F(\phi) \tag{2.32}$$

Where the function F contains all the spatial dependent terms.

The spatial discretization for the time dependent Equation (2.32) is identical to the steady case Equation (2.25). Time discretization involves the integration of every term in the differential equation over a time step Δt. The integration of the transient term can be given using backward differences.

The first order accurate temporal discretization is given by Equation (2.33):

$$\frac{\phi^{n+1} - \phi^{n}}{\Delta t} = F(\phi) \tag{2.33}$$

And the second order accurate temporal discretization is given by Equation (2.34):

$$\frac{3\phi^{n+1} - 4\phi^{n} + \phi^{n-1}}{2\Delta t} = F(\phi) \tag{2.34}$$

Where *n, n+1,* and *n-1* are respectively values at time levels *t, t+Δt* and *t-Δt.*

With the time derivative discretization the time level values of ϕ in the function F has to be defined.

If the time level chosen to evaluate $F(\phi)$ is at n+1 we obtain Equation (2.35) from Equation (2.33) for the first order discretization,

$$\frac{\phi^{n+1} - \phi^{n}}{\Delta t} = F(\phi^{n+1}) \tag{2.35}$$

And Equation (2.36) from Equation (2.34) for the second order discretization,

UNIVERSITAT ROVIRA I VIRGILI
NUMERICAL AND EXPERIMENTAL STUDY OF FLOW AND WALL MASS TRANSFER RATES IN CAPILLARY DRIVEN FLOWS IN MICROFLUIDIC CHANNELS
Salvatore Cito
ISBN:978-84-693-0720-5/DL: T-425-2010

$$\frac{3\phi^{n+1} - 4\phi^{n} + \phi^{n-1}}{2\Delta t} = F\left(\phi^{n+1}\right) \tag{2.36}$$

Then, we have an implicit time integration that for the first order discretization scheme is given by the Equation (2.37):

$$\phi^{n+1} = \phi^{n} + \Delta t F\left(\phi^{n+1}\right) \tag{2.37}$$

And for the second order discretization scheme is given by Equation (2.38):

$$\phi^{n+1} = \frac{1}{3}\left(4\phi^{n} - \phi^{n-1} + 2\Delta t F\left(\phi^{n+1}\right)\right) \tag{2.38}$$

For the study of wall mass transfer rates in CD-Flow the Equation (2.38) has been solved iteratively at each time level before moving to the next step. The advantage of the fully implicit scheme is that is unconditionally stable with respect to the time step.

2.3.4 Fluent solver

The Navier-Stokes equations are no linear differential equation and as we have seen, we can solve them numerically using FVM. One of the issues that have to be faced when the Navier-Stokes equations have to be solved is the fact that they are equations coupled through them by mean of variables like velocity, density and pressure and they have to be solved in a certain order.

The choice of the algorithm that defines the order in which the Navier-Stokes equations are solved is a key element in a CFD simulation, and in the commercial code Fluent there are 4 algorithms proposed:

- The Pressure based segregate algorithm
- The Pressure based coupled algorithm
- The Density based segregate algorithm
- The Density based coupled algorithm.

UNIVERSITAT ROVIRA I VIRGILI
NUMERICAL AND EXPERIMENTAL STUDY OF FLOW AND WALL MASS TRANSFER RATES IN CAPILLARY DRIVEN FLOWS IN MICROFLUIDIC CHANNELS
Salvatore Cito
ISBN:978-84-693-0720-5/DL: T-425-2010

In this study a pressure based coupled algorithm has been selected. It consists in a projection method [35] where the constraint of mass conservation and momentum conservation is achieved by solving a pressure correction equation. Such equation is not available publically (remember that Fluent is not an open source code), but from the Fluent manual [35] we know that is derived from the continuity and the momentum equations in such away that the velocity field, corrected by the pressure, satisfies the continuity.

Since the governing equations are nonlinear and coupled, each governing equation has to be solved iteratively. The set of equations can be solved sequentially (segregated from the others) or using a coupled system of equations comprising momentum equations and the pressure based continuity equation.

Since the momentum and continuity equation are solved in a closely coupled manner the rate of convergence of the solution significantly improves when compared to the segregate algorithm. However, the memory requirements for the coupled algorithm increase by more than 50% of the memory required for the segregate algorithm. This is due to the fact that the matrix system of all momentum and pressure-based continuity equations needs to be stored in the memory at the same time, while solving for the velocity and pressure fields, while in the segregate algorithm only the matrix system of a single equation has to be stored while solving the corresponding equation.

UNIVERSITAT ROVIRA I VIRGILI
NUMERICAL AND EXPERIMENTAL STUDY OF FLOW AND WALL MASS TRANSFER RATES IN CAPILLARY DRIVEN FLOWS IN MICROFLUIDIC CHANNELS
Salvatore Cito
ISBN:978-84-693-0720-5/DL: T-425-2010

Chapter 3

Experimental study of capillary driven flow

3.1 Introduction

Capillary driven flow in a micro-channel is a challenging phenomenon to be visualized and analyzed by means of traditional experimental techniques. Indeed the velocity of the meniscus can be relatively high (≈0.2m/s), the dimensions considered are relatively small (≈100μm) and the interaction between the fluids and the surface of the micro-channel plays a crucial role in the phenomena, such that small variation in wetting properties of the surface can strongly change the dynamic of CD-Flow.

To be successful in the definition of a proper experimental set up able to give useful information about wall mass transfer rate in CD-Flow, we need an instrument able to record large number of images per second and (high number of frames per second), with high spatial resolution (high pixel density PPI pixel per inch), and a micro-fabrication technique able to produce a smooth and reproducible hydrophilic micro-channel surface that can be functionalized to reproduce a fast heterogeneous reaction with the fluid.

Most of the experimental fluid dynamic techniques use tracers (or particles) in the bulk of the flow, to faithfully follow the flow dynamics of the fluid under investigation. [36]

The first who used particles, as an indirect way to visualize fluid flow, was Ludwing Prandl (1875-1953). More recent applications of particle in fluid flow visualization are the Particle Image Velocimetry (PIV) [37] and the Laser Doppler Velocimetry (LDV) [37]. Although these two techniques are very robust and well established, the challenges

UNIVERSITAT ROVIRA I VIRGILI
NUMERICAL AND EXPERIMENTAL STUDY OF FLOW AND WALL MASS TRANSFER RATES IN CAPILLARY DRIVEN FLOWS IN MICROFLUIDIC CHANNELS
Salvatore Cito
ISBN:978-84-693-0720-5/DL: T-425-2010

of analyzing the flow field generated by CD-Flow of blood, required us to use a novel technique called Optical Doppler Tomography (ODT) [38] that combined with a video framing analysis gave us good insight in the fluid dynamic of CD-Flow with blood.

3.1.1 Video frame analysis

A video is a sequence of images called frames. The projection of the frames at the same velocity at which they has been taken allows the visualization in real time of time dependent phenomena like capillary driven flow. The higher the number of frame per second "fps" recorded the higher the amount of information that can be used to analyze the phenomenon.

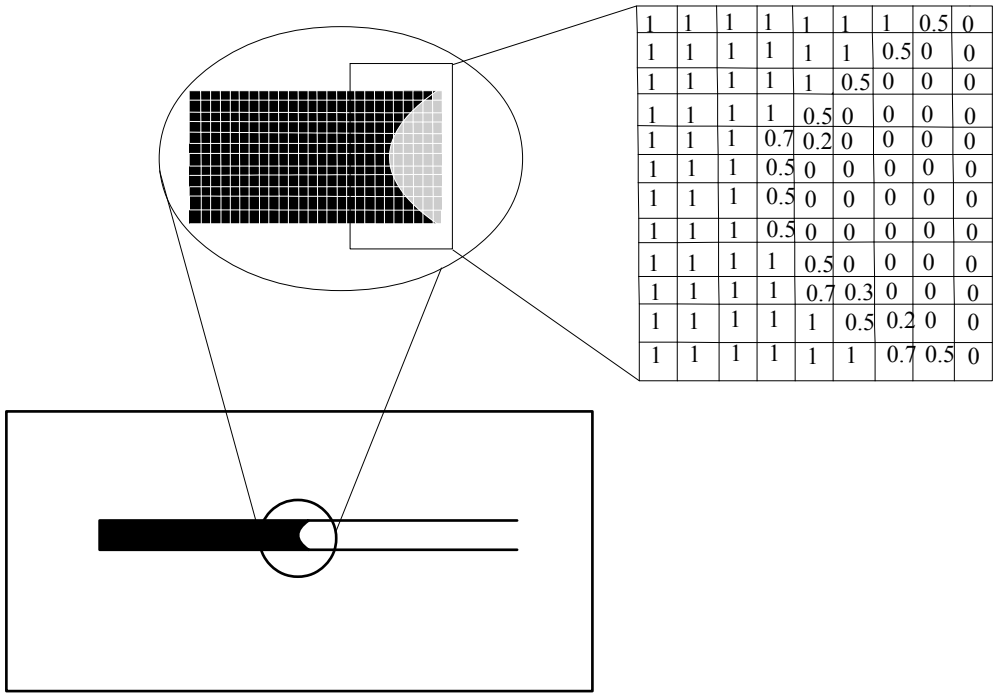

Figure 7: Schematic of a digital picture of meniscus with zoom at pixel level and representation of matrix formulation of the picture.

A digital frame is an image constituted by an array of pixels. A pixel is the smallest element that forms an image. Each pixel can be mathematically expressed with a number corresponding to its intensity. Then a frame can be seen as a 2D matrix $n \times m$, where the

UNIVERSITAT ROVIRA I VIRGILI
NUMERICAL AND EXPERIMENTAL STUDY OF FLOW AND WALL MASS TRANSFER RATES IN CAPILLARY DRIVEN FLOWS IN MICROFLUIDIC CHANNELS
Salvatore Cito
ISBN:978-84-693-0720-5/DL: T-425-2010

position of each number corresponds to the geometrical position of the picture (see Figure 7). n and m are respectively the maximum number of pixels along the vertical and horizontal direction of the image (see Figure 7).

If the frame is in black and white then the pixels can have two values, 0 for white and 1 for black. If the frame is intensity scaled grey picture then the image is a matrix in which each pixel can have an integer value between 0 and 255. If the frame is a coloured picture then each pixel is the composition of the three basic colours, red, green, and blue and the matrix is the composition of three matrices or a 3D matrix $n \times m \times p$ where $p = 3$. The coloured picture can be understood as the composition of three matrixes in which the element in the i-j position of each matrix has an integer value between 0 and 255. The value in the i-j position in each of the three matrices represents, respectively the intensity of red, green and blue of the picture in that position.

3.2 Optical Doppler tomography

Optical Doppler tomography (ODT) is a technique that couples the Doppler effect to optical coherence tomography (OCT) to measure the instantaneous velocity of particles immerged in a fluid while it is flowing [39].

The Doppler effect was described in 1842 by J. C. Doppler who observed that waves emitted from a source moving toward an observer/receiver decrease their wavelength and increase their frequency, while waves emitted from a source moving away from an observer/receiver decrease their wavelength and increase their frequency. Doppler Effect can be used as indirect way to measure the flow velocity in several experimental techniques.

Laser Doppler Velocimetry (LDV) has been the first experimental technique that implemented the Doppler effect to measure the flow velocity [40]. Indeed, LDV is a technique able to measure the velocity of a particle in a fluid with high temporal resolution. LDV uses two beams of collimated monochromatic and coherent laser lights

UNIVERSITAT ROVIRA I VIRGILI
NUMERICAL AND EXPERIMENTAL STUDY OF FLOW AND WALL MASS TRANSFER RATES IN CAPILLARY DRIVEN FLOWS IN MICROFLUIDIC CHANNELS
Salvatore Cito
ISBN:978-84-693-0720-5/DL: T-425-2010

(two waves are said to be coherent if they have a constant relative phase). To ensure coherence of the two beams, a Michelson interferometer can be implemented. In a Michelson interferometer a beam of monochromatic light is split in two paths and properly recombined to create alternating interference fringes on a back detector see Figure 8. Using a proper post-processing of the fringes, the velocity of the scattering particles can be obtained [40].

In LDV the two beams intersect across the target area at a known angle α as shown in Figure 9

The spacing δ of the interference fringes where the combined laser light intensity is zero can be obtained from simple trigonometric considerations that lead to the equation:

$$\delta = \frac{\lambda}{2\cos(\alpha)} \tag{3.1}$$

Where λ is the vacuum centre wavelength of the target laser beam.

When the target area is within a flow field as shown in Figure 10, the moving particles passing through the fringe produce a scattered light having a Doppler shifted Δf equal to:

$$\Delta f = \frac{v_p}{\delta} = \frac{2v_p}{\lambda}\cos(\alpha) \tag{3.2}$$

Form which we obtain the velocity of the particle as:

$$v_p = \frac{\Delta f \cdot \lambda}{2\cos(\alpha)} \tag{3.3}$$

UNIVERSITAT ROVIRA I VIRGILI
NUMERICAL AND EXPERIMENTAL STUDY OF FLOW AND WALL MASS TRANSFER RATES IN CAPILLARY DRIVEN FLOWS IN MICROFLUIDIC CHANNELS
Salvatore Cito
ISBN:978-84-693-0720-5/DL: T-425-2010

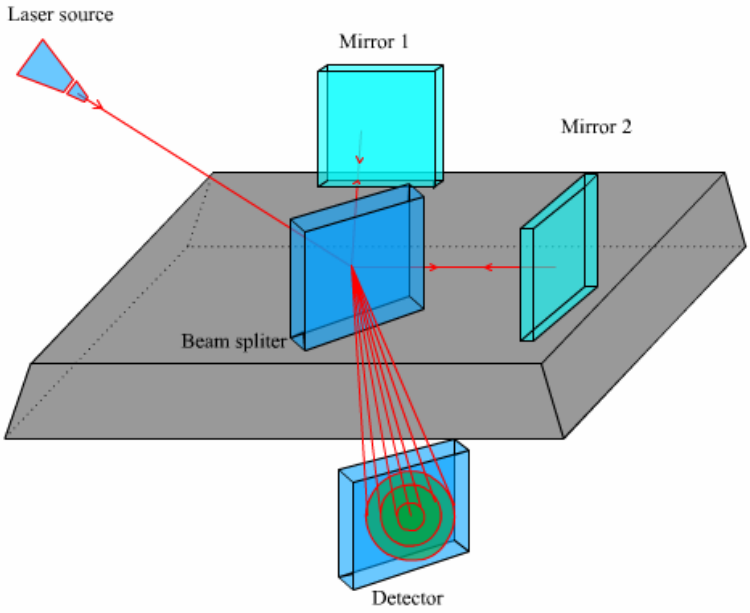

Figure 8: Schematic of a Michelson interferometer.

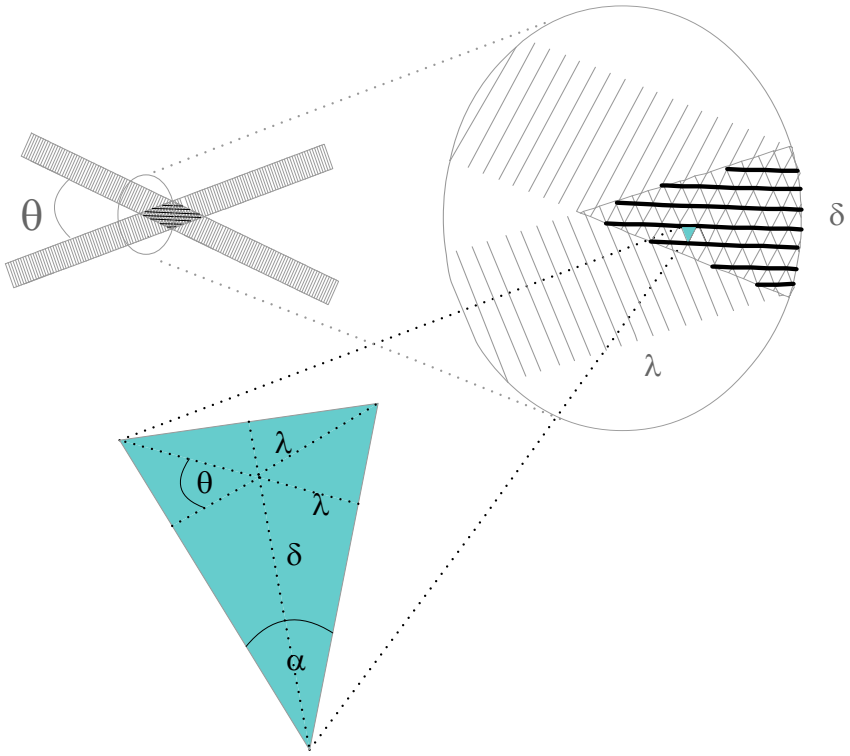

Figure 9: Schematic of interference fringe formation due to the intersection of two coherent beams.

UNIVERSITAT ROVIRA I VIRGILI
NUMERICAL AND EXPERIMENTAL STUDY OF FLOW AND WALL MASS TRANSFER RATES IN CAPILLARY DRIVEN FLOWS IN MICROFLUIDIC CHANNELS
Salvatore Cito
ISBN:978-84-693-0720-5/DL: T-425-2010

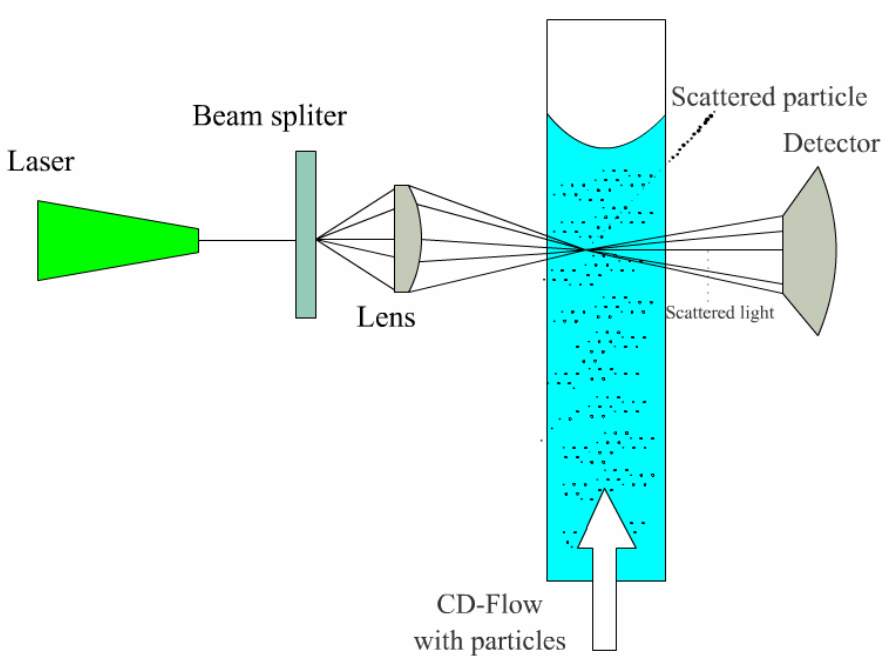

Figure 10: Schematic of Laser Doppler Velocimetry.

In the last two decades, LDV and PIV (Particles image velocimetry), have been the most used techniques in experimental fluid dynamics. One of the limitations of these two techniques is that they need a transparent fluid to be properly implemented. Consequently it is difficult to use such techniques to investigate flow in turbid fluids like blood. Nevertheless both techniques have been implemented by several authors to study flow in blood, but the interpretation of the result is often difficult and may cause conflicting reports [30].

To overcome the difficulties related with turbid flows, optical coherence tomography (OCT) techniques can be used in combination with LDV [41, 42].

OCT is an optical method based on the interferometric technique that employs near-infrared light to investigate and visualize the optical scattering target (like red blood cells).

UNIVERSITAT ROVIRA I VIRGILI
NUMERICAL AND EXPERIMENTAL STUDY OF FLOW AND WALL MASS TRANSFER RATES IN CAPILLARY DRIVEN FLOWS IN MICROFLUIDIC CHANNELS
Salvatore Cito
ISBN:978-84-693-0720-5/DL: T-425-2010

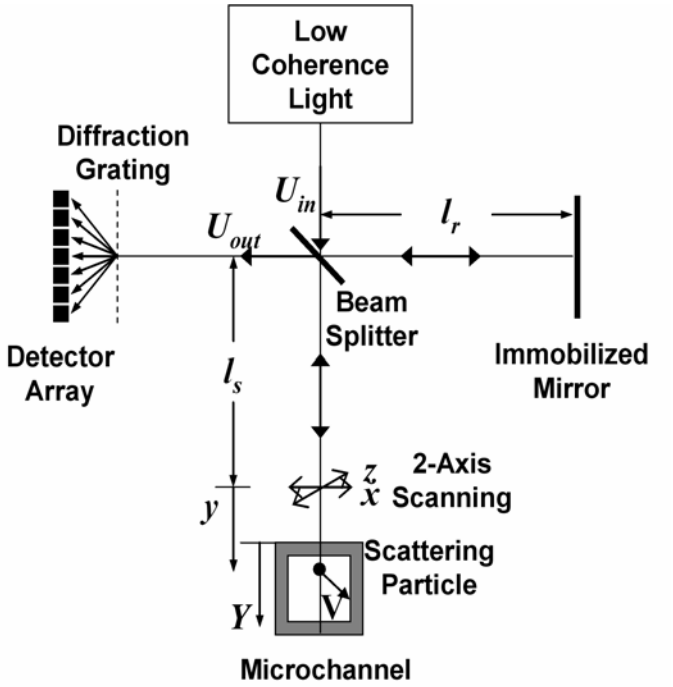

Figure 11: Schematic of Spectral domain Doppler optical coherence tomography with Michelson interferometer [43].

Spectral-domain Doppler optical coherence tomography SDDOCT is a fusion of laser Doppler velocimetry and optical coherence tomography based on a Michelson interferometer shown in Figure 11.

Four arms around a 50:50 beam splitter in the Michelson interferometer are assigned by a low-coherence light source at the source arm, a spectrometer with a line array of detectors and a diffraction grating at the detector arm, an immobilized mirror at the reference arm, and a 2-axis scanner and a sample with moving scatterers at the sample arm. Reflected lights from the immobilized mirror and each scattering particle in the sample make a signal in spectral domain which is detected by the spectrometer [43].

UNIVERSITAT ROVIRA I VIRGILI
NUMERICAL AND EXPERIMENTAL STUDY OF FLOW AND WALL MASS TRANSFER RATES IN CAPILLARY DRIVEN FLOWS IN MICROFLUIDIC CHANNELS
Salvatore Cito
ISBN:978-84-693-0720-5/DL: T-425-2010

3.3 Confocal microscopy

Wall mass transfer rate in a micro-channel is a challenging issue that cannot be endorsed detecting the velocity of particles immersed in the fluid. Then all the particles based technique need to be further developed, for example introducing analysis of fluorescence property of the fluid particle system. Indeed it is well known that quenching depends on several properties like temperature or concentration of certain substance (i.e. Ph).

SDDOCT needs to be coupled with a fluorescence detector to properly visualize wall mass transfer rates in capillary driven flow. But this modification is far from being implemented, and alternative way has to be used to study mass transfer in capillary driven flow.

In this work an experimental set up based on the use of confocal microscopy has been developed to detect wall mass transfer rate in micro-channel.

In a confocal microscopy the fluorescence is detected by a photodetector or camera and this is done using a point illumination and a pinhole in an optically conjugate plane in front of the detector to eliminate out-of-focus information - the name "confocal" stems from this configuration. As only light produced by fluorescence very close to the focal plane can be detected the image resolution, particularly in the direction perpendicular to the sample, is much better than that of wide-field microscopes. However, much of the light from the sample fluorescence is blocked at the pinhole. This increased resolution is at the cost of decrease of the signal intensity. Consequently long exposures are often required and a high frame per second recording system has a big inconvenience to work with confocal microscopy.

UNIVERSITAT ROVIRA I VIRGILI
NUMERICAL AND EXPERIMENTAL STUDY OF FLOW AND WALL MASS TRANSFER RATES IN CAPILLARY DRIVEN FLOWS IN MICROFLUIDIC CHANNELS
Salvatore Cito
ISBN:978-84-693-0720-5/DL: T-425-2010

Chapter 4

Microfabrication of micro-channels

4.1 Introduction

Microfluidic devices are commonly fabricated by photolithography, dry and wet etching and hot embossing [11]. Such methods allow incorporation of functional elements such as sensors and actuators, valves and passive or active elements with different degrees of complexity and cost depending on if the final realization is done on plastic or silicon. Work in the clean room is often required. For such methods prototyping has a long iteration cycle and it is feasible but laborious to produce hybrid devices especially incorporating sensors and active elements. For many applications the cost of these methods can be considerably high and careful study of production volumes has to be undertaken before product development. For many products, the low resolution required for the microfluidic elements (in the order of hundred microns) does not warrant the expense of high resolution techniques.

4.2 Soft photolithography and micro-molding

Photolithography (from Greek *photo* 'light', *lithos* 'stone' and *grapho* 'to write') is a microfabrication technique that uses light to transfer a geometric pattern from a mask to a light-sensitive chemical photo-resist on a substrate (i.e. SU-8).

SU-8 is a negative photoresist resin highly transparent in the ultraviolet region; it contains eight epoxy groups per molecule which gives the polymer very high

UNIVERSITAT ROVIRA I VIRGILI
NUMERICAL AND EXPERIMENTAL STUDY OF FLOW AND WALL MASS TRANSFER RATES IN CAPILLARY DRIVEN FLOWS IN MICROFLUIDIC CHANNELS
Salvatore Cito
ISBN:978-84-693-0720-5/DL: T-425-2010

functionality. It is a very viscous polymer that can be poured over a thickness ranging from 0.1 micrometer up to 2 millimetres and its maximum absorption is for ultraviolet light with a wavelength of 365 nm. When exposed to UV light the optical absorption of the resin in the near-UV is very low so that its long molecular chains cross-link causes the solidification of the material allowing fabrication of relatively thick structures with nearly vertical side walls. When this resin is photosensitized with a mixture of triarylsulfonium/hexafluroantimonate salt, the exposed regions polymerize, resulting in an extremely high crosslink density. The high cross-linking degree gives SU-8 good thermal stability.

SU-8 was developed as a photoresist for microelectronics devices, and it main property is that provides a high-resolution mask for fabrication of semiconductor devices. Nowadays is mainly used together with PDMS in the micro-fabrication of microfluidics and MEMS parts.

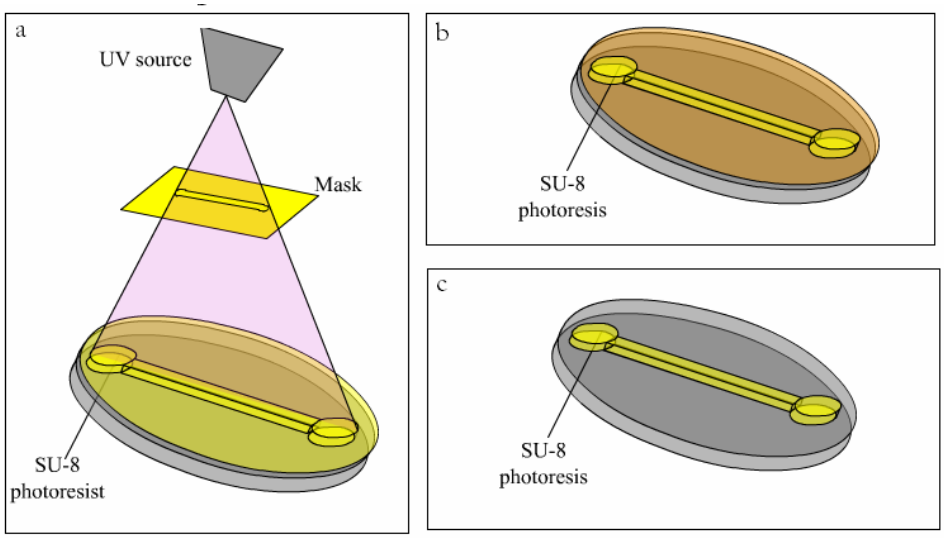

Figure 12: Schematic of SU-8 cross-linking under UV light exposition.

Liquid SU-8 is poured over a spinning silicon wafer, leaving a controlled thin layer of liquid monomer. Exposing this layer to ultraviolet light through a high-resolution transparency mask Figure 12a and baking the wafer to crosslink the SU-8 forms a

UNIVERSITAT ROVIRA I VIRGILI
NUMERICAL AND EXPERIMENTAL STUDY OF FLOW AND WALL MASS TRANSFER RATES IN CAPILLARY DRIVEN FLOWS IN MICROFLUIDIC CHANNELS
Salvatore Cito
ISBN:978-84-693-0720-5/DL: T-425-2010

permanent mold master (Figure 12b). The no cross-linked SU-8 is washed out using a proper solvent (Figure 12c). This master wafer can be used indefinitely with PDMS to reproduce its shape.

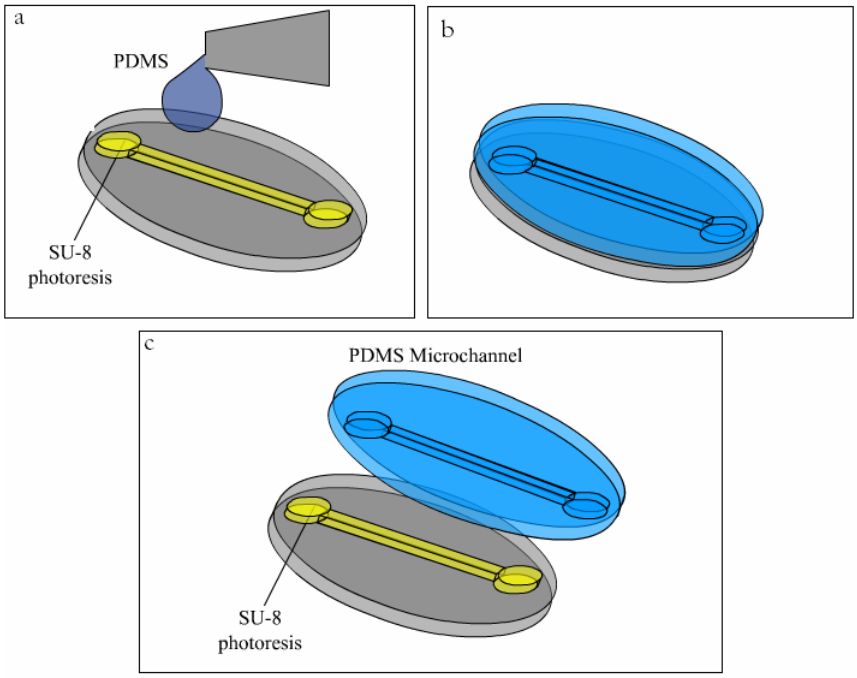

Figure 13: Schematic of micro-channel fabrication through soft lithography of SU-8 and PDMS micro-molding.

PDMS oligomer is a viscous, oily liquid with very low surface tension. To microfabricate a PDMS micro-channel liquid PDMS is poured over the SU-8 master mold and polymerized at an optimized temperature. Because of its low surface tension, it can flow into the micron-sized features of a master mold (i.e. SU-8 master mold) (see Figure 13a) and be polymerized to become a tough, transparent rubber (see Figure 13b).

Once the molded PDMS has been cured is remove, mold release agents or solvents such as ethanol can be used to reduce adhesion during this step (see Figure 13c).

Once PDMS is pilled out from the SU-8 mold master has the micro-channel shape with an external transparent hydrophobic surface [44] (see Figure 13c). This surface

UNIVERSITAT ROVIRA I VIRGILI
NUMERICAL AND EXPERIMENTAL STUDY OF FLOW AND WALL MASS TRANSFER RATES IN CAPILLARY DRIVEN FLOWS IN MICROFLUIDIC CHANNELS
Salvatore Cito
ISBN:978-84-693-0720-5/DL: T-425-2010

chemistry makes it difficult for polar solvents like H_2O to wet the PDMS surface, and may lead to adsorption of hydrophobic contaminants. Plasma oxidation can be used to alter the surface chemistry, adding silanol (SiOH) groups to the surface. This treatment renders the PDMS surface hydrophilic, allowing water to wet and CD-Flow to occur in a PDMS micro-channel. The oxidized surface resists adsorption of negatively charged and hydrophobic species and can be further functionalized by reaction with trichlorosilanes. Oxidized surfaces are stable for not longer then 30 minutes in air. To maintain PDMS surface hydrophilic can be stored in several ways, but after a certain time hydrophobic recovery of the surface is inevitable independently of the surrounding medium whether it is vacuum, air or water [45].

The immense flexibility of SU-8 in cross-linking channel layouts can be used as master mold for PDMS micro-channels to quickly fabricate nearly any two-dimensional channel geometry. Three dimensional shapes require more difficult multilevel bonding, and remain the greatest limitation of micro-fabrication techniques. One of the micro-fabrication techniques that can face this challenge is screen-printing.

4.3 Screen-printing

Screen-printing is a lower resolution thick film technology that can be applied to plastic substrates as well as glass or silicon. This technique has been used mainly in the microelectronics industry for fabrication of printed circuit boards in two dimensions.

A summary of a typical Screen-printing fabrication procedure is shown in Figure 9; A squeegee pas over a mask where the ink is deposited in its paste form, the ink paste is printed in the substrate under the mask replicating the shape present in the mask.

In order for screen-printing to be used as a Microsystems fabrication technique all that is needed is to realize the 3-D nature of the ink deposit (see Figure 14). Seen as a layer-by-layer 3-D element fabrication method, the flexibility of the technique lies in that almost any substrate can be used, in the possibility of printing different

UNIVERSITAT ROVIRA I VIRGILI
NUMERICAL AND EXPERIMENTAL STUDY OF FLOW AND WALL MASS TRANSFER RATES IN CAPILLARY DRIVEN FLOWS IN MICROFLUIDIC CHANNELS
Salvatore Cito
ISBN:978-84-693-0720-5/DL: T-425-2010

commercially available inks that can be functionalized by adding different catalysts or enzymes, and in the possibility of printing different layers with various inks allowing an unlimited variety of designs and for the incorporation of active elements. These advantages as well as the low cost and fast prototyping cycle make the technique ideal as a manufacturing approach for microfluidic elements.

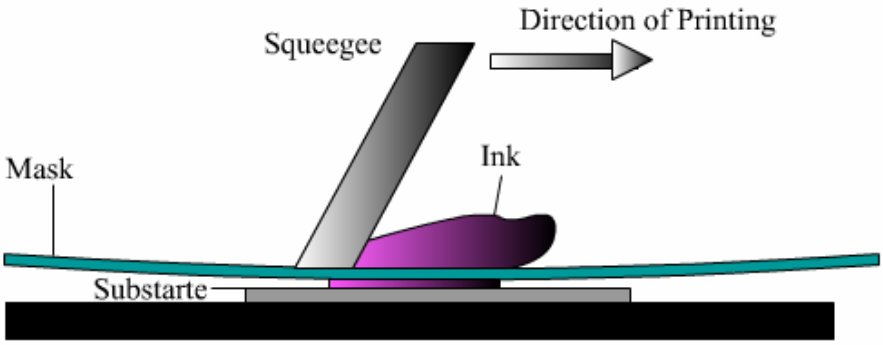

Figure 14: Schematic of screen-printing process.

Screen-printing is used already in fields such as clinical, environmental or industrial analysis [12], and in fuel [13] and solar cells [14]. In these applications screen printed inks are limited to be used as the reactive element and little has been reported, although it has been claimed in some patents [46-49], about using screen-printing as a 3-D element reproduction. The use of screen-printing technique in the biosensors manufacturing area has produced microfluidic devices based on the production of micro-channels combined with electrodes [15]. These devices show a similar architectural concept to the one presented in this work but with a difference: the reported microfluidic device is composed of well-differentiated structural (fluidics) and functional parts (electrodes).

UNIVERSITAT ROVIRA I VIRGILI
NUMERICAL AND EXPERIMENTAL STUDY OF FLOW AND WALL MASS TRANSFER RATES IN CAPILLARY DRIVEN FLOWS IN MICROFLUIDIC CHANNELS
Salvatore Cito
ISBN:978-84-693-0720-5/DL: T-425-2010

UNIVERSITAT ROVIRA I VIRGILI
NUMERICAL AND EXPERIMENTAL STUDY OF FLOW AND WALL MASS TRANSFER RATES IN CAPILLARY DRIVEN FLOWS IN MICROFLUIDIC CHANNELS
Salvatore Cito
ISBN:978-84-693-0720-5/DL: T-425-2010

Chapter 5

Results and discussions

5.1 Introduction

In this chapter we will show the main results of this thesis. For the sake of clarity, we divided it in three different sections. The first section contains the CFD model developed and the analysis of the results obtained for wall mass transfer rates in capillary driven flow. The second section contains a detailed description of the PDMS micro-channel micro-fabrication, and the results obtained using SDDOCT to visualize capillary driven flow of water in PDMS micro-channel and of bovine blood in Glass micro-channel, and a comparison between the numerical solution and the experimental results is proposed. Finally, in the third section we described the screen-printing micro-fabrication approach employed to obtain micro-channels with electro-active walls. The screen printed micro-channels have been used to produce an electrochemical reaction. The pH gradient of the electrochemical reaction has been visualized using confocal microscopy.

UNIVERSITAT ROVIRA I VIRGILI
NUMERICAL AND EXPERIMENTAL STUDY OF FLOW AND WALL MASS TRANSFER RATES IN CAPILLARY DRIVEN FLOWS IN MICROFLUIDIC CHANNELS
Salvatore Cito
ISBN:978-84-693-0720-5/DL: T-425-2010

5.2 Numerical simulation of wall mass transfer rates in capillary driven flow

5.2.1 Physical model

We consider micro-channels of circular and high aspect ratio rectangular cross section with reactive hydrophilic walls (see Figure 2). The diameter d of the circular micro-channel and the height h of the rectangular micro-channel are of the order of $200\ \mu m$. The width W of the rectangular micro-channel is assumed to be much larger than h. The inlet and the outlet of the micro-channels, with a length L larger than $1\ cm$, are open. The flow is assumed to be generated by surface tension forces and as the liquid advances, it wets a region of the walls with length l(t) of the micro-channel on which a heterogeneous reaction occurs (see Figure 15). The effect of gravity is considered to be negligible and the circular shape of the meniscus is assumed to be constant with time [27, 28]. The prediction of the variation of the contact angle as function of time and velocity of the meniscus is complex and it requires the resolution of the triple point problem. Most of the analytical and numerical simulations reported in the literature assume that the contact angle θ is constant as the meniscus moves, and its value depends on the hydrophobicity of the wall of the micro-channel and on the physical properties of the liquid. In this study we considered a range of contact angles between 10^o and 70^o, bearing in mind that if the contact angle is larger than 90^o, the walls are hydrophobic.

For Reynolds number smaller than one [27], the CD-Flow field can be divided into three different zones (see Figure 15), the entry zone, the Poiseuille zone and the surface traction zone. The entry zone is the first to form near the inlet; it extends from the inlet to a streamwise distance of $L_1=0.35h$. This first region is characterized by very high and time dependent velocities and accelerations of the meniscus. The second region, the Poiseuille zone, begins after the entry regime zone and it ends at the beginning of

UNIVERSITAT ROVIRA I VIRGILI
NUMERICAL AND EXPERIMENTAL STUDY OF FLOW AND WALL MASS TRANSFER RATES IN CAPILLARY DRIVEN FLOWS IN MICROFLUIDIC CHANNELS
Salvatore Cito
ISBN:978-84-693-0720-5/DL: T-425-2010

Surface Traction Regime zone. The Surface Traction Regime zone begins just after the Poiseuille zone and it ends at a distance $L_3=0.35h$ (that corresponds to the meniscus position). The flow in the Poiseuille zone has the classical fully developed parabolic profile [27] with the mean velocity equal to the meniscus velocity.

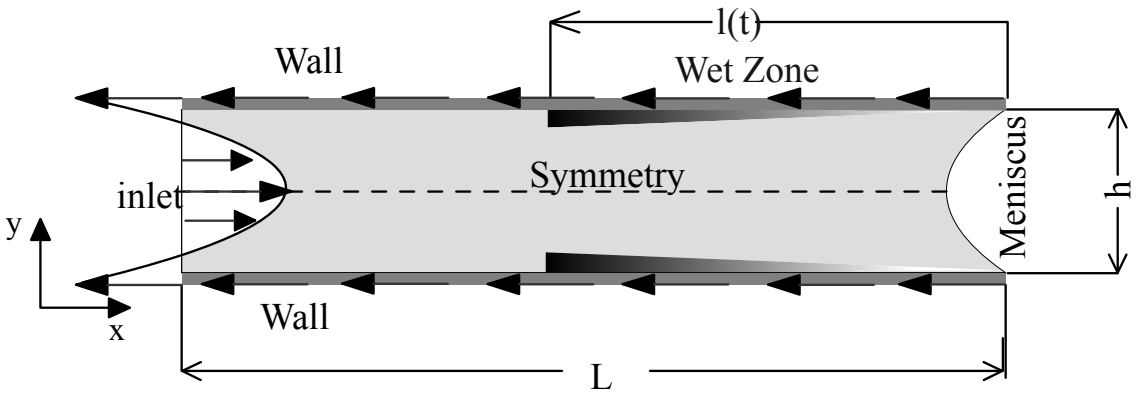

Figure 15: Schematic representation of the boundary condition of a 2d micro-channel in steady condition.

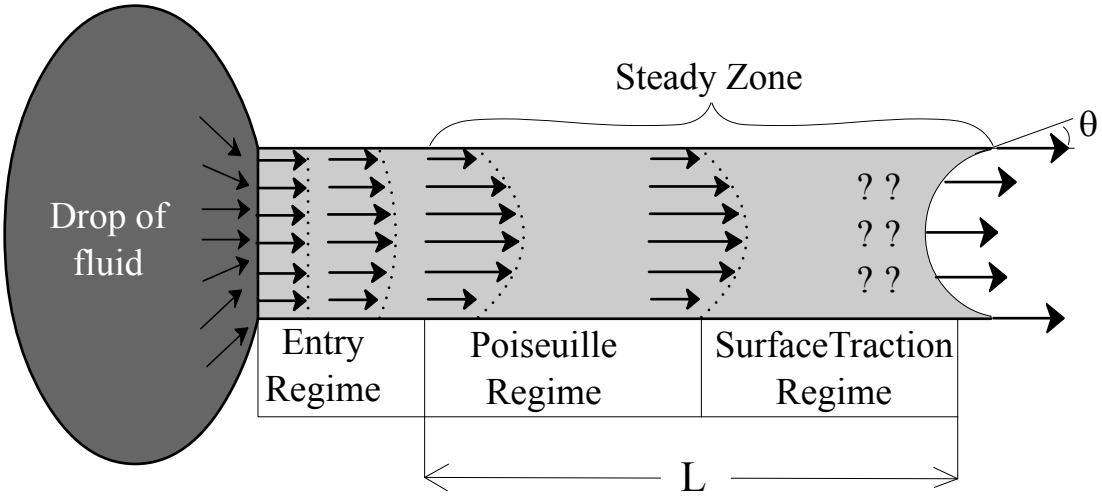

Figure 16: Schematic representation of the three main velocity flow field of a capillary driven flow in a hydrophilic channel with rectangular or circular cross section.

UNIVERSITAT ROVIRA I VIRGILI
NUMERICAL AND EXPERIMENTAL STUDY OF FLOW AND WALL MASS TRANSFER RATES IN CAPILLARY DRIVEN FLOWS IN MICROFLUIDIC CHANNELS
Salvatore Cito
ISBN:978-84-693-0720-5/DL: T-425-2010

Although the triple point is part of the wall, the fluid velocity at this point is not equal to zero [25] as supposed by the no slip condition. The computational domain considered in this study includes the Poiseuille zone and the Surface Traction Regime zone, while the Entry zone is not considered (see Figure 16).

The velocity of the meniscus has been calculated assuming that the capillary driving pressure is:

$$\Delta P = -\frac{4\sigma\cos\theta}{h} \tag{5.1}$$

Where we assumed the analogy between circular cross section of radius r and rectangular cross section with thickness h=2·r.

And that the averaged velocity of the fully developed Poiseuille flow for a plane channel is:

$$V_m = -\frac{h^2\Delta P}{12\mu L} \tag{5.2}$$

Combining Equations (5.1) and (5.2), the velocity of the meniscus, for a rectangular cross section micro-channel with large aspect ratio, can be estimated as (see for example [28]),

$$V_m = \frac{h\sigma\cos\theta}{6\mu L} \tag{5.3}$$

For a circular micro-channel, with diameter *d*, the velocity of the meniscus can be written as,

$$V_m = \frac{d\sigma\cos\theta}{6\mu L} \tag{5.4}$$

The acceleration of the meniscus for a plane micro-channel can be calculated as (see for example[28]),

UNIVERSITAT ROVIRA I VIRGILI
NUMERICAL AND EXPERIMENTAL STUDY OF FLOW AND WALL MASS TRANSFER RATES IN CAPILLARY DRIVEN FLOWS IN MICROFLUIDIC CHANNELS
Salvatore Cito
ISBN:978-84-693-0720-5/DL: T-425-2010

$$L(t) = \sqrt{t\frac{h\sigma\cos\theta}{3\mu}};$$
$$V_m = \frac{dL(t)}{dt} = \sqrt{\frac{h\sigma\cos\theta}{12\mu\cdot t}} \qquad (5.5)$$
$$a_m = \frac{d^2L(t)}{dt^2} = -\frac{L}{4t^2}$$

Using Equation (5.4), we observe that for a glass-made micro-channel with $h\approx 200\ \mu m$, and $\theta=45^o$ filled with water ($\rho\approx 10^3\ kg/m^3$, $\mu\approx 10^{-3}\ Pa\text{-}s$, and surface tension $\sigma\approx 0.072\ N/m$), the acceleration of the meniscus at a penetration distance L equal to 1 *cm* is about $-2.88\ m/s^2$. This means that for the case considered in this study and for micro-channels with $h\leq 200\mu m$ or $d\leq 200\ \mu m$, the variation of the meniscus velocity, between two different meniscus positions in the micro-channel having a distance of 3h *cm* between them and minimum 1 cm far from the inlet is less than *10%*. This variation of velocity is sufficiently small to reasonably assume a constant velocity of the meniscus and that the flow can be considered, approximately, steady with respect to a reference frame moving at that velocity. Consequently, we adopted a coordinate system moving at a constant velocity V_m along the axial direction of the channel. With respect to the moving reference frame, the meniscus axial velocity component is zero and the micro-channel's wall velocity is $-V_m$ (see Figure 15).

For the range of Reynolds numbers, ($\mathrm{Re} = \frac{V_m h}{\nu}$ or $\mathrm{Re} = \frac{V_m d}{\nu}$) considered, $1\leq Re\leq 500$ and adopting the physical properties of water, the sizes of the micro-channels are $h\leq 1000\ \mu m$ or $R\leq 1000\ \mu m$ for $L=1\ cm$. The corresponding ranges of Weber, Capillary and Bond numbers are given in Table 1. For example, if we consider a case of a glass tube with $h=100\ \mu m$ filled with water ($\rho=10^3\ kg/m^3$, $\mu=10^{-3}\ kg/m\cdot s$, $\sigma=0.072$ and N/m $\theta=70^o$) we obtain: $V_m=0.0821 m/s$, $Re=16$, $We=3.74\cdot 10^{-2}$, $Ca=1.14\cdot 10^{-3}$, $Bo=2.18\cdot 10^{-2}$. The small values of the Bond numbers support the hypothesis of a meniscus with a constant curvature adopted in the simulations. The physical properties of the Newtonian fluid and the mass diffusion coefficient are assumed to be constant. The Schmidt number has been

UNIVERSITAT ROVIRA I VIRGILI
NUMERICAL AND EXPERIMENTAL STUDY OF FLOW AND WALL MASS TRANSFER RATES IN CAPILLARY DRIVEN FLOWS IN MICROFLUIDIC CHANNELS
Salvatore Cito
ISBN:978-84-693-0720-5/DL: T-425-2010

fixed at 10^3, typical of liquids. The flow is assumed to be isothermal, laminar and steady with respect to the reference frame considered. The Marangoni effect caused by concentration gradients along the meniscus is neglected.

Re	θ	We	Ca	Bo
500	10	1.64	3.3·10-3	5.8·10-2
	70	0.57	1.1·10-3	1.6·10-1
1	10	3.3·10-3	3.3·10-3	1.2·10-4
	70	1.1·10-3	1.1·10-3	3.3·10-4

Table 1: Ranges of minimum and maximum values for Reynolds number, contact angle, Weber number, and Capillary number.

The models considered for the plane channel and for the circular micro-channel are, respectively, symmetric and axisymmetric about the x axis (see Figure 15). The flow at $x=0$, *1 cm* far from the meniscus, is assumed to be fully developed. As indicated in Figure 15, the wet zone, that is the region of the wall where the chemical reaction and the mass transfer take place, increases its length as time evolves (i.e. $l(t) = V_m \cdot t$). The concentration in this region of the wall is assumed to be constant. The inactive region of the wall for mass transfer with length $L - l(t)$ is assumed to be impermeable. Note that at $t=0$ all the extension of the wall is inactive.

5.2.2 Mathematical model

According to the previous hypotheses, the flow is governed by the continuity equation and the momentum equations and the distribution of the concentration of the reacting species is governed by the unsteady differential mass balance. This set of governing equations can be written in Cartesian coordinates of the moving reference frame as:

UNIVERSITAT ROVIRA I VIRGILI
NUMERICAL AND EXPERIMENTAL STUDY OF FLOW AND WALL MASS TRANSFER RATES IN CAPILLARY DRIVEN FLOWS IN MICROFLUIDIC CHANNELS
Salvatore Cito
ISBN:978-84-693-0720-5/DL: T-425-2010

$$\frac{\partial u_i}{\partial x_i} = 0 \tag{5.6}$$

$$u_j \frac{\partial u_i}{\partial x_j} = -\frac{1}{\rho}\frac{\partial p}{\partial x_i} + \nu \frac{\partial^2 u_i}{\partial x_j^2} \tag{5.7}$$

and

$$\frac{\partial C}{\partial t} + u_i \frac{\partial C}{\partial x_i} = D \frac{\partial^2 C}{\partial x_i^2} \tag{5.8}$$

respectively.

The model described corresponds to the physical situation in which, chemical specie dissolved in the fluid reacts at the wall of the micro-channel. The kinetic of the heterogeneous reaction is assumed to be fast enough to consider the mass transfer process at the wall as limited by diffusion. According to this assumption the concentration of the reactant is zero on the active part of the wall. The local non-dimensional mass transfer rate, or Sherwood number, is defined as:

$$Sh = \frac{hK}{2D} \tag{5.9}$$

The dimensional mass transfer coefficient K can be calculated from the instantaneous local wall mass transfer rate $N''|_w$ defined, for the plane channel, as:

$$N''|_w = -D\left.\frac{\partial C}{\partial y}\right|_w = K(C_o - C_w) \tag{5.10}$$

Where C_o is the initial concentration of the reactant, C_w is the value of the concentration at the wall (i.e. C_w=0 under the mass diffusion limited hypothesis).

The boundary conditions for momentum are non-slip at the walls ($y=h/2$ for the plane channel or $r=R$ for the circular micro-channel) and symmetry conditions at the symmetry plane, $y=0$ for the plane channel and at $r=0$ for the circular micro-channel. Fully developed velocity profiles have been imposed at the inlet of the channel.

$$u_x = \frac{3}{2}V_m\left(\frac{1-y^2}{(h/2)^2}\right) - V_m,\ u_y = 0 \tag{5.11}$$

UNIVERSITAT ROVIRA I VIRGILI
NUMERICAL AND EXPERIMENTAL STUDY OF FLOW AND WALL MASS TRANSFER RATES IN CAPILLARY DRIVEN FLOWS IN MICROFLUIDIC CHANNELS
Salvatore Cito
ISBN:978-84-693-0720-5/DL: T-425-2010

for the plane channel. And

$$u_x = 2V_m\left(\frac{1-y^2}{R^2}\right) - V_m, u_r = 0 \tag{5.12}$$

for the circular channel.

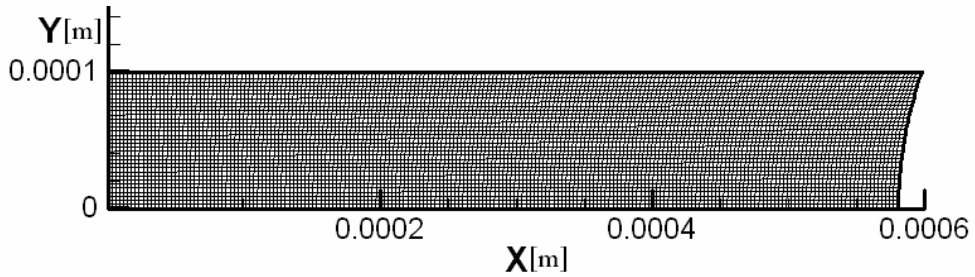

Figure 17: Mesh used to obtain a grid independent solution for the flow-field of the micro-channel with θ=70º.

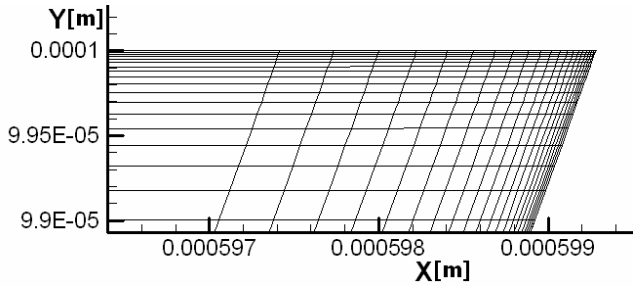

Figure 18: Mesh close to the wall for micro-channel with θ=70º used to obtain a grid independent solution. A finer mesh is located near the wall and near the meniscus.

UNIVERSITAT ROVIRA I VIRGILI
NUMERICAL AND EXPERIMENTAL STUDY OF FLOW AND WALL MASS TRANSFER RATES IN CAPILLARY DRIVEN FLOWS IN MICROFLUIDIC CHANNELS
Salvatore Cito
ISBN:978-84-693-0720-5/DL: T-425-2010

	Mesh1	Mesh2	Error%
Nodes	11934	47187	
Time step	$4 \cdot 10^{5}$ s	$2 \cdot 10^{-5}$ s	
$< Sh > \begin{cases} \theta = 70^{\circ} \\ \mathrm{Re} = 500 \\ T = 0.03 \end{cases}$	468	458	2.2%
$< Sh > \begin{cases} \theta = 70^{\circ} \\ \mathrm{Re} = 500 \\ T = 0.06 \end{cases}$	329	334	1.6%

Table 2: Mesh size and time step used to make the grid independence analysis.

The shear stress at the meniscus is considered to be zero since Marangoni effect has not been considered.

The concentration of the reactant at the reactive region of the wall with length $l(t) = V_m \cdot t$ is equal to zero. The meniscus and the inactive part of the wall are considered impermeable. At the inlet of the channel, the diffusion flux of the reacting chemical species is set zero. A uniform distribution of concentration of the reacting specie is considered as initial condition.

5.2.3 Numerical model

The set of governing equations and boundary conditions has been solved numerically with the finite volume commercial code Fluent. The time and spatial discretization chosen have second order accuracy. The steady state velocity distributions have been calculated for each Reynolds numbers and contact angle, and the solution of the flow field has been used to compute the unsteady concentration distribution using the same grid resolution. The same has been done for the micro-channels with circular cross section.

UNIVERSITAT ROVIRA I VIRGILI
NUMERICAL AND EXPERIMENTAL STUDY OF FLOW AND WALL MASS TRANSFER RATES IN CAPILLARY DRIVEN FLOWS IN MICROFLUIDIC CHANNELS
Salvatore Cito
ISBN:978-84-693-0720-5/DL: T-425-2010

The grid nodes have been stretched towards the wall of the channel (see Figure 17) to capture the development of the thin mass transfer boundary layer. Figure 18 shows the details of the grid used. The grid independence and the time step independence tests show that for the largest Reynolds number considered Re=500 and θ=70º, simulations carried out with the grids indicated in Table 2, Mesh1 ($\Delta t=4\cdot10^{-5}$ s) and Mesh2 ($\Delta t=2\cdot10^{-5}$ s) predict differences on the averaged Sherwood number over the active region of the wall of about 2.2% at $t=0.03\ h/V_m$ and 1.6% at $t=0.06\ h/V_m$. The simulations have been performed using Mesh 1.The time-dependent boundary conditions at the wall are not directly available in the code and they have been implemented using a user-defined function.

5.2.4 CFD results

The simulations were carried out for 11 different Reynolds numbers in the range $1 \leq Re \leq 500$ and for 7 different contact angles ($10^o \leq \theta \leq 70^o$). As an example we consider the cases corresponding to $Re=1$ and $Re=500$ for $\theta=10^o$ (see Figure 19). It can be seen that; there is, in the relative reference frame, a backflow behind the meniscus. The effect of such recirculation in the dissolution of the product in the bulk, at different times T can be seen in Figure 20 a, b, and c for $Re=1$ and in Figure 20 d, e, and f for $Re=500$. At $Re=1$ the thickness of the mass transport boundary layer is of the order of 10 μm, while for $Re=500$ the thickness of the mass transfer boundary layer is of the order of 1μm. In order to evaluate the mass transfer rate from the wall we have considered an averaged value of Sherwood number along the wall of the channel (see Equation. 5.13) and a non-dimensional value of time (see Equation 5.14):

$$< Sh >= \frac{1}{l(t)} \int_{L-l(t)}^{l(t)} Sh\, dx \tag{5.13}$$

$$T = \frac{t \cdot Vmen}{L} \tag{5.14}$$

Where L is the longitude of the channel.

UNIVERSITAT ROVIRA I VIRGILI
NUMERICAL AND EXPERIMENTAL STUDY OF FLOW AND WALL MASS TRANSFER RATES IN CAPILLARY DRIVEN FLOWS IN MICROFLUIDIC CHANNELS
Salvatore Cito
ISBN:978-84-693-0720-5/DL: T-425-2010

When the meniscus reach a distance from the inlet equal to 1cm, its velocity is almost constant, that why in all the simulations we have considered *L=1* cm. The solution of the flow field shows that behind the meniscus two symmetrical recirculations are generated. The presence of these recirculations is due to the fact that the relative velocity of the fluid in the main flow is higher than the velocity of the meniscus, so a recirculation is forced behind the meniscus as shown in Figure 19. Such simulation has been performed for a plane channel and for circular channel. In both cases we found the same kind of flow field.

Once computed the flow field for the 77 cases corresponding to the combination of the Reynolds number and contact angles considered, we solved the mass transfer equation for each case considering a Schmidt number equal to 10^3. For each simulation we computed the value of Sherwood number and we obtained for each case a similar behaviour.

The local Sherwood number used to evaluate the wall mass transfer in the capillary driven can be evaluated considering the following equation:

$$Sh = \frac{K \cdot h}{2D}$$
$$N\Big|_w^{"} = -D\frac{\partial C_A}{\partial n}\bigg|_w = K\left(C_{A_0} - C_{A_W}\right) \qquad 5.15$$

The local Sherwood Vs longitude is shown in Figure 21 for $\theta=10^o$ and *Re=1*. It can be seen that the peak of mass transfer is behind the meniscus, where the recirculation occurs.

UNIVERSITAT ROVIRA I VIRGILI
NUMERICAL AND EXPERIMENTAL STUDY OF FLOW AND WALL MASS TRANSFER RATES IN CAPILLARY DRIVEN FLOWS IN MICROFLUIDIC CHANNELS
Salvatore Cito
ISBN:978-84-693-0720-5/DL: T-425-2010

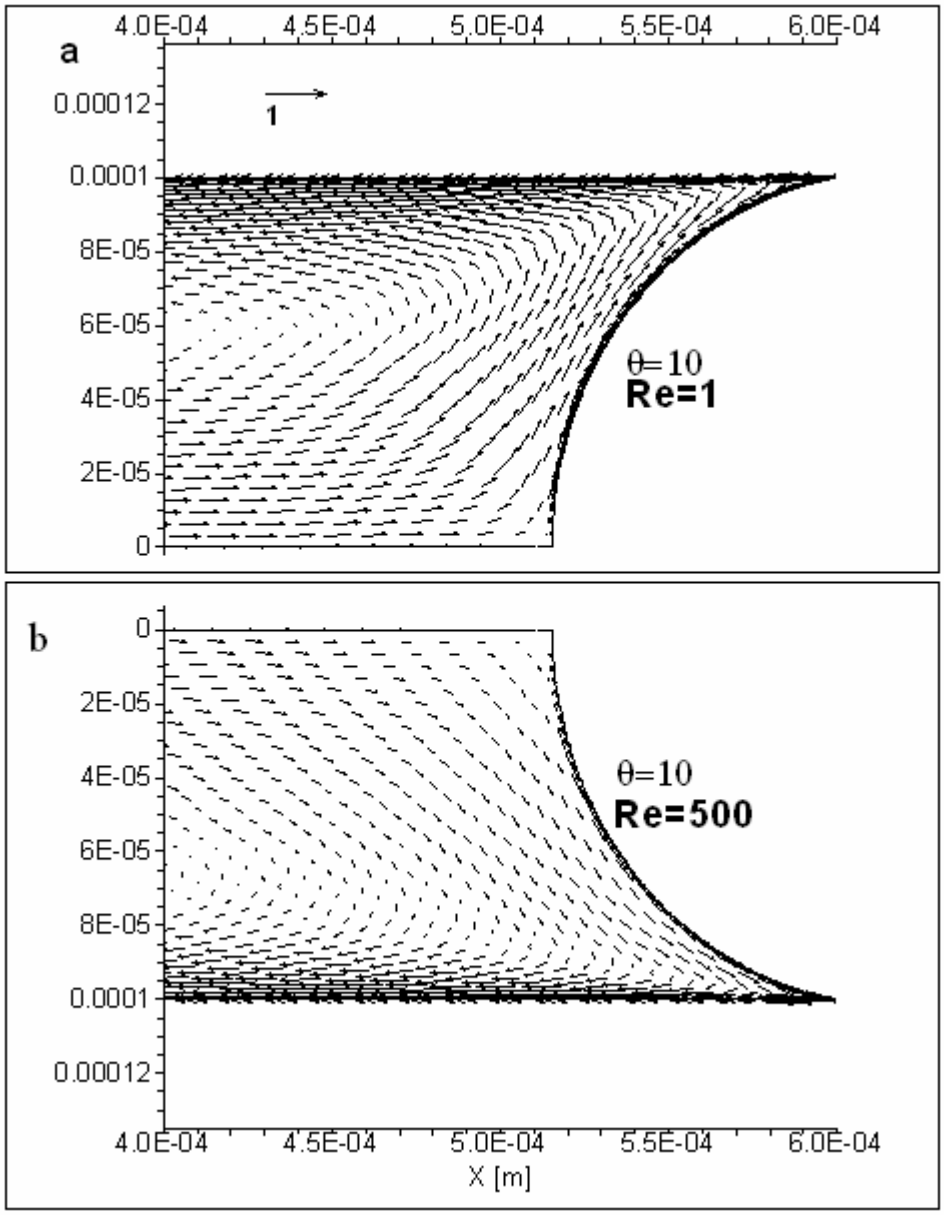

Figure 19: Schematic velocity field for a CD-Flow having contact angle θ=10º a) Vector velocity field for Re=1, b) vector velocity field for Re=500.

UNIVERSITAT ROVIRA I VIRGILI
NUMERICAL AND EXPERIMENTAL STUDY OF FLOW AND WALL MASS TRANSFER RATES IN CAPILLARY DRIVEN FLOWS IN MICROFLUIDIC CHANNELS
Salvatore Cito
ISBN:978-84-693-0720-5/DL: T-425-2010

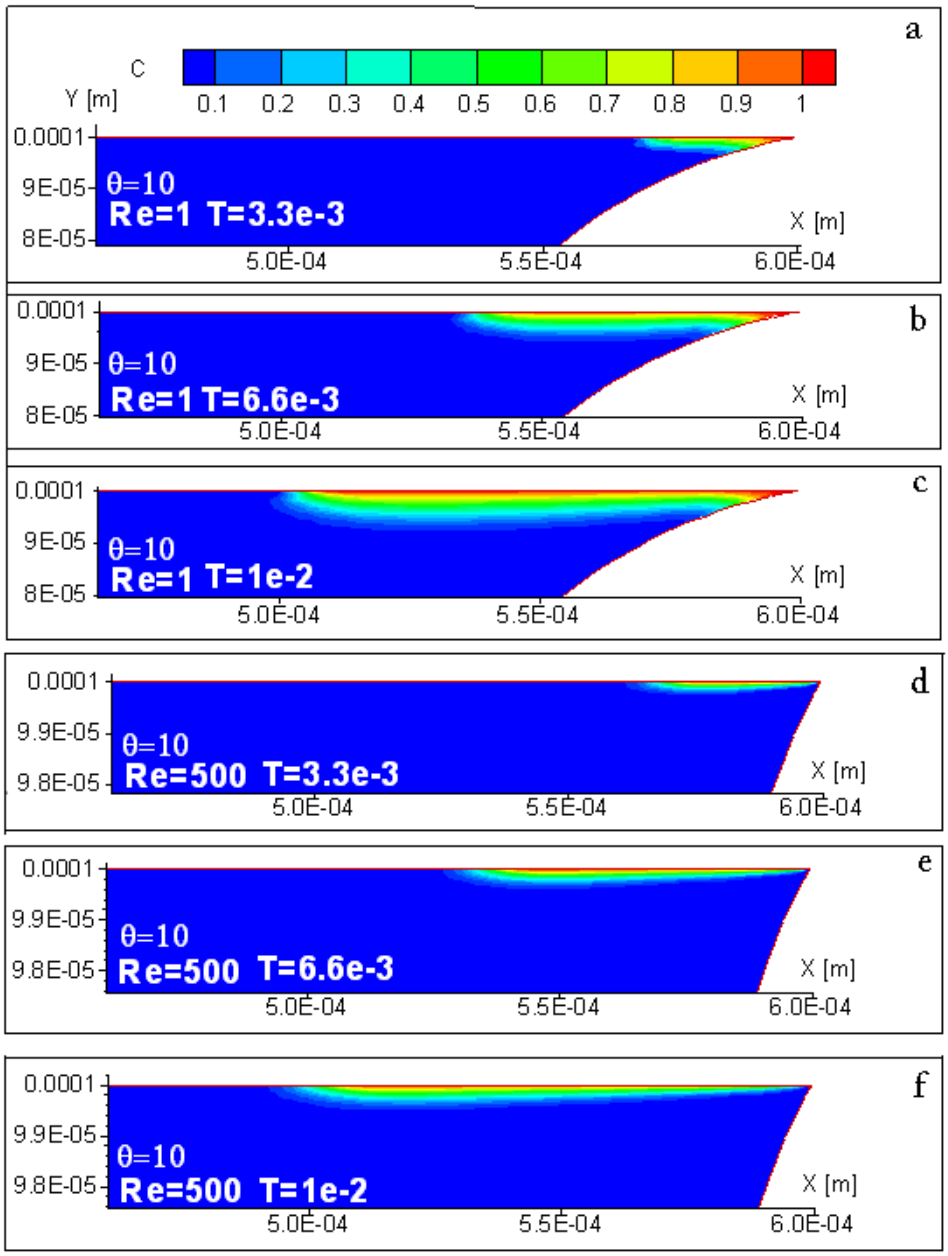

Figure 20: Schematic concentration field for a CD-Flow having contact angle θ=10º. a) Contour of concentration field at time $T=3.3\cdot10^{-3}$ for Re=1 b) Contour of concentration field at time $T=6.6\cdot10^{-3}$ for Re=1, c) Contour of concentration field at time $T=1\cdot10^{-2}$ for Re=1, d) Contour of concentration field at time $T=3.3\cdot10^{-3}$ for Re=500 e) Contour of concentration field at time $T=6.6\cdot10^{-3}$ for Re=500 f) Contour of concentration field at time $T=1\cdot10^{-2}$ for Re=500.

UNIVERSITAT ROVIRA I VIRGILI
NUMERICAL AND EXPERIMENTAL STUDY OF FLOW AND WALL MASS TRANSFER RATES IN CAPILLARY DRIVEN FLOWS IN MICROFLUIDIC CHANNELS
Salvatore Cito
ISBN:978-84-693-0720-5/DL: T-425-2010

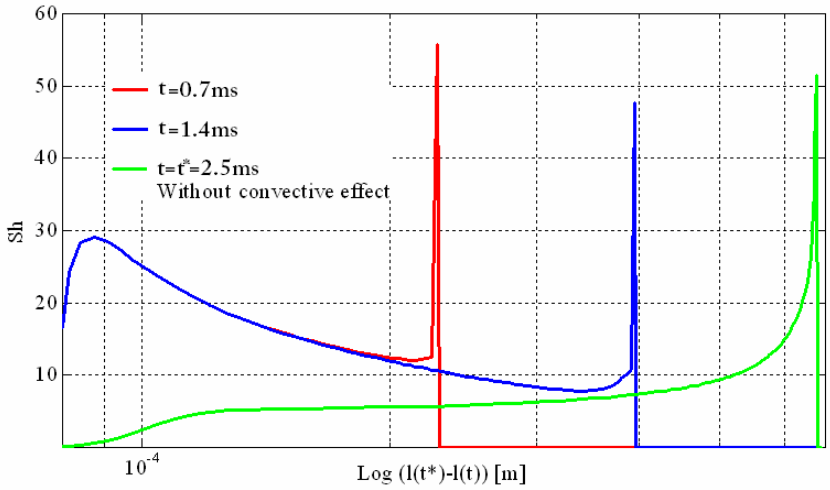

Figure 21: Local Sherwood number at different time (t=0.7ms t=1.4ms t=t* 2.5ms, where t^* is the time it takes the meniscus to reach the position l=3·h starting from the end of the entry zone) in a capillary micro-channel with rectangular cross section (h=200), with and without convective effect in wall mass transfer, contact angle θ =10º V_m=0.23m/s and Reynolds number Re=1.

In Figure 20 can be see as well, that there is a clear effect of the flow field on the mass transfer of the product in the mass transfer boundary layer. To understand the effect of the meniscus in the mass transfer we calculated a case for which we have considered the flow field velocity equal to zero (no convective effect considered). Comparing the two curves we can notice that there is a big effect of convective forces close to the meniscus (i.e. small values of $Log(l(t^* - l(t)))$. Indeed for a case of Re =1 and contact angle θ=10º the Sherwood has relatively high value close to the meniscus compared with the case without convective effect, (see Figure 21).

To compare the effect of Reynolds number and/or contact angle on the wall mass transfer rate, Figure 22 shows the averaged Sherwood number (see Equation 5.13) <Sh> vs the longitude of the micro-channel for different values of Reynolds number. We can observe that the average Sherwood number decreases with the square root of Reynolds number for a fixed contact angle. This is typical of laminar boundary layers.

UNIVERSITAT ROVIRA I VIRGILI
NUMERICAL AND EXPERIMENTAL STUDY OF FLOW AND WALL MASS TRANSFER RATES IN CAPILLARY DRIVEN FLOWS IN MICROFLUIDIC CHANNELS
Salvatore Cito
ISBN:978-84-693-0720-5/DL: T-425-2010

Figure 22-25 shows the effect of the contact angle, on <Sh>, such effect is very small and become important only for high value of Reynolds number.

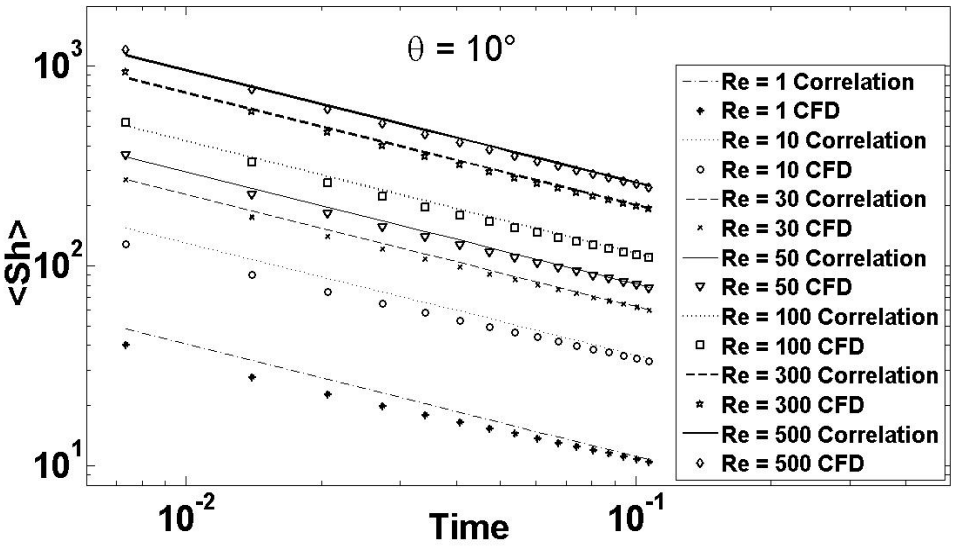

Figure 22: Sherwood number vs. T for θ equal to 10° and Re between 1 and 500 for a micro-channel with rectangular section.

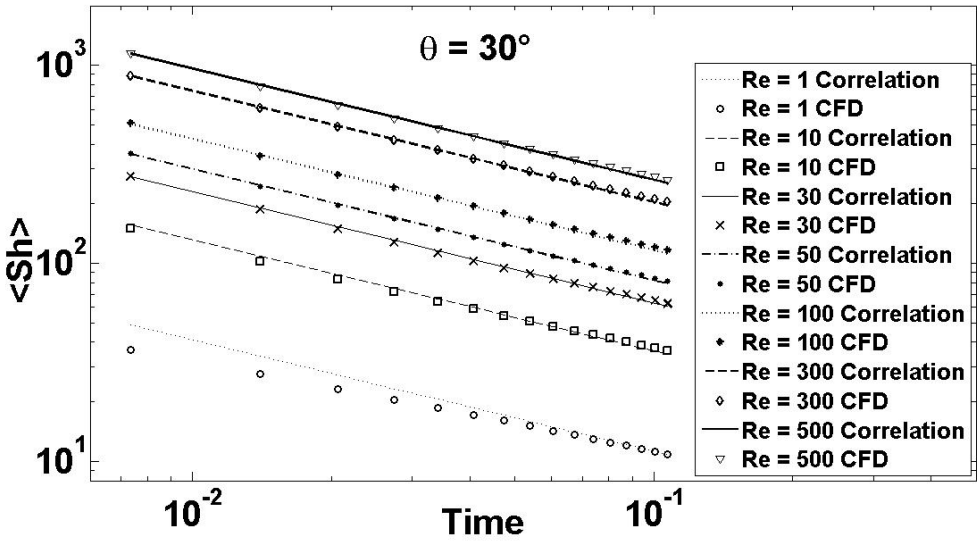

Figure 23: Sherwood number vs. T for θ equal to 30° and Re between 1 and 500 for a micro-channel with rectangular section.

UNIVERSITAT ROVIRA I VIRGILI
NUMERICAL AND EXPERIMENTAL STUDY OF FLOW AND WALL MASS TRANSFER RATES IN CAPILLARY DRIVEN FLOWS IN MICROFLUIDIC CHANNELS
Salvatore Cito
ISBN:978-84-693-0720-5/DL: T-425-2010

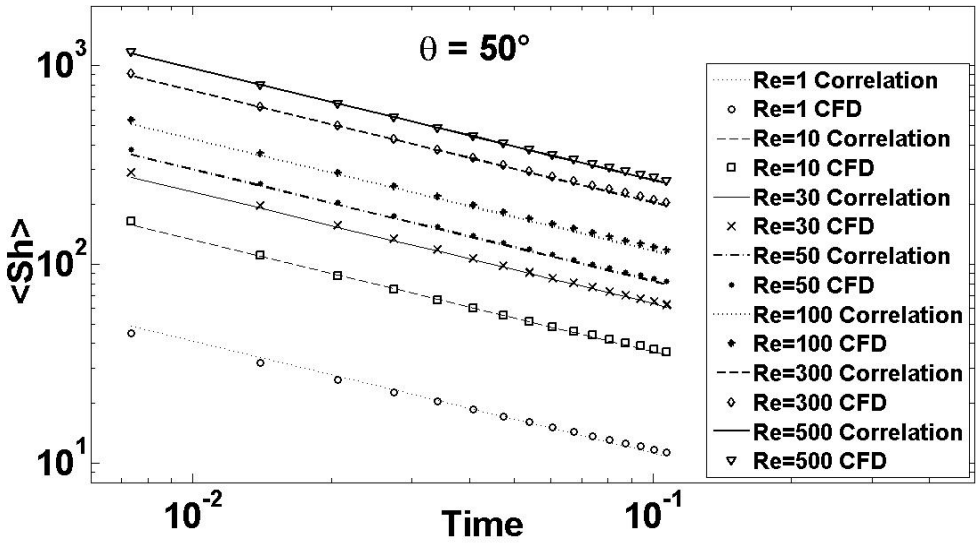

Figure 24: Sherwood number vs. T for θ equal to 50° and Re between 1 and 500 for a micro-channel with rectangular section.

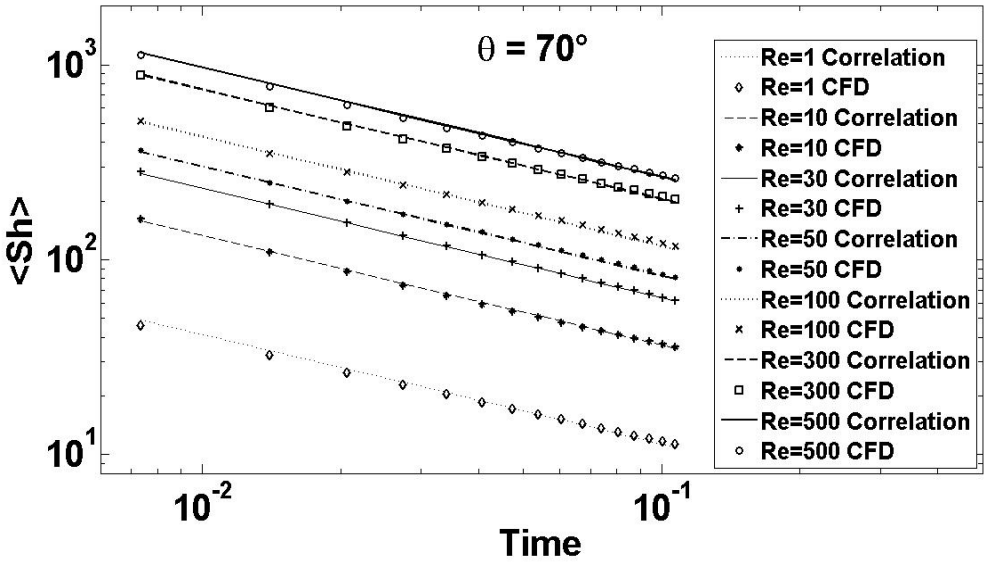

Figure 25: Sherwood number vs. T for θ equal to 70° and Re between 1 and 500 for a micro-channel with rectangular section.

UNIVERSITAT ROVIRA I VIRGILI
NUMERICAL AND EXPERIMENTAL STUDY OF FLOW AND WALL MASS TRANSFER RATES IN CAPILLARY DRIVEN FLOWS IN MICROFLUIDIC CHANNELS
Salvatore Cito
ISBN:978-84-693-0720-5/DL: T-425-2010

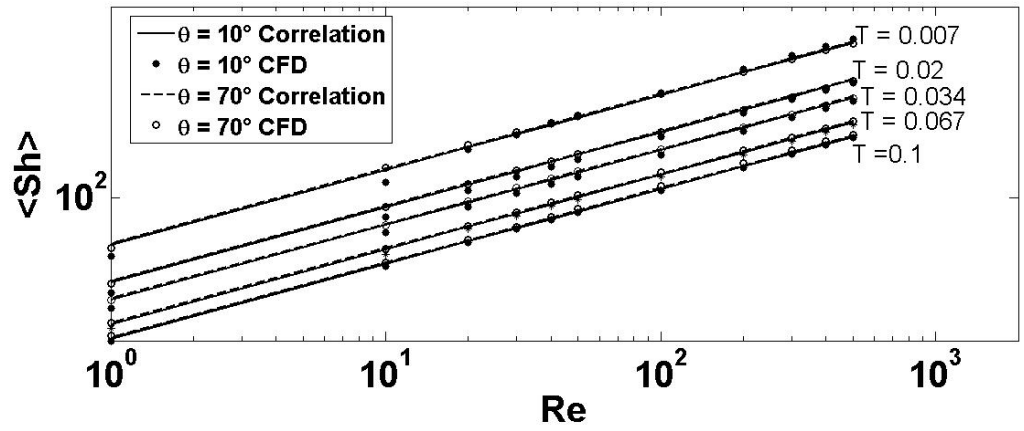

Figure 26: Sherwood number vs. Reynolds number for a micro-channel with rectangular, at different values of T between $7 \cdot 10^3$ and 0.1.

The values of <*Sh*> calculated can be resumed correlating them to a power function of *Re,* θ and *T*. This has been done using non linear least-squares regression models of Gauss-Newton algorithm with Levenberg-Marquardt) modifications (implemented in MATLAB) for global convergence function of Reynolds number Time and contact angle. The resolution of such problem gave us the coefficient $A, \alpha \beta$ and γ (See Equation 5.16).

$$< \overline{Sh} >= A T^{a} \, \mathrm{Re}^{\beta} \, \theta^{\gamma} \begin{cases} A = 3.15 \\ \alpha = -0.55 \\ \beta = 0.5 \\ \gamma = 0.0088 \end{cases} \tag{5.16}$$

The correlation predicts the averaged Sherwood number <*Sh*> with a mean absolute error *MAE%=2.2%* See Equation 5.17).

$$MAE = \frac{1}{n} \sum_{i=1}^{n} \left| \frac{< \overline{Sh} > - < Sh >}{< Sh >} \right| \tag{5.17}$$

Considering the correlation given in Equation 5.16 we can introduce a non dimensional capillary driven flow wall mass transfer rate coefficient *Wc* given as:

UNIVERSITAT ROVIRA I VIRGILI
NUMERICAL AND EXPERIMENTAL STUDY OF FLOW AND WALL MASS TRANSFER RATES IN CAPILLARY DRIVEN FLOWS IN MICROFLUIDIC CHANNELS
Salvatore Cito
ISBN:978-84-693-0720-5/DL: T-425-2010

$$W_c = \frac{< Sh >}{\sqrt{\mathrm{Re}}} \tag{5.18}$$

And substituting Equation 5.16 in Equation 5.18 we obtain:

$$W_c = 3.15 \frac{\theta^{0.0088}}{T^{0.55}} \tag{5.19}$$

The coefficient Wc can be used as a design parameter to predict and understand the wall mass transfer rate in a micro-biosensor that has fast heterogeneous reactions in the wall of its hydrophilic micro-channels and that need to have a response time in the order of 10 ms. An example of the use of the parameter Wc can be seen in Figure 27 in which Wc vs. Time for Re=1 and different values of contact angles θ is shown. Observing Figure 27, we can see that the coefficient Wc is in practice contact angle independent, and that such parameter can predict the variation of wall mass transfer rate with time.

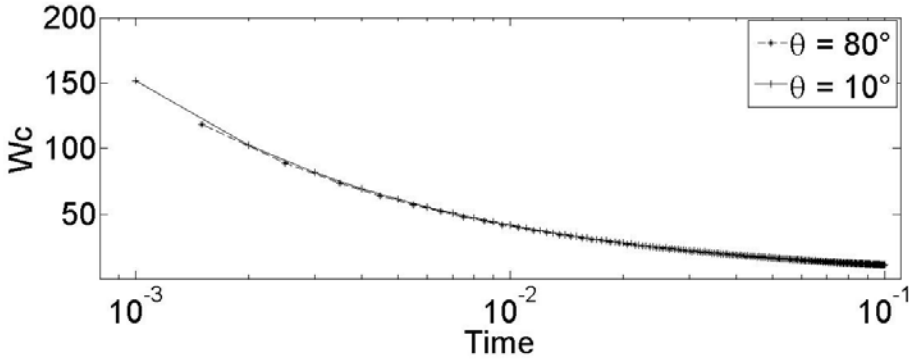

Figure 27 WC vs. Time for Re=1 and different values of contact anglesθ.

Considering that in viscous laminar boundary layer <Sh> depends with the power of 0.5 of Re and so it is the value of β obtained in Equation 5.16. Then, we can conclude that the laminar behaviour of the cases considered still maintains the phenomena mostly diffusive.

After comparing, the mass transfer rate for a two dimensional case with certain contact angle and Reynolds number, with a cylindrical case that has the same values of Reynolds and contact angle, we can see that we obtain practically the same result, as

UNIVERSITAT ROVIRA I VIRGILI
NUMERICAL AND EXPERIMENTAL STUDY OF FLOW AND WALL MASS TRANSFER RATES IN CAPILLARY DRIVEN FLOWS IN MICROFLUIDIC CHANNELS
Salvatore Cito
ISBN:978-84-693-0720-5/DL: T-425-2010

example we plot, in Figure 28, Sherwood vs. Time for θ=50º and Re=500 for micro-channels with rectangular cross section and circular cross section.

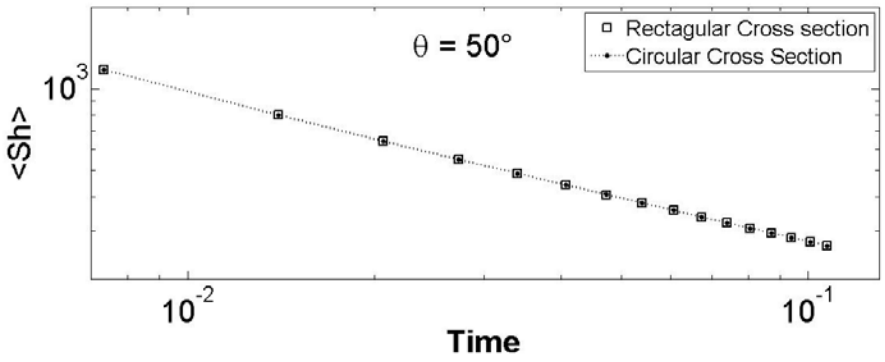

Figure 28: Sherwood vs. Time for θ=50º and Re=500 for micro-channels with rectangular cross section and circular cross section.

UNIVERSITAT ROVIRA I VIRGILI
NUMERICAL AND EXPERIMENTAL STUDY OF FLOW AND WALL MASS TRANSFER RATES IN CAPILLARY DRIVEN FLOWS IN MICROFLUIDIC CHANNELS
Salvatore Cito
ISBN:978-84-693-0720-5/DL: T-425-2010

5.3 Experimental visualization and analysis of capillary driven flow

5.3.1 Spectral-domain Doppler optical coherence tomography (SDDOCT) experimental set up

The schematic of SDDOCT is shown in Figure 29 .

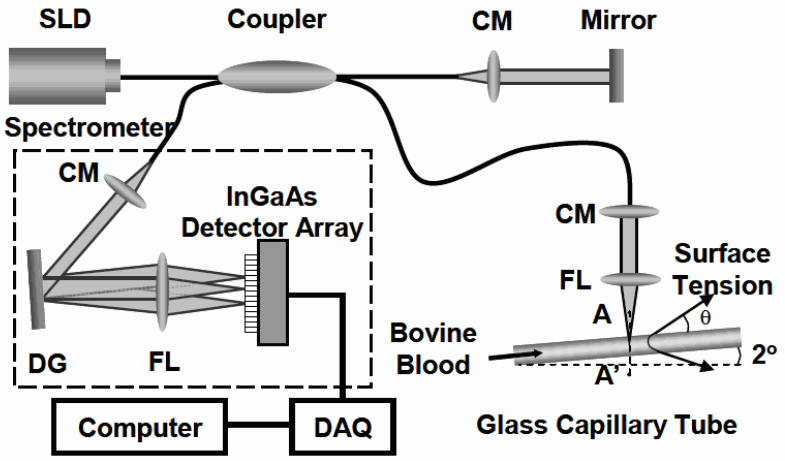

Figure 29: Schematic diagram for spectral-domain Doppler optical coherence tomography. SLD: Super luminescent Diode; CM collimator; DG: diffraction grating; FL: focusing lens.

Low-coherence light having a 1310 nm centre wavelength with a full width at half maximum of 95 nm was coupled into the source arm of a fiber-based Michelson interferometer. Backscattered lights from the reference and sample arms were guided into a spectrometer. Interference fringes were sampled by the spectrometer with a 1×1024 InGaAs detector array at 7.7 kHz. The wavelength range on the array was 130 nm, corresponding to a spectral resolution of 0.13 nm and an imaging depth (from *A* to *A*') of 3.4 mm in air. The probe beam with a 15 μm spot at the focal point was fixed at the centre of the micro-channel. The micro-channel was tilted by 2° from the horizontal

UNIVERSITAT ROVIRA I VIRGILI
NUMERICAL AND EXPERIMENTAL STUDY OF FLOW AND WALL MASS TRANSFER RATES IN CAPILLARY DRIVEN FLOWS IN MICROFLUIDIC CHANNELS
Salvatore Cito
ISBN:978-84-693-0720-5/DL: T-425-2010

position using an accurate goniometric to avoid possible detector saturation by a strong backscattering from the micro-channel surface. This angle sets Doppler angle between the backscattered light and the velocity of blood cells. We used PDMS and glass micro-channels. The PDMS micro-channel has been obtained from an SU-8 master mold that has rectangular cross sections with height of 100 μm and width of 500 μm. The Commercial glass micro-channels have different sizes: three circular micro-channels with inner diameters of 300 μm, 400 μm, and 500 μm. [43]

5.3.2 SU-8 master mold fabrication

The master mold for the PDMS micro-channel has been done using The Integrated Nanosystems Research Facility (INRF) of the University of California Irvine. The SU-8 used is the SU-8 3050 provided by MICRO-CHEM.

SU-3050 has been chosen for this work because it is ideally suited for its high resolution near vertical side wall and its high viscosity allows film thicknesses up to 100 μm in a single coat.

Due to the liquid state of SU-8 it has to be poured in a uniform layer over a substrate, spin coated in spinner, soft baked in a hot plate, exposed to a source of UV light, post baked after exposure in a hot plate, and finally developed using an SU-8 Developer such as ethyl lactate and diacetone alcohol.

Before pouring SU-8 3050 in the silicon wafer, the substrates have been cleaned with a piranha wet etch (using H_2SO_4 + H_2O_2) followed by de-ionized water rinse and finally dried in a hot plate.

UNIVERSITAT ROVIRA I VIRGILI
NUMERICAL AND EXPERIMENTAL STUDY OF FLOW AND WALL MASS TRANSFER RATES IN CAPILLARY DRIVEN FLOWS IN MICROFLUIDIC CHANNELS
Salvatore Cito
ISBN:978-84-693-0720-5/DL: T-425-2010

Figure 30: Laurell photoresist spinner. Courtesy of INFR centre of University of California Irvine.

To obtain a uniform channel height the Laurell photoresist spinner has been used to spin the silicon wafer in which, 1ml of resist for each 25mm of substrate diameter, was poured (see Figure 30.

Optimization of the spinning velocity was done to obtain a layer thickness of 100 μm. A set of 33 trials has been done changing the velocity of spinning between 800 and 4000 rpm and an optimum velocity of 900 rpm have been used to obtain an SU-8 layer of 100 μm. The spin program has been accelerated according to the following step acceleration: (1) Spin at 500 rpm for 5-10 sec with acceleration of 100 rpm/second, (2) Spin up to 4000 rpm for 30 sec with acceleration of 300 rpm/second.

After spinning the substrate with SU-8 layer has been backed in a levelled hot plate at 95ºC for 50 sec.

Once the solvent of the SU-8 has been relied with the soft bake step, the UV source aligner Karl Suss Model MJB3 Contact Aligner (vacuum) (see Figure 31) located in the INFR's clean room has been used to transfer the pattern of the photo-mask to the dried SU-8. In this step the SU-8 has been exposed for 15 sec to the ultraviolet photolithography (λ = 365 nm) with an exposure energy of 250 mJ/cm^2.

UNIVERSITAT ROVIRA I VIRGILI
NUMERICAL AND EXPERIMENTAL STUDY OF FLOW AND WALL MASS TRANSFER RATES IN CAPILLARY DRIVEN FLOWS IN MICROFLUIDIC CHANNELS
Salvatore Cito
ISBN:978-84-693-0720-5/DL: T-425-2010

Figure 31: Karl Suss Model MJB3 Contact Aligner (vacuum). Courtesy of INFR centre of University of California Irvine.

After the cross linking of the SU-8 with the UV light it has been baked again for 1 minute at 65 °C (to avoid stress in the structure) and for 5 minute at 95 °C to polymerize the exposed material. Finally, the master mold of the micro-channel has been developed in propylene-glycol-methyl-ether-acetate (PGMEA) to remove the unexposed SU-8. The finished SU-8 structures have been finally released from the handling substrate by wet etching of the sacrificial metal layer. To clean the surface has been spray-washed with isopropyl alcohol for 10 second and dried with filtered, pressurized nitrogen.

Figure 32: Nanospec thin film monitor Courtesy of INFR centre of University of California Irvine.

Before obtaining an optimal procedure to fabricate a 100 μm micro-channel several temperature and times for each steps has been considered in a trial and error procedure. The key step of the procedure has been the optimization of the spin speed. The thickness of 33 SU-8 layer trials on the silicon wafer obtained from different values of spin speed has been measured using the Nanospec Thin Film monitor (See Figure 32) and the Film thickness vs. the spin speed is reported in Figure 33.

UNIVERSITAT ROVIRA I VIRGILI
NUMERICAL AND EXPERIMENTAL STUDY OF FLOW AND WALL MASS TRANSFER RATES IN CAPILLARY DRIVEN FLOWS IN MICROFLUIDIC CHANNELS
Salvatore Cito
ISBN:978-84-693-0720-5/DL: T-425-2010

The photo-mask used to transfer the pattern of the micro-channel has been done using the drawing program Illustrator (Adobe System Inc.) to draw the micro-channel and it has been saved as a Post Script file successively printed using a 4000-dpi resolution printer on a transparency (see Figure 34).

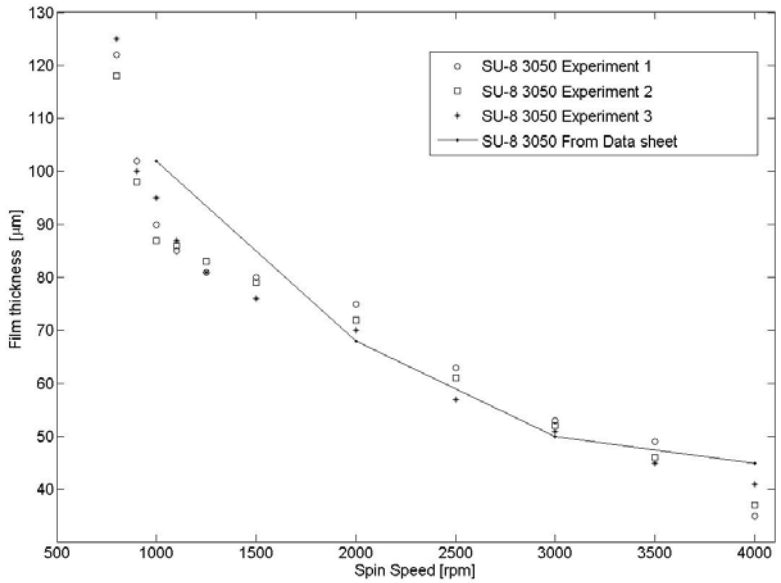

Figure 33: Spin speed vs Thickness for SU-8 3050 resist.

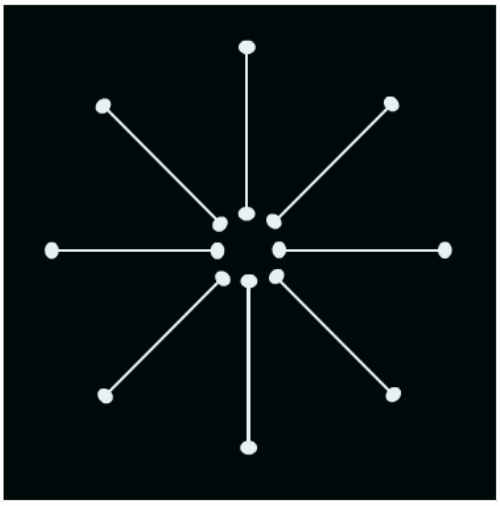

Figure 34: Photo mask used to fabricate the SU-8 master mold.

UNIVERSITAT ROVIRA I VIRGILI
NUMERICAL AND EXPERIMENTAL STUDY OF FLOW AND WALL MASS TRANSFER RATES IN CAPILLARY DRIVEN FLOWS IN MICROFLUIDIC CHANNELS
Salvatore Cito
ISBN:978-84-693-0720-5/DL: T-425-2010

Figure 35: Technics Plasma Etcher of INFR centre of University of California Irvine.

5.3.3 PDMS micro-channel

PDMS micro-channel has been done using Sylgard 184 base mixed with Sylgard 184 curing agent. The equipments used for PDMS microfabrication were an analytical balance, a Vacuum Chamber and Curing Oven. At first we placed the SU-8 master mold on a 150mm plastic petri dish. The silicon wafer has been secured to the bottom of petri dish using clean room vinyl tape and We placed large (250 ml weight boat) on weighing scale and measured the out Sylgard 184 curing agent (using 10% of the amount of Sylgard 184 pre-polymer base desired). After tarring the balance we added the desired amount of Sylgard 184 pre-polymer base. we wiped the plastic fork with 2-propanol acetone to clean and remove impurities and we have used it to mix well the PDMS (until a milky colour has been achieved). The milky PDMS so obtained has been poured onto the petri dish silicon wafer assembly, and the whole assembly has been placed inside vacuum chamber for the removal of air bubbles. Degassing of PDMS achieved keeping it under vacuum (between 25 and 20 inches of mercury) for at least one hour (until all the bubbles were relied). Once the PDMS has been totally degassed the all assembly has been placed in the curing oven at 65ºC for 24 hours. To remove the molded PDMS, a scalpel has been used to manually cut out the device from the master. Once cut out the PDMS micro-channel as well as glass substrates were exposed for 1 minute to oxygen plasma using the Technics Plasma Etcher available in the INRF clean room (see Figure

UNIVERSITAT ROVIRA I VIRGILI
NUMERICAL AND EXPERIMENTAL STUDY OF FLOW AND WALL MASS TRANSFER RATES IN CAPILLARY DRIVEN FLOWS IN MICROFLUIDIC CHANNELS
Salvatore Cito
ISBN:978-84-693-0720-5/DL: T-425-2010

35) to activate their surfaces. The PDMS and glass substrate were brought together to form a closed hydrophilic micro-channel.

5.3.4 Visualization of CD-Flow of water with particles in PDMS micro-channels

In this section, we report the observation of secondary flow in CD-Flow in a PDMS micro-channel using spectral-domain Doppler optical coherence tomography (SDDOCT).

Deionised water and a 2.5% aqueous suspension of polystyrene beads (0.2 mm in diameter and 1.05 g/cm^3 in density) were injected with a pipe into a PDMS micro-channel with dimension of cross-section between inlet and outlet of 100 μm x 500 μm.

Since the density of polystyrene beads is almost the same as that of water, the beads follow the mean liquid movement faithfully. The average distance between beads is sufficiently smaller than the current imaging resolution with a particle concentration of 2.5%. Hence, the resolution is not limited by the particle number density.

SDDOCT measures the vertical-component of the velocity field which is the particle velocity projected on the incident light. When the incident light is normal at the top or bottom surface of the meandering micro-channel, the detected velocity does not include the primary flow. However, high backscattering from the top and bottom surfaces give rise to saturation of the detector in the spectrometer so that the micro-channel is slightly tilted with respect to the X-axis by α =-2º from the normal illumination (see Figure 29). If the normal illumination has a relationship between two frames: x = X, y = Y, and z = Z, the new relationship due to the tilting is x = X, y = Ycosα+ Zsinα, and z = Ysinα + Zcosα. Because of the -2º tilting, the effect of the primary flow is included.

CD-Flow of deionised water and a 2.5% aqueous suspension of polystyrene beads in a PDMS micro-channel has been detected by mean of SDDOCT. The meniscus is clearly detected and two recirculations behind it are developed due to the presence of relatively strong component of velocity in the radial direction (see Figure 36).

UNIVERSITAT ROVIRA I VIRGILI
NUMERICAL AND EXPERIMENTAL STUDY OF FLOW AND WALL MASS TRANSFER RATES IN CAPILLARY DRIVEN FLOWS IN MICROFLUIDIC CHANNELS
Salvatore Cito
ISBN:978-84-693-0720-5/DL: T-425-2010

A similar behaviour between the CD-Flow predicted by CFD model and CD-Flow observed by SDDOCT has been found see Figure 36 and Figure 37.

Due to the limitations of PDMS surface wattability property we have considered to use glass made micro-channel to set up a quantitative analysis of CD-Flow.

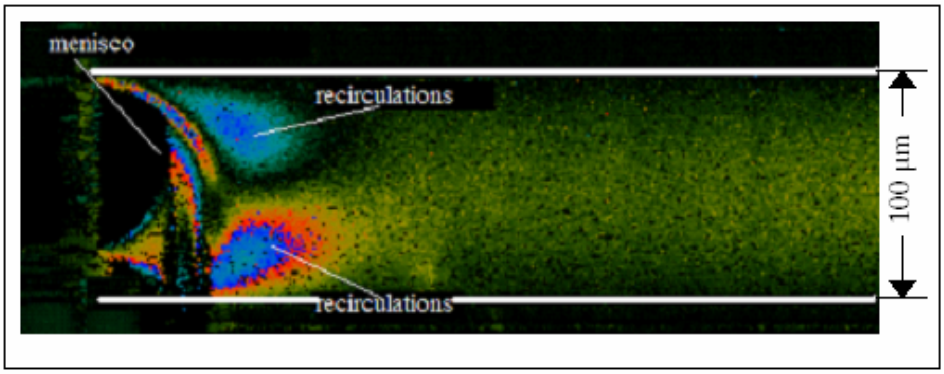

Figure 36: Secondary flow in CD-Flow of deionised water and a 2.5% aqueous suspension of polystyrene beads in a PDMS micro-channel using spectral-domain Doppler optical coherence tomography (SDDOCT).

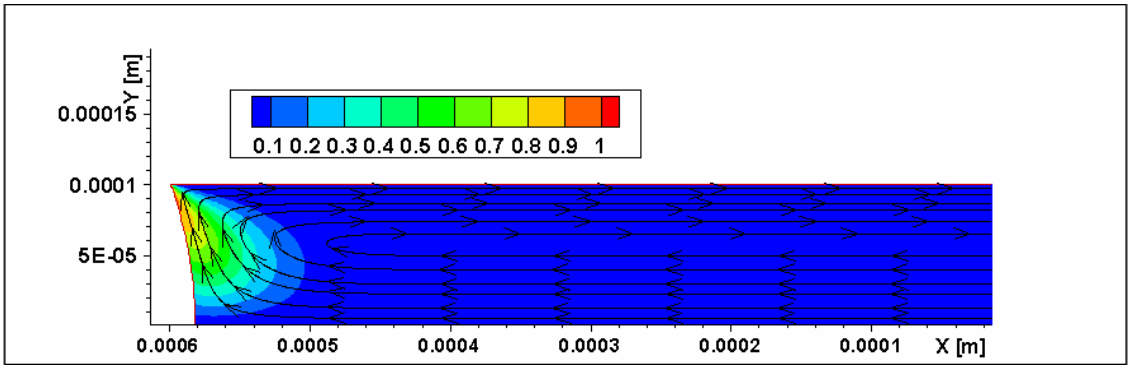

Figure 37: Contour of normalized y component of the velocity and stream line of velocity that underline the secondary flow in CD-Flow obtained by mean of CFD model using water with contact angle equal to 70º in a micro-channel with rectangular cross section and h=100 µm.

UNIVERSITAT ROVIRA I VIRGILI
NUMERICAL AND EXPERIMENTAL STUDY OF FLOW AND WALL MASS TRANSFER RATES IN CAPILLARY DRIVEN FLOWS IN MICROFLUIDIC CHANNELS
Salvatore Cito
ISBN:978-84-693-0720-5/DL: T-425-2010

Figure 38: Video frames of bovine blood CD-Flow in a glass micro-channel with circular cross section and internal diameter of 300 µm CD-Flow. (a) Frame nº 173 (b) frame nº 190 (c) frame nº 200.

5.3.5 CD-Flow of bovine blood in glass micro-channel

The Glass micro-channels with circular cross section or rectangular cross section has been pasted along a standard ruler, a drop of blood has been dropped just over the inlet and the surface tension drawn the blood inside the micro-channel and the hole dynamic of the CD-Flow of bovine blood in the micro-channel has been recorded using a commercial video camera working at 29 frames per second. Figure 38a to Figure 38c show, respectively, the frame number 173, 190, 200 and 300, of the blood CD-Flow in a glass micro-channel with circular cross section and internal diameter of 300 µm.

UNIVERSITAT ROVIRA I VIRGILI
NUMERICAL AND EXPERIMENTAL STUDY OF FLOW AND WALL MASS TRANSFER RATES IN CAPILLARY DRIVEN FLOWS IN MICROFLUIDIC CHANNELS
Salvatore Cito
ISBN:978-84-693-0720-5/DL: T-425-2010

5.3.5.1 Video analysis of CD-Flow of blood in glass micro-channels

In this section, we report the analyses of meniscus velocity of CD-Flow of bovine blood in a glass micro-channels post-processing the video recorded as a sequence of frames treated as numerical matrixes.

As we have seen in section 3.1.1, every frame can be seen as a matrix. In a CD-Flow video each frame is a matrix equal to the previous one, except from the fact that the meniscus has changed slightly its position. This means that the only pixels of the matrix that have changed are those where the meniscus has moved. Then using an algorithm able to read iteratively each frame and compare them, the position of the meniscus can be obtained.

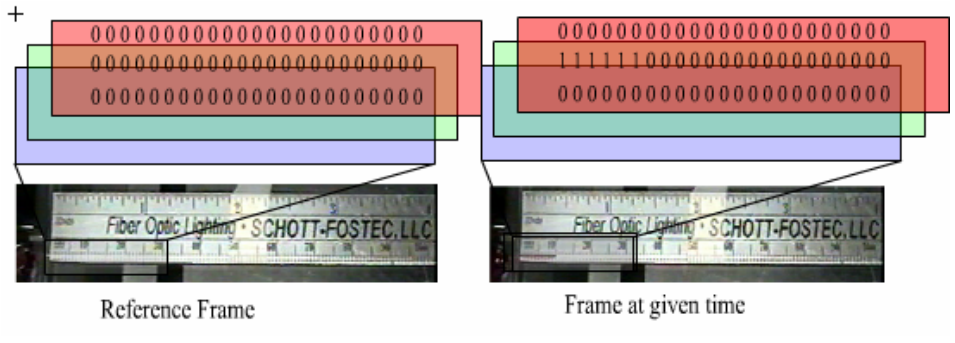

Figure 39: Schematic of RGB extrapolation of the reference frame and a frame at given time with emphasis in changing values of matrix value in the meniscus position from 0 to 1.

In this work we have taken the first frame as the reference matrix. We have subtracted from each matrix frame the reference matrix frame and since our image is a RGB picture we considered only the matrix associated with the red colour, in this way we reduced the background noise (see Figure 39). Then we defined a threshold value to establish where the blood in present and where is not and we have assigned to each frame a new matrix having values equal to 1 where the blood is present and 0 in the rest of the matrix. Now since we know the dimension of each pixel the number of frame and

UNIVERSITAT ROVIRA I VIRGILI
NUMERICAL AND EXPERIMENTAL STUDY OF FLOW AND WALL MASS TRANSFER RATES IN CAPILLARY DRIVEN FLOWS IN MICROFLUIDIC CHANNELS
Salvatore Cito
ISBN:978-84-693-0720-5/DL: T-425-2010

that each frame has been recorded every 1/29 sec, we can compute the position of the meniscus just finding the total sum of the matrix components.

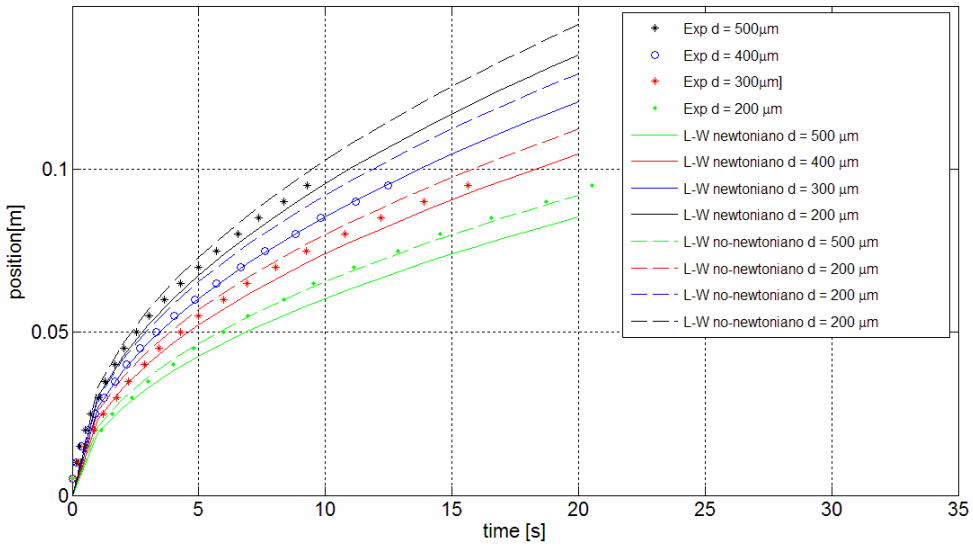

Figure 40: The meniscus position over time for the different micro-channels was obtained by video analysis and the meniscus speed was computed for each position.

From the described video analysis, we first measured the meniscus position over time for the different micro-channels and computed the meniscus speed for each position as shown in Figure 40. Then we fitted the meniscus position data from the circular micro-channels (within the range (200 μ m – 500 μ m) using the Lucas–Washburn one-dimensional model, Equation (2.20) and the generalized Lucas–Washburn one-dimensional model (with Non-Newtonian model), Equation (2.21) (with n=0.92), and found the best fit with θ=60º. The property of blood used are: $\mu = 0.0027$ [Pa·s] and $\sigma = 0.05\,\mathrm{N/m^2}$.

UNIVERSITAT ROVIRA I VIRGILI
NUMERICAL AND EXPERIMENTAL STUDY OF FLOW AND WALL MASS TRANSFER RATES IN CAPILLARY DRIVEN FLOWS IN MICROFLUIDIC CHANNELS
Salvatore Cito
ISBN:978-84-693-0720-5/DL: T-425-2010

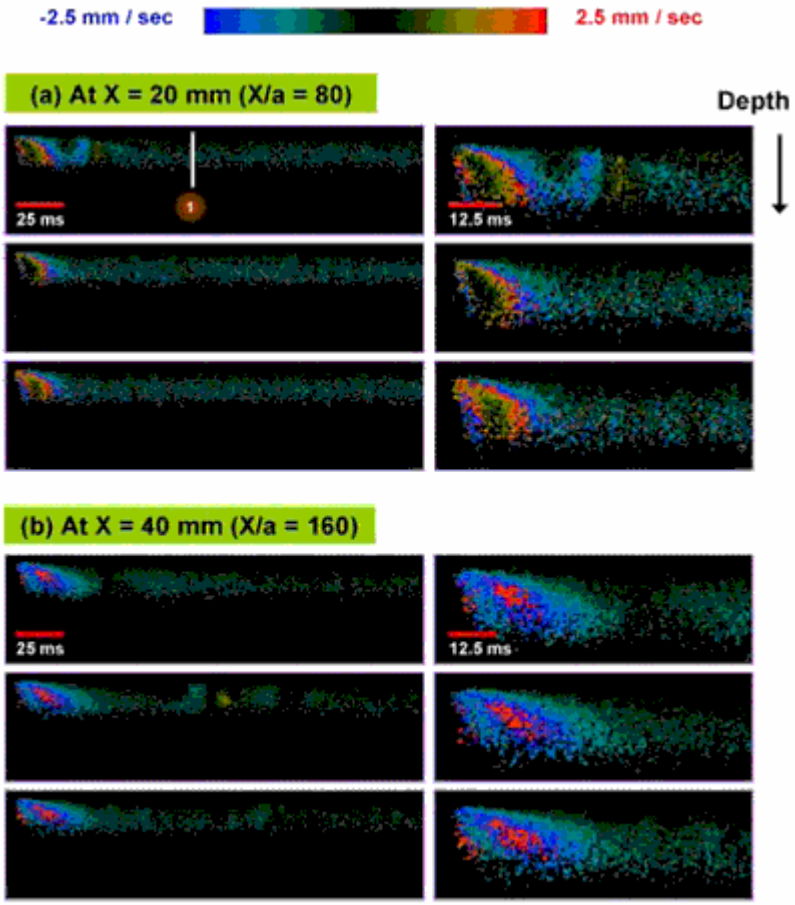

Figure 41: The radial velocity imaged by SDDOCT is shown. All cases are for the circular micro-channel with an inner diameter of 500 µm. The images are depth versus time plots at different fixed positions (X = 20 mm and 40 mm) which mean time histories of the radial velocity along the diameter of the micro-channel. Here, X is the distance from the inlet of the micro-channel. The time history was taken three times for each position corresponding to three rows. The second column shows enlarged upper half images. Left side of each image indicates the time when menisci reached the probe beam of SDDOCT.

UNIVERSITAT ROVIRA I VIRGILI
NUMERICAL AND EXPERIMENTAL STUDY OF FLOW AND WALL MASS TRANSFER RATES IN CAPILLARY DRIVEN FLOWS IN MICROFLUIDIC CHANNELS
Salvatore Cito
ISBN:978-84-693-0720-5/DL: T-425-2010

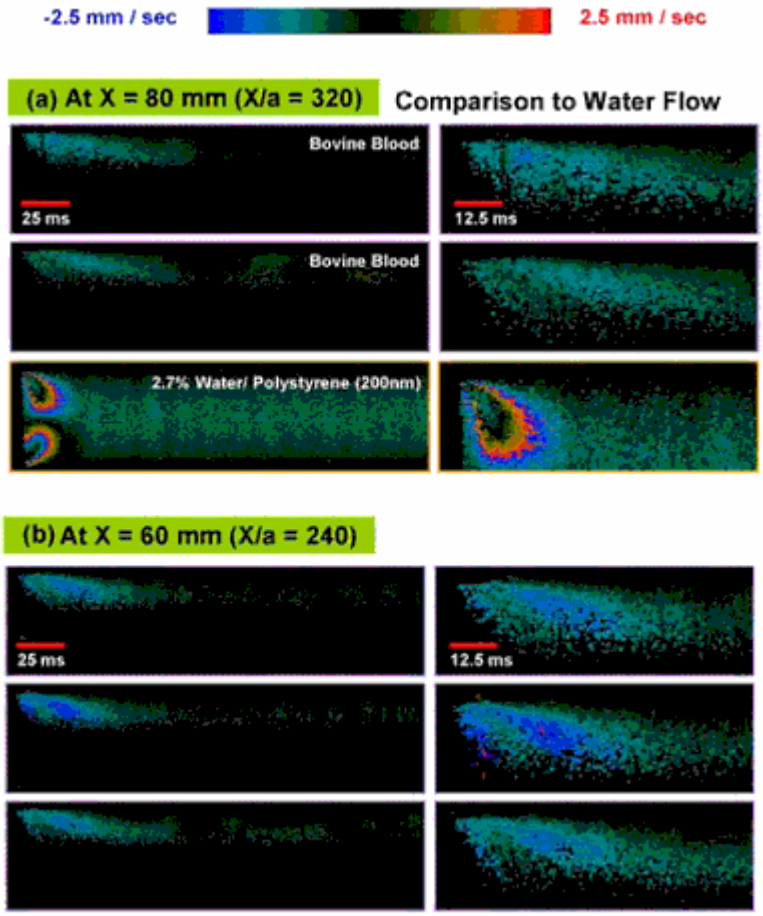

Figure 42: The radial velocity imaged by SDDOCT is shown. All cases are for the circular micro-channel with an inner diameter of 500 μm. The images are depth versus time plots at different fixed positions (X = 60, and 80 mm) which mean time histories of the radial velocity along the diameter of the micro-channel. Here, X is the distance from the inlet of the micro-channel. The time history was taken three times for each position corresponding to three rows in (a) and only two of three are shown in (b). The second column shows enlarged upper half images. Left side of each image indicates the time when menisci reached the probe beam of SDDOCT. The radial blood flow pattern is compared to the radial water flow pattern in (b).

The radial velocity imaged by SDDOCT is shown in Figure 41 and Figure 42. All cases are for the circular micro-channel with an inner diameter of 500 μ m. The images in Figure 41 and Figure 42 are depth versus time plots at different fixed positions (X =

UNIVERSITAT ROVIRA I VIRGILI
NUMERICAL AND EXPERIMENTAL STUDY OF FLOW AND WALL MASS TRANSFER RATES IN CAPILLARY DRIVEN FLOWS IN MICROFLUIDIC CHANNELS
Salvatore Cito
ISBN:978-84-693-0720-5/DL: T-425-2010

20, 40, 60, and 80 (mm) which mean time histories of the radial velocity along the diameter of the micro-channel. Here, X is the distance from the inlet of the micro-channel. The time history was taken three times for each position corresponding to three rows in Figure 41 (a)-(b) and Figure 42 (a)-(b) (Only two of three are shown in Figure 42(b). Blood has a strong light scattering because of the difference of refractive indices between erythrocytes and plasma and a strong absorption by hemoglobin. Hence, light penetration depth into the blood was limited to 300 μm out of 500 μm inner diameter. By considering an axisymmetric flow pattern, we showed enlarged upper half images at the second column in Figure 41 (a)-(b) and Figure 42 (a)-(b). Left side of each image indicates the time when menisci reached the probe beam of SDDOCT. The radial velocity was mapped in the colour as shown in the colour map of Figure 41 and Figure 42. Each image has an elliptic colour pattern. The outermost colour in the pattern indicates the direction of the radial velocity. The outermost colour of all images Figure 41 and Figure 42 is blue which means that the direction of the radial velocity is upward (negative). The red colour at the centre of the elliptic pattern, for instance, in Figure 41 (b) does not mean positive velocity but more negative because there is an abrupt colour change from blue to red. A strong negative velocity caused an aliasing effect or a phase wrapping.[43] The strong radial velocity toward the wall implies that the axial blood velocity at the centre of the micro-channel is faster than the meniscus speed, in order to satisfy the equation of continuity. If an observer rides on the moving meniscus, he will observe a clockwise recirculation near meniscus.

Reminding the flow is axisymmetric, we can infer the recirculation from the core of the circular micro-channel to the wall along the interface between blood and gas. The decreasing tendency of the radial velocity against the probe beam position was almost same as that of the meniscus speed. Additionally, we compared the radial blood flow pattern against the radial water flow pattern in Figure 42(b). We used neutrally buoyant polystyrene beads with a mean diameter of 200 nm as seeding particles in a water experiment. Because of low absorption by the water, we could see the entire cross

UNIVERSITAT ROVIRA I VIRGILI
NUMERICAL AND EXPERIMENTAL STUDY OF FLOW AND WALL MASS TRANSFER RATES IN CAPILLARY DRIVEN FLOWS IN MICROFLUIDIC CHANNELS
Salvatore Cito
ISBN:978-84-693-0720-5/DL: T-425-2010

section along the channel diameter. Surface tension of blood is half of water and viscosity is 4 times greater than water. The meniscus speed in the water experiment was much faster and so the radial velocity more intense.

The difference of the meniscus speed and the maximum axial blood velocity at the centre of the micro-channel in the downstream far enough from the meniscus to have a negligible radial velocity ia a measure of strength of the radial velocity at a certain time.

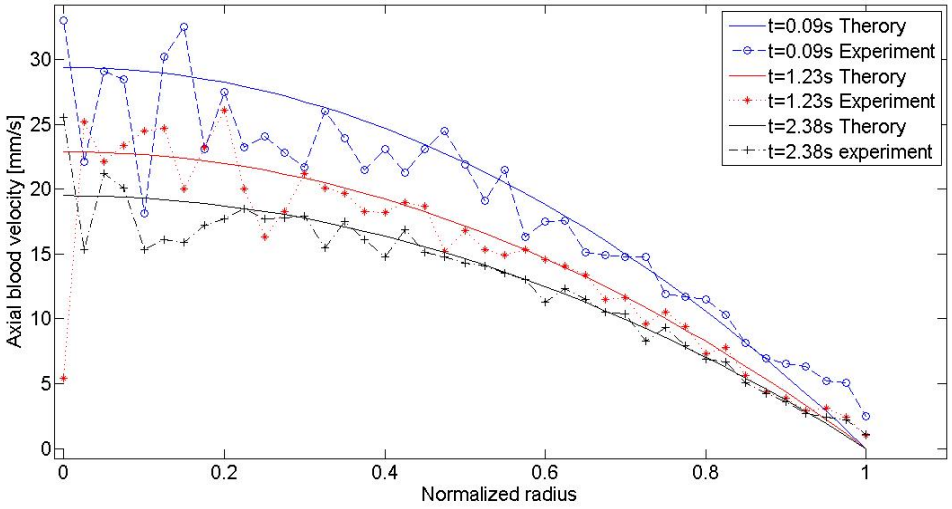

Figure 43:In the downstream far enough not to have any radial velocity, the axial velocity profile of blood flow at X = 20 mm was measured at three different times (0.09, 1.23, and 2.38 second later after the meniscus reached the probe beam located at X = 20 mm).

We measured the axial velocity profile of blood flow at $X = 20$ mm at three different times (0.09, 1.23, and 2.38 second later after the meniscus reached the probe beam located at $X = 20$ mm) and plotted it in Figure 43. In the downstream far enough not to have any radial velocity, the velocity has only axial component and, therefore, Doppler angle is easily determined if we consider the tilted angle 2^{o} of the micro-channel. Then, the axial blood velocity can be obtained from the Doppler shift measured by SDDOCT. The number 1 indicated in Figure 41 (a) is corresponding to the case of 0.09 second. The axial blood velocity decreased with time. Assuming the profile follows Poiseuille's law,

UNIVERSITAT ROVIRA I VIRGILI
NUMERICAL AND EXPERIMENTAL STUDY OF FLOW AND WALL MASS TRANSFER RATES IN CAPILLARY DRIVEN FLOWS IN MICROFLUIDIC CHANNELS
Salvatore Cito
ISBN:978-84-693-0720-5/DL: T-425-2010

we provided parabolic curve fits with the same flow rates (calculated from the experimental data) for three cases. Maximum velocities were 29.4, 22.9, and 19.5 mm/sec respectively. Since the meniscus speed is almost constant (23 mm/sec from the Figure 43) during such a short time of 0.09 second, the measure of strength of the radial velocity was 6.4 mm/sec and it was 28% of the meniscus speed.

UNIVERSITAT ROVIRA I VIRGILI
NUMERICAL AND EXPERIMENTAL STUDY OF FLOW AND WALL MASS TRANSFER RATES IN CAPILLARY DRIVEN FLOWS IN MICROFLUIDIC CHANNELS
Salvatore Cito
ISBN:978-84-693-0720-5/DL: T-425-2010

5.4 Experimental analysis of wall mass transfer rates in screen-printed micro-channels

5.4.1 Introduction

One of the goals of the work presented here is to set a game field where the microdevice fabrication is further simplified by making all parts both structural and functional; this is, making the fluidics part be also electrochemically active as depicted in Figure 44. In addition to that it has also been explored the influence of some screen-printing process tuneable variables on the principal characteristics of Microsystems components: definition, resolution, and thickness or aspect ratio. Little has been previously reported on predictive analysis of geometrical dimensions, to our knowledge there are only some preliminary studies on fixed variables like screen pattern design and squeegee – screen attack angle [50].

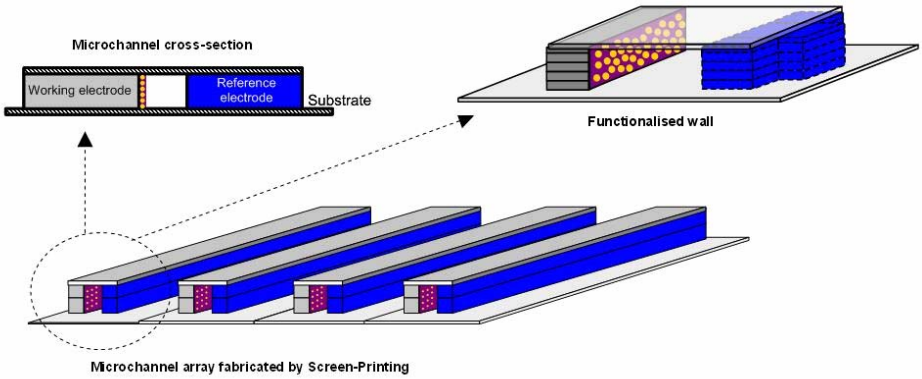

Figure 44: Schematic of the screen-printed Microsystems.

A demonstrator of a screen-printed micro-channel was built and its functionality characterized. First using confocal microscopy to visualize the occurrence of electrochemical process within the channel and then modifying under electrochemical

UNIVERSITAT ROVIRA I VIRGILI
NUMERICAL AND EXPERIMENTAL STUDY OF FLOW AND WALL MASS TRANSFER RATES IN CAPILLARY DRIVEN FLOWS IN MICROFLUIDIC CHANNELS
Salvatore Cito
ISBN:978-84-693-0720-5/DL: T-425-2010

control such micro-channel by depositing a conductive polymer (polyaniline) and supraparamagnetic beads in spatially defined positions, opening the possibility of *in-situ* multifunctional modification of such Microsystems. Electropolymerisation is an efficient enzyme immobilization method used in biosensor development [51]. Conducting polymers such as, polythiophene, polyaniline, polyindole and polypyrrole can be grown electrochemically on an electrode surface. The thickness of the growing polymer film can be controlled by measuring the charge transferred during the electrochemical polymerisation process [52]. The main advantage of having an electrode covered by a layer of a conducting film is that it can entrap enzymes if they are electropolymerised together with the conducting polymer or if the polymer is already in the surface the enzyme can be adsorbed by electrostatic charges. The spatial distribution of the immobilised enzyme can be controlled [52]. The polymer layer can act as the transducer and/or the platform to immobilize the recognition element in a reactive layer that can be applied in a biosensor design. In the case of paramagnetic particles electrophoretic deposition is the method used where colloidal particles suspended in a liquid medium migrate under the influence of an electric field and are deposited onto an electrode [53, 54].

5.4.2 Materials and equipment

The substrate for printing was a polyester film with a thickness of 175 μm provided by Cadillac Plastic S.A. (Spain). The substrate was cut according to the design printed.

The ink (7102 CONDUCTOR PASTE based on carbon and 5874 CONDUCTOR PASTE based on Ag/AgCl) and the specific thinner used to decrease the viscosity (3610 THINNER) were provided by DuPont Ltd. (UK). The screens were designed in house and manufactured by DEK International (France). Three different screens with different specification parameters were used: to perform the resolution test of lines a stainless steel mesh 300 SDS (65/20), emulsion thickness $6.0 \cdot 10^{-6}$ m, to perform the resolution test of micro-channels a polyester mesh 380 (150/27) and to carry out the micro-channel

UNIVERSITAT ROVIRA I VIRGILI
NUMERICAL AND EXPERIMENTAL STUDY OF FLOW AND WALL MASS TRANSFER RATES IN CAPILLARY DRIVEN FLOWS IN MICROFLUIDIC CHANNELS
Salvatore Cito
ISBN:978-84-693-0720-5/DL: T-425-2010

fabrication by optical alignment a stainless steel mesh 200 (90/40). The screens are specified mainly with the material of the strands used, the strands per inch (mesh), the opening between the strands and the wire diameter.

The squeegee used was made of polyurethane and provided by DEK International. (Model SQA152 with a contact angle of 45º and a hardness factor of 70). The adhesive used to close the micro-channel is a commercial Arcare 90485 provided by Adhesives Research Inc (UK). It is a PET tape, coated with acrylic medical grade adhesive on both sides with a total thickness of 254 μm.

Poly(vinylsulfonic acid) aniline and fluorescein were provided by Sigma-Aldrich (Spain), hydrochloric acid 1 M, di-sodium hydrogen phosphate and sodium dihydrogen phosphate provided by Scharlau (Spain) and Dynabead M-270 Epoxy beads provided by Invitrogen (Norway).

The screen-printing apparatus was a DEK-248 (DEK International). The machine has a DEK Align 4 Vision System Module that is a 2-point optical alignment system.

The viscosity of the inks was determined with a Brookfield DV-E Viscosimeter equipped with a Small Sample Adapter and a SC4-21 spindle (Brookfield, UK).

The profilometries were performed with a Mitutoyo SJ-301 profilometer and the data received was analyzed with the software SURFPAK-SJ Version 1.401 (Mitutoyo Messgeräte GmbH, Japan). The curing of the ink was carried out in a Digiheat 150L oven (JP Selecta S.A, Spain).

The Environmental Scanning Electron Microscope (ESEM) is a FEI model QUANTA 600 manufactured by FEI (USA). A Confocal Scanning Laser Microscope (NIKON model TE2000-E) was used. The electrodeposition was performed with a potentiostat CHI420A from CH Instruments (USA).

UNIVERSITAT ROVIRA I VIRGILI
NUMERICAL AND EXPERIMENTAL STUDY OF FLOW AND WALL MASS TRANSFER RATES IN CAPILLARY DRIVEN FLOWS IN MICROFLUIDIC CHANNELS
Salvatore Cito
ISBN:978-84-693-0720-5/DL: T-425-2010

5.4.3 Deposition of polyaniline and supraparamagnetic beads

A solution of 20 % v/v PVS, 78.1 % HCl 1M and 1.9% aniline was introduced in the micro-channel and polymerisation was performed using cyclic voltammetry between –500 and 1100 mV at a scan rate of 100 mV/s.

For the deposition of paramagnetic beads, the Microsystems used was the same as the one used for poly(aniline) electropolymerisation. In this case a solution of 4.75 % v/v of Dynabeads® in PBS 0.1 M was prepared and placed inside the micro-channel. A positive potential of 1 V was applied at the working electrode for 10 minutes.

5.4.4 Screen-printing variables study

Since the objective of this study is to establish that screen-printing can be used to transfer onto a substrate 3-D patterns that can form microfluidic elements it is necessary to fine-tune the process parameters that can optimize such 3-D transfer.

A large number of process parameters have been identified that affect to a greater or lesser extent the architecture, geometry and appearance of the designs produced [55]. Kobs and Voigt [55] in their study they performed a parametric experimental evaluation of 50 variables and compared the results on the basis of a “rating system” based on image analysis primarily and only supported by resistance and profilometry of the patterns. Although their work is the first published, systematic approach to the screen printed process is only of marginal help for the purposes of the present study. Still, it helped to identify a subset of important process parameters.

Much more valid insight could be obtained from the theoretical analysis and modelling of the process since from such models a predictable effect on the printed pattern can be discerned and verified. The off-contact screen-printing is essentially the passing of a non-Newtonian fluid through a barrier under the pressure exerted by the squeegee. As the squeegee moves, the screen is deformed, the ink passes through the barrier and after the pass of the squeegee the screen returns to its initial position. Several attempts have been reported in the literature to model this process [56-65]. Of these

UNIVERSITAT ROVIRA I VIRGILI
NUMERICAL AND EXPERIMENTAL STUDY OF FLOW AND WALL MASS TRANSFER RATES IN CAPILLARY DRIVEN FLOWS IN MICROFLUIDIC CHANNELS
Salvatore Cito
ISBN:978-84-693-0720-5/DL: T-425-2010

attempts Riemer's [57-59] represent the earliest reports in the literature modelling the process. This effort was extended to include non-Newtonian fluids [60] and the gap between the substrate and the screen [56]. These models are not easily exploited for the purposes of this work because they lack the detail necessary for taking into account the geometry of the squeegee attack or the screen permeability and deflection, all of them parameters that should be taken into account when the 3-D transfer of patterns is sought to be optimised. In addition, they are solved for the pressure exerted by the squeegee, a variable with little value for evaluation of the print result. Subsequent attempts have used lubrication theory for the flow of ink through the screen [61, 62] but still failed to account for the geometry of the process, whereas a more complete solution (including non-Newtonian behaviour) is limited to the simpler stencil process [64].

Another characteristic that most of the models fail to address consistently is the existence of the hydrodynamic film under the squeegee during its pass over the screen. Most models account for it in order to achieve continuity of the mathematical solution, but experience shows that this is not the case. Finally, the quantification of the ink left on the substrate (which is one of the most important parameters relevant to this study) was only undertaken directly in one work [65]. However, the model in this work is solved numerically and does not provide a clear insight into the process and the squeegee geometry (roller type) is different than the one used in this work. Lately [63] another study provides a solution for the flux of ink through the screen and although it does so only for Newtonian fluids. It establishes some dimensionless numbers that could be used at least for a first approximation to assigning importance to process parameters. White *et al*. [63] conclude that, other parameters kept constant, it is the magnitude of $(L/h_f)(\kappa_s H_a)^{0.5}$ (L is the screen length, h_f the frame height, κ_s the squeegee tip curvature, and H_a the squeegee tip height) that controls the flux of ink through the screen, whereas Fox et al. [65] ascertain that the deposited thickness is directly proportional to this flux modulated only by the mesh ruling and the screen open area. Knowing that screen characteristics and squeegee geometric parameters are important for ink flow and therefore 3-D transfer of patterns, it was decided in this first approximation of

UNIVERSITAT ROVIRA I VIRGILI
NUMERICAL AND EXPERIMENTAL STUDY OF FLOW AND WALL MASS TRANSFER RATES IN CAPILLARY DRIVEN FLOWS IN MICROFLUIDIC CHANNELS
Salvatore Cito
ISBN:978-84-693-0720-5/DL: T-425-2010

parametric evaluation to vary only the parameters directly related to the screen-printing process.

The parameters considered that may have greater effect on the final product quality are the pressure of the squeegee (P), the speed of the squeegee over the screen (S) and the print gap between the substrate and the screen (G). It was also examined preliminarily if the viscosity affects significantly the quality of the print although it is intuitively obvious that this "raw material" property will be of primary importance for further optimizations. However, the present study focuses on process parameters rather than on raw material properties. As a result, the screen characteristics (tension, length, void area, etc) and the squeegee angle of attack and geometry were fixed as indicated in Table 3, which refers only to the 300 SDS (65/20) screen used for the study. The printing temperature was fixed to 22 ºC. The curing of the ink is performed in the oven at 120 ºC for 10 minutes. The separation speed of the substrate is adjusted to $2 \cdot 10^{-3}$ m/s.

Parameter	Symbol	Value
Frame height	h_f	$5 \cdot 10^{-4}$ m
Screen tension	T	$2 \cdot 10^{3}$ N m^{-1}
Screen length	L	$2.5 \cdot 10^{-1}$ m
Squeegee tip height	H_a	$4.2 \cdot 10^{-4}$ m
Squeegee tip curvature	κ_s	$3 \cdot 10^{3}$ m^{-1}
Open area fraction	ϕ	0.38
Wire diameter	w_d	$2 \cdot 10^{-5}$ m
Wire separation	l	$6.5 \cdot 10^{-5}$ m
Emulsion Thickness		$6.0 \cdot 10^{-6}$ m

Table 3: Fixed 300 SDS (65/20) screen and squeegee parameters.

The evaluation was performed against three properties of the print: once the designs were cooled, the *resistance(R)* of the printed figure was measured with a two-point

UNIVERSITAT ROVIRA I VIRGILI
NUMERICAL AND EXPERIMENTAL STUDY OF FLOW AND WALL MASS TRANSFER RATES IN CAPILLARY DRIVEN FLOWS IN MICROFLUIDIC CHANNELS
Salvatore Cito
ISBN:978-84-693-0720-5/DL: T-425-2010

probe. The ink is made of carbon and it has an electrical conductivity. The measurement of the resistance provides preliminary information about the quality of the printing. Optimum values of up to 500 ohms were considered valid, based on the practical experience that the resistance still ensures good electrochemical responses of the material. Secondly the thickness (δ) of the ink deposited was measured with the profilometer. These data provide information about the uniformity of the ink deposited and the roughness of the surface (this is roughly the aspect ratio that can be achieved per pass). Finally, a characteristic distance of the design (which is called here resolution) was measured. In the case of printed lines, this characteristic distance was the width of the thinnest printable line (a characteristic of the print process) and in the case of the micro-channels, it was the width of the micro-channel (a characteristic of alignment).

5.4.5 Maximum line resolution

First, the highest resolution that can be achieved with the screen-printing equipment was determined. To carry out this objective a screen with lines of different widths was used. The mesh is one of the most important elements that control what line width can be achieved. A well-known rule in the industry is that the limit of the line width that can be printed can be no thinner than three times the width of the mesh threads. The finest stainless steel mesh available in the market has a thread diameter of 16 μm so the minimum width that could be achieved following this rule is 48 μm. The mesh used in this experiment had a thread diameter of 20 μm, so the minimum width expected was 60 μm. Therefore, in this sense "resolution" has a lowest limit that is characteristic of the screen and the objective was to see how this limit can be approached as a function of the varied parameters.

The parametric dependence was determined using a statistical central composite design with the statistical software Design-Expert (V.7.0). The limit values of each factor can be defined according to previous experience with the equipment. The pressure of the squeegee fixed had a maximum value of $4.23 \cdot 10^4$ Pa. At higher values there is a

UNIVERSITAT ROVIRA I VIRGILI
NUMERICAL AND EXPERIMENTAL STUDY OF FLOW AND WALL MASS TRANSFER RATES IN CAPILLARY DRIVEN FLOWS IN MICROFLUIDIC CHANNELS
Salvatore Cito
ISBN:978-84-693-0720-5/DL: T-425-2010

high risk to break the mesh. The minimum pressure value was fixed to $1.15 \cdot 10^4$ Pa. The limits in the speed of the squeegee were fixed by the limitations of the equipment that have a minimum speed of $6.4 \cdot 10^{-2}$ m/s and a maximum of $2.26 \cdot 10^{-1}$ m/s. The print gap limits were also fixed by experience. The minimum print gap was fixed at $5 \cdot 10^{-4}$ m and the maximum at $1 \cdot 10^{-3}$ m.

Central composite design is a surface response method used to quantify the relationships between one or more measured responses and the vital input factors. The method is based on the estimation of a quadratic model that relates all the factors and the responses. The factors can have four different values that are the extreme points, the central point between the extremes and a limiting value. The software used (Design-Expert V.7.0) is able to define the design of the experiments in order to have enough information to do the calculations. In this case, with three factors and three responses, it was necessary to do 20 experiments. The results obtained correspond to the narrowest line printed; they were the narrowest lines that could be printed from a series of lines on a screen design.

The results have been treated in the software and the model obtained can be summarized in a quadratic model.

$$\delta = 3.93 \cdot 10^{-6} + \left(2.10 \cdot 10^{-2} \cdot G\right) + \left(2.88 \cdot 10^{-7} \cdot S\right) - \left(4.83 \cdot 10^{-10} \cdot P\right) - \left(2.40 \cdot 10^{-2} \cdot G \cdot S\right) - \ldots \left(3.89 \cdot 10^{-8} \cdot G \cdot P\right) + \left(1.66 \cdot 10^{-10} \cdot S \cdot P\right) - \left(9.40 \cdot G^2\right) + \left(9.93 \cdot 10^{-6} \cdot S^2\right) \quad (5.20)$$

$$R = 9.36 \cdot 10^4 - \left(1.75 \cdot 10^8 \cdot G\right) - \left(1.88 \cdot 10^5 \cdot S\right) + \left(1.14 \cdot P\right) + \left(3.38 \cdot 10^8 \cdot G \cdot S\right) + \left(3.28 \cdot 10^2 \cdot G \cdot P\right) - \ldots \left(1.00 \cdot S \cdot P\right) + \left(7.14 \cdot 10^{10} \cdot G^2\right) - \left(1.14 \cdot 10^5 \cdot S^2\right) \quad (5.21)$$

$$\text{Resolution} = 2.58 \cdot 10^{-4} - \left(1.38 \cdot 10^{-1} \cdot G\right) - \left(3.87 \cdot 10^{-4} \cdot S\right) - \left(3.10 \cdot 10^{-9} \cdot P\right) + \left(4.80 \cdot 10^{-1} \cdot G \cdot S\right) + \ldots \left(1.75 \cdot 10^{-6} \cdot G \cdot P\right) + \left(8.52 \cdot 10^{-9} \cdot S \cdot P\right) \quad (5.22)$$

Where δ is the thickness in m, R is the resistance in ohms, Resolution is the highest resolution in m, G is the print gap in m, S is the speed of the squeegee in m/s and P is the pressure of the squeegee in Pa.

UNIVERSITAT ROVIRA I VIRGILI
NUMERICAL AND EXPERIMENTAL STUDY OF FLOW AND WALL MASS TRANSFER RATES IN CAPILLARY DRIVEN FLOWS IN MICROFLUIDIC CHANNELS
Salvatore Cito
ISBN:978-84-693-0720-5/DL: T-425-2010

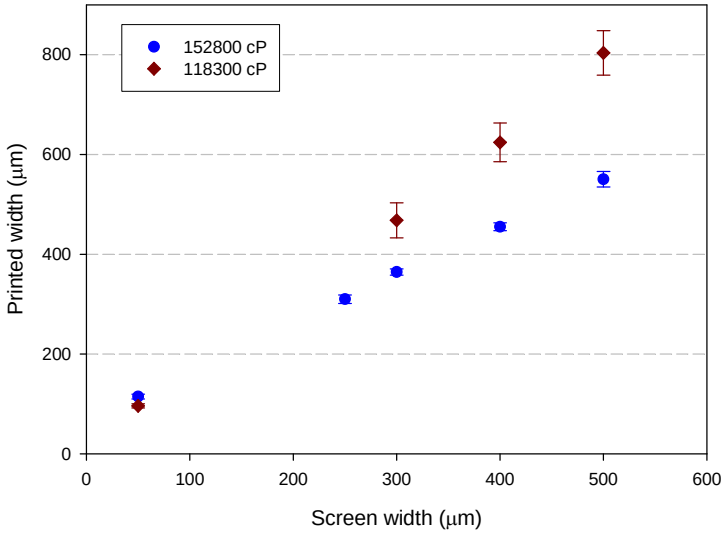

Figure 45: Variation of printed line width as a function of screen width. Speed=$6.40 \cdot 10^{-2}$ m/s. Print gap=$1.0 \cdot 10^{-3}$ m. Pressure=$1.15 \cdot 10^{4}$ Pa (n = 40, 95% Confidence).

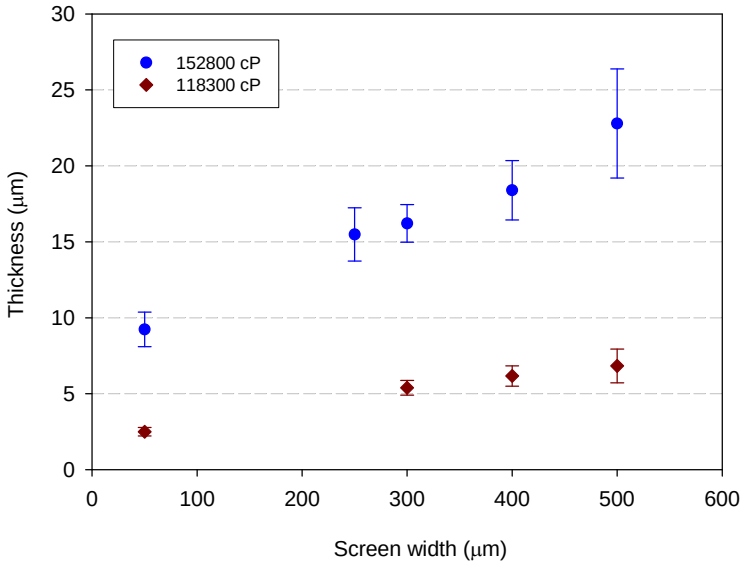

Figure 46: Variation of printed line thickness as a function of screen width. Speed=$6.40 \cdot 10^{-2}$m/s. Print gap=$1.0 \cdot 10^{-3}$ m. Pressure=$1.15 \cdot 10^{4}$ Pa. (n = 40; 95% Confidence).

From the statistical model equations can be seen that the speed of the squeegee is the parameter that less profoundly affects the print quality.

As it was mentioned, “raw material” properties were used only as an indicator of possible process improvements. In order to examine the effect of ink viscosity on the print and establish the repeatability of the process, two inks were prepared with viscosities 152800 and 118300 cP and a series of 20 substrates were printed with the fixed process parameters predicted for highest resolution. The results are summarized in Figure 45 and Figure 46.

Observation of the results indicates that a lower viscosity ink permits that the lines can be printed with a lower width and smaller designs could be manufactured despite the fact that the print spreads more. On the other hand the thickness achieved is smaller with lower viscosity. Both results are expected from intuition and the modelling efforts mentioned above. Also of importance is the fact that repeatability is better when thinner line patterns are transferred and it also improves with the higher viscosity ink. Overall, it appears that the tuning of the viscosity of the inks used is an important parameter to control in order to achieve high resolution and reproducible results.

5.4.6 Maximum micro-channel resolution

In order to determine the capacity to print micro-channels, a screen was used with micro-channel designs of different widths between lines. A polyester screen with a larger space between strands was used because the tension during the separation of the substrate and the mesh was so high that the screen could break.

The same experimental design as before was applied. The resolution reported is the width of the printed micro-channel as measured by acquiring a transversal profilometry of the entire figure printed and reporting the peak of the profile on both sides of the channel. Obviously, the real width of the printed channel is smaller since the ink printed forms a sloping deposit that peaks approximately in the middle of the wall width. Efforts to quantify the slope of the deposit are in progress since it is another quality

UNIVERSITAT ROVIRA I VIRGILI
NUMERICAL AND EXPERIMENTAL STUDY OF FLOW AND WALL MASS TRANSFER RATES IN CAPILLARY DRIVEN FLOWS IN MICROFLUIDIC CHANNELS
Salvatore Cito
ISBN:978-84-693-0720-5/DL: T-425-2010

characteristic in 3-D ink transfer for Microsystems production. The resistance is measured between the extreme points of the transferred design. The thickness corresponds to the ink printed. In this case the thickness of the ink is the thickness of the walls of the micro-channel, and again, is reported as the maximum thickness of the deposit.

The best model where all the variables fit is a linear model for the thickness and resistance prediction and a quadratic model for the width with the following equations:

$$\delta = +4.19\cdot10^{-6} + 1.83\cdot10^{-2}\cdot G + 4.82\cdot10^{-5}\cdot S - 2.54\cdot10^{-10}\cdot P \quad (5.23)$$

$$R = +4.83\cdot10^{2} - 2.31\cdot10^{5}\cdot G - 3.70\cdot10^{2}\cdot S + 4.15\cdot10^{-3}\cdot P \quad (5.24)$$

$$\text{Resolution} = +1.84\cdot10^{-3} - 5.07\cdot G - 6.49\cdot10^{-3}\cdot S + 1.39\cdot10^{-8}\cdot P + 2.50\cdot10^{1}\cdot G\cdot S - \ldots$$
$$3.21\cdot10^{-5}\cdot G\cdot P + 1.13\cdot10^{-7}\cdot S\cdot P + 3.05\cdot10^{3}\cdot G^{2} - 3.96\cdot10^{-2}\cdot S^{2} \quad (5.25)$$

Where δ is the thickness in m, R is the resistance in ohms, Resolution is the highest resolution in m, G is the print gap in m, S is the speed of the squeegee in m/s and P is the pressure of the squeegee in Pa. As before, the speed of the squeegee appears to have the least effect on the resulting prints and for this reason fixing the speed at 64 mm/s (the optimum speed observed).

In order to examine the effect of ink viscosity on the print and establish the repeatability of the process, two inks were prepared with viscosities 152800 and 118300 cP and a series of 6 substrates were printed with the process parameters fixed as predicted from the model for highest resolution. The results are summarized in Figure 47 and Figure 48.

.

UNIVERSITAT ROVIRA I VIRGILI
NUMERICAL AND EXPERIMENTAL STUDY OF FLOW AND WALL MASS TRANSFER RATES IN CAPILLARY DRIVEN FLOWS IN MICROFLUIDIC CHANNELS
Salvatore Cito
ISBN:978-84-693-0720-5/DL: T-425-2010

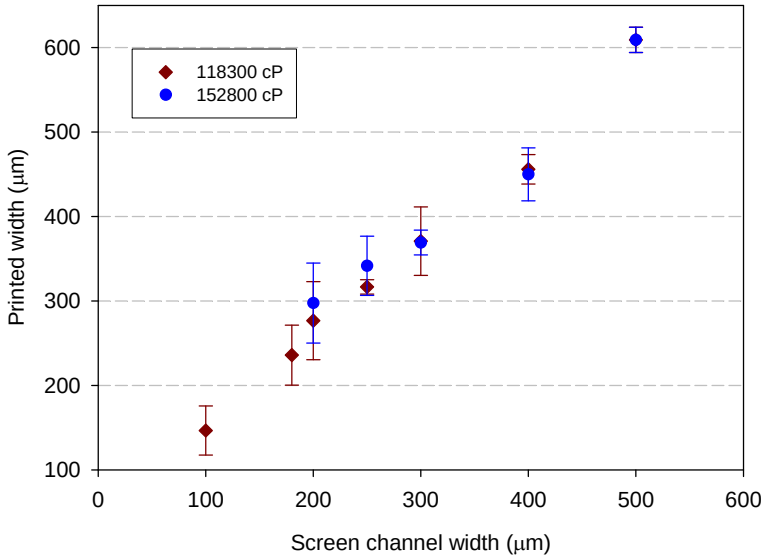

Figure 47: Variation of micro-channel width as a function of screen width. Speed=6.40·10^{-2}m/s. Print gap = 5.0·10^{-4}m. Pressure = 4.23·10^{4} Pa (n = 6; 95% Confidence).

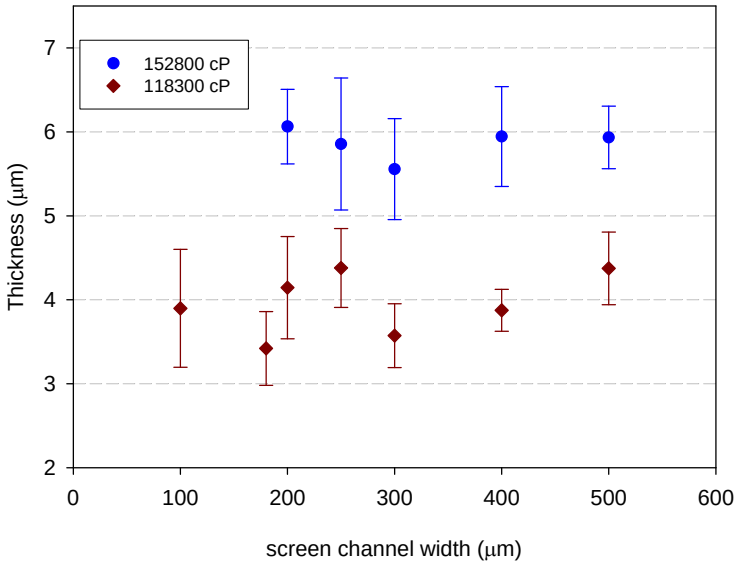

Figure 48: Variation of micro-channel thickness as a function of screen width. Speed=6.40·10^{-2}m/s. Print gap=5.0·10^{-4}m. Pressure=4.23·104 Pa (n=6; 95% Confidence).

UNIVERSITAT ROVIRA I VIRGILI
NUMERICAL AND EXPERIMENTAL STUDY OF FLOW AND WALL MASS TRANSFER RATES IN CAPILLARY DRIVEN FLOWS IN MICROFLUIDIC CHANNELS
Salvatore Cito
ISBN:978-84-693-0720-5/DL: T-425-2010

Observation of the results shows that, as expected, the channel width does not influence the thickness of the deposition which has also the expected behaviour as a function of the viscosity of the ink. The repeatability of the process is not such a strong function of dimensions as before. The lower viscosity ink permits to print finer channels being of 146 ± 3 μm the minimum width with wall thickness of 3.90 ± 0.66 μm. It was also noticed that lower viscosity produced the accumulation of ink in the back of the screen and in the case of the printing of micro-channels; lower print gaps should be used in order to avoid this leakage. It is important also to use higher pressures in order to improve the quality of the print

5.4.7 Micro-channel fabrication with optical alignment

The thickness achieved printing the micro-channel directly from a screen design is small and to obtain a higher thickness it will be necessary to print several layers. To increase the thickness printed a screen with higher separation between wires could be used but at the expense of resolution. In addition, it is of interest to be able to print different materials in different parts of the microfluidic device. For these reasons, it was decided that a multistep process should be developed where different screens with different designs should be aligned over the substrate. To achieve this alignment, the Align Vision System Module of the screen-printing equipment was used. This alignment module has micrometric precision and needs two reference points that can be incorporated in the screen design.

The minimum width that can be achieved with the optical alignment and the accuracy of the equipment to print several layers of ink in order to increase the thickness while maintaining the width were decided with a series of exploratory experiments. The desired width is fixed manually in the equipment. The print gap used was 0.9 mm, the pressure was $3.08 \cdot 10^4$ Pa and the squeegee speed was 64 mm/s. Three different separation settings were tested until the optimum conditions could be decided. In our hands, the best micro-channel obtained had a thickness of 18.86 ± 4.41 μm and a width

UNIVERSITAT ROVIRA I VIRGILI
NUMERICAL AND EXPERIMENTAL STUDY OF FLOW AND WALL MASS TRANSFER RATES IN CAPILLARY DRIVEN FLOWS IN MICROFLUIDIC CHANNELS
Salvatore Cito
ISBN:978-84-693-0720-5/DL: T-425-2010

of 198 ± 60 μm. The printing of several layers was performed using this optimum equipment separation.

The results obtained after printing four layers (Figure 49) show that the thickness increases gradually when the number of layers printed increases while we were able to maintain the channel width within acceptable limits. The effect of multilayer printing was that the walls of the micro-channel are not vertical and tend to slope outwards having the channel a higher width in the upper than in the lower part. It is therefore concluded that it is feasible to align the screens in order to print different materials in the microfluidic device and the multilayer printing can achieve a big variety of aspect ratios.

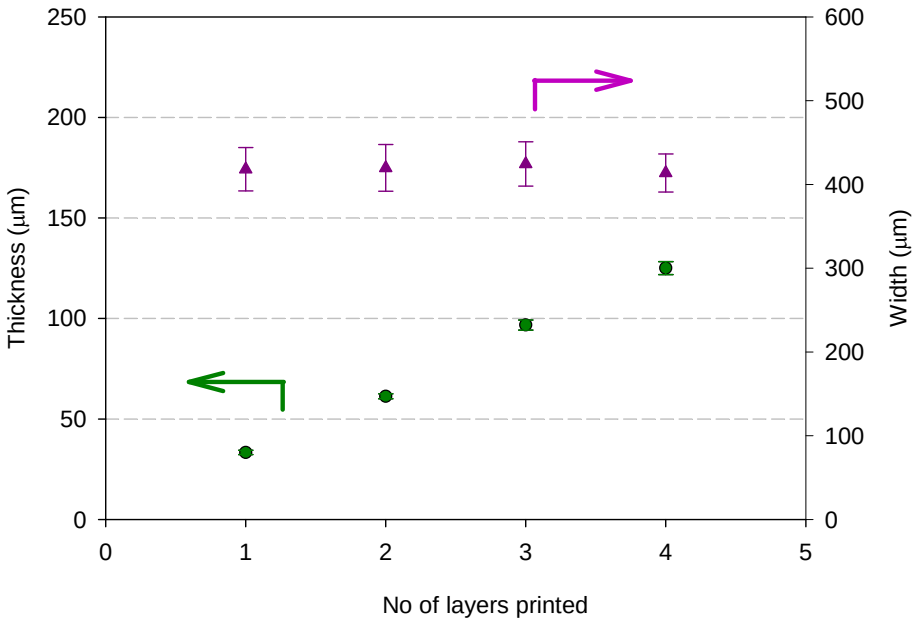

Figure 49: Variation of micro-channel width and thickness with optical alignment in multilayer printing. Speed=6.40·10^{-2}m/s. Print-gap=9.0·10^{-4}m. Pressure=3.08·10^{4} Pa. Ink viscosity=152800 cP. (n=20; 95% Confidence).

UNIVERSITAT ROVIRA I VIRGILI
NUMERICAL AND EXPERIMENTAL STUDY OF FLOW AND WALL MASS TRANSFER RATES IN CAPILLARY DRIVEN FLOWS IN MICROFLUIDIC CHANNELS
Salvatore Cito
ISBN:978-84-693-0720-5/DL: T-425-2010

5.4.8 Optical monitoring of an electrochemical reaction within the screen printed micro-channel

Once it has been demonstrated that micro-channels can be printed with an approximate width of 200 μm and thickness of 25 μm and that several layers can be printed, a demonstrator of a functional screen-printed micro-channel was undertaken. For this purpose a micro-channel was constructed with carbon ink as one wall (working electrode) and Ag/AgCl ink as the opposite (counter/reference electrode). A micro-electrochemical cell was thus produced. A plastic substrate layer coated with adhesive on both sides was used to manually seal the top of the micro-channel.

A screen printed micro-channel was filled with 0.1 M fluorescein and a voltage of 2 V was applied across the 200 μm distance between the electrodes creating a water electrolysis that generates a change of pH and hence an accumulation of protons in the proximities of the electrode. This induced pH change makes the fluorescein change colour and this is monitored by confocal microscopy. As it is observed in the confocal microscopy image, Figure 50, the reaction takes place specifically in the working electrode (top of the confocal image) and it is clearly observed the reaction products diffusion within the micro-channel.

The demonstrator involves the electropolymerisation of a conductive polymer (poly(aniline)) and the electrophoretic deposition of paramagnetic particles on the channel wall, both processes that can only be realized if functional electrodes are incorporated in the micro-channel. However, a plastic layer coated with adhesive on both sides was used. The total thickness was 254 μm to simulate the walls of the micro-channel. Once a single-layer micro-channel was printed and closed a different number of cycles (2, 5, 10 and 20) the micro-channels were tested in order to verify the growth of the polyaniline layer on the working electrode by microscopy and cyclic voltammetry. Cyclic voltammetry showed the characteristic poly(aniline) peaks in buffer (results not shown) while the microscopy results are shown in Figure 51. With two cycles no polyaniline deposition was observed whereas after five cycles the deposition becomes

UNIVERSITAT ROVIRA I VIRGILI
NUMERICAL AND EXPERIMENTAL STUDY OF FLOW AND WALL MASS TRANSFER RATES IN CAPILLARY DRIVEN FLOWS IN MICROFLUIDIC CHANNELS
Salvatore Cito
ISBN:978-84-693-0720-5/DL: T-425-2010

discernible. The increase of the amount of polymer deposited on the electrode can be observed comparing the results after 20 cycles.

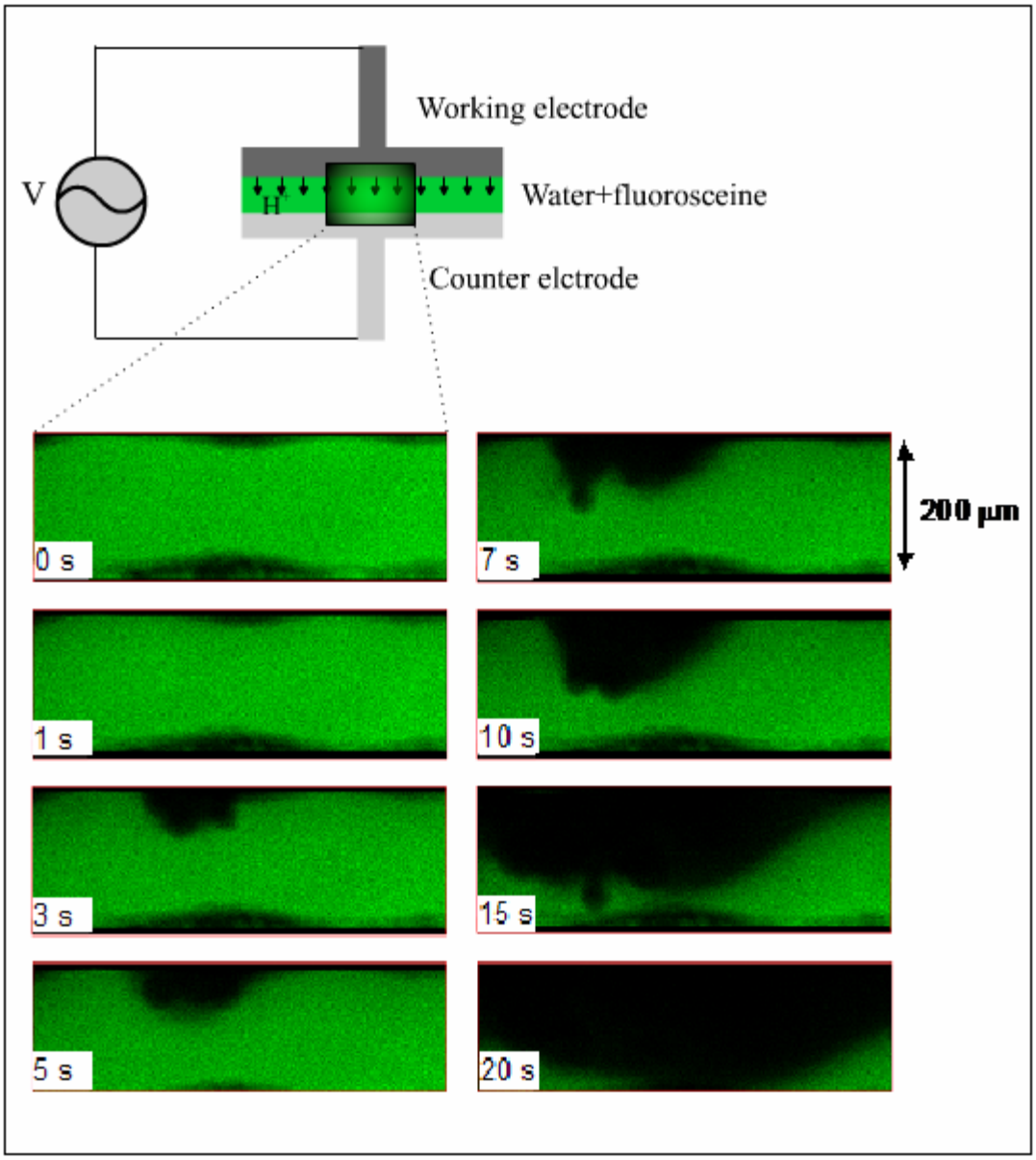

Figure 50: Confocal microscopy images monitoring the formation and diffusion of electrochemical reaction products within a micro-channel deposition of polyaniline and superparamagnetic beads in screen printed micro-channels.

UNIVERSITAT ROVIRA I VIRGILI
NUMERICAL AND EXPERIMENTAL STUDY OF FLOW AND WALL MASS TRANSFER RATES IN CAPILLARY DRIVEN FLOWS IN MICROFLUIDIC CHANNELS
Salvatore Cito
ISBN:978-84-693-0720-5/DL: T-425-2010

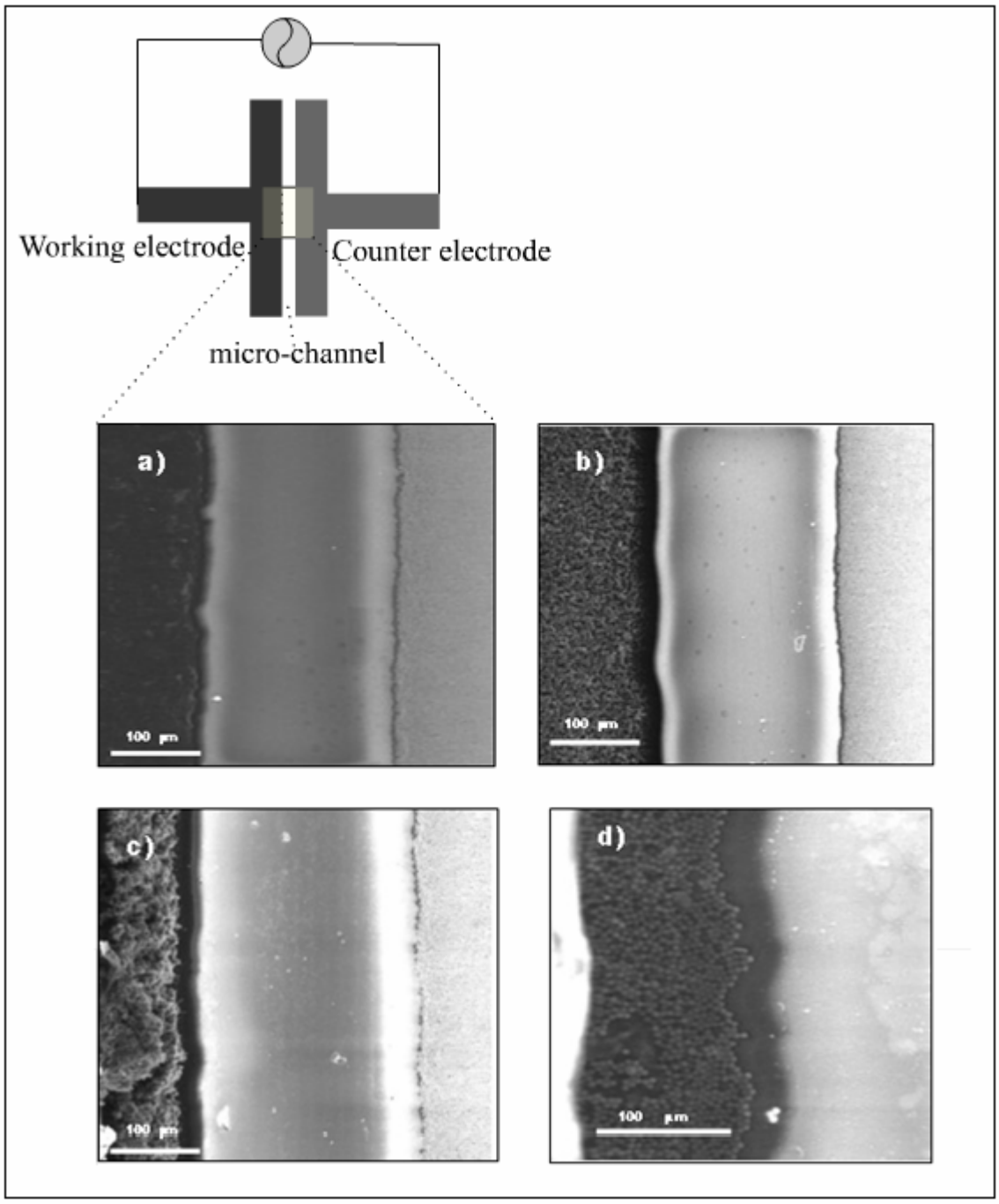

Figure 51: ESEM image of the deposition of polyaniline in a screen-printed micro-channel a) 2 cycles, b) 5 cycles, c) 20 cycles, d) ESEM image of the deposition of paramagnetic particles in a screen-printed micro-channel.

UNIVERSITAT ROVIRA I VIRGILI
NUMERICAL AND EXPERIMENTAL STUDY OF FLOW AND WALL MASS TRANSFER RATES IN CAPILLARY DRIVEN FLOWS IN MICROFLUIDIC CHANNELS
Salvatore Cito
ISBN:978-84-693-0720-5/DL: T-425-2010

In the case of the immobilization of paramagnetic particles inside the micro-channels it was observed in the ESEM. That the particles can be seen deposited on the working electrode demonstrating the functionality of the microfluidic element for selective deposition.

UNIVERSITAT ROVIRA I VIRGILI
NUMERICAL AND EXPERIMENTAL STUDY OF FLOW AND WALL MASS TRANSFER RATES IN CAPILLARY DRIVEN FLOWS IN MICROFLUIDIC CHANNELS
Salvatore Cito
ISBN:978-84-693-0720-5/DL: T-425-2010

UNIVERSITAT ROVIRA I VIRGILI
NUMERICAL AND EXPERIMENTAL STUDY OF FLOW AND WALL MASS TRANSFER RATES IN CAPILLARY DRIVEN FLOWS IN MICROFLUIDIC CHANNELS
Salvatore Cito
ISBN:978-84-693-0720-5/DL: T-425-2010

Chapter 6

Conclusions

The fluid dynamics field of a capillary driven flow in a rectangular and cylindrical cross section micro-channel for different value of Reynolds and different value of contact angle has been computed, two recirculations has been identified behind the meniscus.

The effect of the two recirculation in the mass transfer rate from the wall has been calculated for several values of Reynolds number. We have seen that the phenomena is mostly diffusive and that the recirculation does not increase significantly the average mass transfer on the wall. Comparison between the mass transfer rates for different values of the contact angle has been done and it has shown that it does not have an important effect

The fluid dynamics field of a cylindrical micro-channel and a rectangular micro-channel is different but close to the wall this difference is very small so the wall mass transfer rate for a rectangular case and a cylindrical case with the same value of Reynolds number and contact angle, results to be similar. A correlation between Sh number and (Re θ and T) has been obtained to fit the results obtained from the simulations. Such correlation can be a useful tool to predict mass transfer phenomena in micro-channel pumped by mean of CD-Flow with Reynolds number between 1 and 500.

An extended version of Lucas-Washburn equations able to give the velocity of the meniscus of non-Newtonian fluid has been formulated. And a good agreement has been obtained with the experimental results performed on CD-Flow of bovine blood in micro-channel with circular cross section. The detection of flow of bovine blood in glass made micro-channels has been recorded using a commercial video camera to measure the

UNIVERSITAT ROVIRA I VIRGILI
NUMERICAL AND EXPERIMENTAL STUDY OF FLOW AND WALL MASS TRANSFER RATES IN CAPILLARY DRIVEN FLOWS IN MICROFLUIDIC CHANNELS
Salvatore Cito
ISBN:978-84-693-0720-5/DL: T-425-2010

average axial velocity of the meniscus in the micro-channels. The non-Newtonian behaviour of blood has been investigated and the experimental results have been compared with the extended version of Lucas-Washburn equations.

The optical Doppler tomography ODT has been implemented for the first time, to measure the radial velocity of fluid under capillary driven flow in glass and PDMS made micro-channels. The results given by ODT confirmed the presence of the recirculation predicted by the simulations. The Mathematical model based in the numerical resolution of Navier-Stokes equation has been developed to reproduce the flow dynamic field of capillary driven flow in micro-channel for Newtonian and non-Newtonian fluids, and has been validated by means of the ODT.

It has been demonstrated that screen-printed functional microfluidic elements can be produced. This fabrication technique is of low cost and of acceptable, reproducibility so that it can be considered for the prototyping and production of commercial products.

An experimental factorial design to gain insight on the effect of process conditions on the resolution of the 3-D pattern transfer yielded a mathematical model that permits to optimize the process as a function of print gap, squeegee pressure and speed.

Micro-channels of minimum dimensions of as low as 100 μm could be printed with variable aspect ratios and the channels could be functionalized at will. The limitations of the work are that it was designed with a specific ink composition and screen design and type and does not have therefore universal application. Refinement of the existing fluid dynamic models and combination with experimental studies should allow the generalization of a predictive recipe for process conditions.

A first attempt to measure wall mass transfer rate in micro-channel has been done and the gradient of pH has been visualized with good resolution.

UNIVERSITAT ROVIRA I VIRGILI
NUMERICAL AND EXPERIMENTAL STUDY OF FLOW AND WALL MASS TRANSFER RATES IN CAPILLARY DRIVEN FLOWS IN MICROFLUIDIC CHANNELS
Salvatore Cito
ISBN:978-84-693-0720-5/DL: T-425-2010

Chapter 7

Future work

In this work the main challenges of CD-Flow has been faced and some of them have been successfully solved but still there is a lot of room to be investigated in this field.

1) Fast heterogeneous reaction has been considered in this work, but this is not always true and in the future we plan to refine the CFD model of CD-Flow developed in this work. The introduction of several reaction of first and second order with given reaction rate will be considered.
2) Since the mathematical problem of triple point need to still to be solved in more rigorous, is difficult to predict the unsteady behaviour of the meniscus at the entrance of the channel. As future work we plan to find a mathematical condition for the triple point that coherently describe the unsteady behaviour of CD-Flow and gives its fluid dynamic field.
3) Once obtained the solution of the CFD unsteady problem a parametrical study of the main dimensionless parameter can be done and a correlation useful for design purpose could be obtained.
4) In the future the numerical solution of wall mass transfer rate in CD-Flow needs to be validated by mean of experimental results. A first attempt to visualize a fast heterogeneous reaction has been done in this work, but the art of screen-printing and/or other microfabrication technique should be further investigated to make possible the production of hybrid micro-channels with controlled hydrophilic surface and at least one reactive wall. Without such micro-device would not be possible to make a reproducible experimental set-up.

UNIVERSITAT ROVIRA I VIRGILI
NUMERICAL AND EXPERIMENTAL STUDY OF FLOW AND WALL MASS TRANSFER RATES IN CAPILLARY DRIVEN FLOWS IN MICROFLUIDIC CHANNELS
Salvatore Cito
ISBN:978-84-693-0720-5/DL: T-425-2010

5) This work opened the prospect of several ideas in which mass transfer phenomena in capillary driven flow can be exploited and used in new generation micro-devices. One of these ideas that are worth to be mentioned here is the evaporation driven membraneless micro-fuel cell (EDM-FC).

The mechanism used by trees to feed themselves drawing water from the root up to the leaf is possible thanks to the huge number of micro-capillary that use surface tension and evaporation to pump water all over the tree (See Figure 52).

The same principle can be applied to the membraneless fuel cell (or microfluidic fuel cell) developed by Choban et al [66].

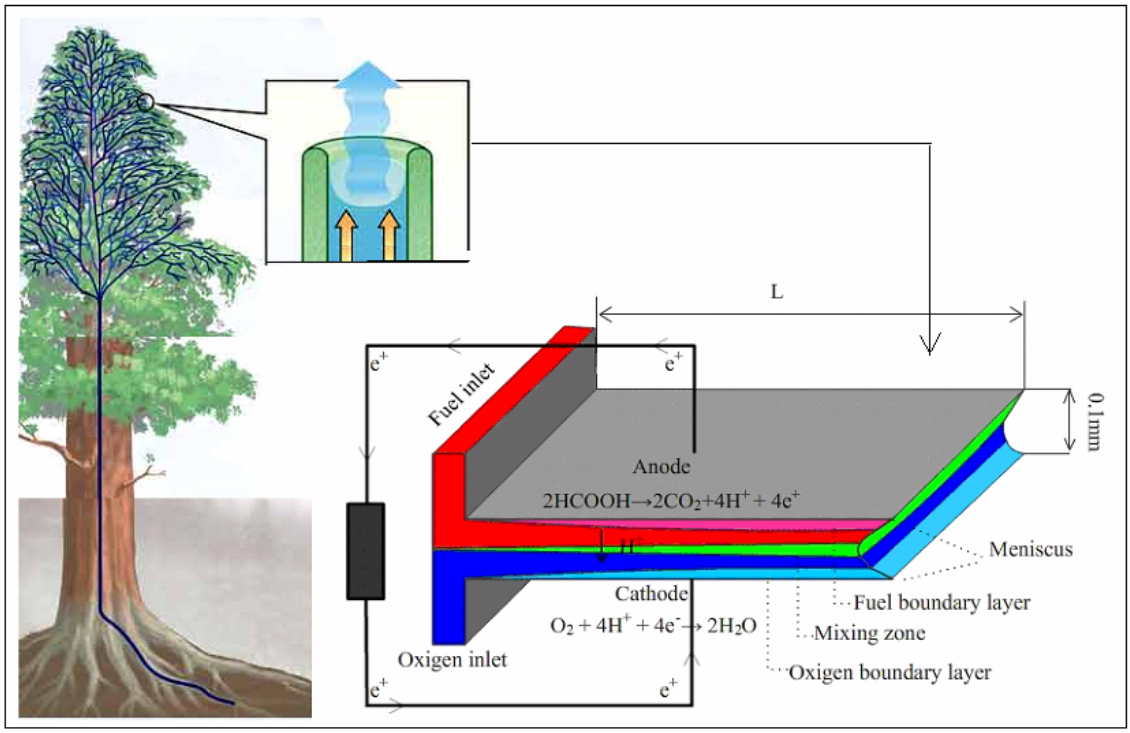

Figure 52: Schematic representation of EDM-FC with focus on the principle of work derived from trees feeding by mean of evaporation driven flow.

UNIVERSITAT ROVIRA I VIRGILI
NUMERICAL AND EXPERIMENTAL STUDY OF FLOW AND WALL MASS TRANSFER RATES IN CAPILLARY DRIVEN FLOWS IN MICROFLUIDIC CHANNELS
Salvatore Cito
ISBN:978-84-693-0720-5/DL: T-425-2010

Indeed the laminar behaviour, of the flow make mixing a difficult phenomena, the Marangoni effect in a evaporation driven flow produce a recirculation behind the meniscus [67, 68]similar to the ones we have seen in this work.

From the results of this thesis and the phenomenological description of evaporation driven flow given by Buffone et al [67, 68] it is reasonable to expect that the recirculation behind the meniscus should not enhance too much the wall mass transfer rate close to the meniscus and so is for performance degradation of the Fuel cell due to cross flow in the micro-channel.

The considerations aforementioned are the basis of the future work plan in which investigation in the development of EDM-FC is the main objective.

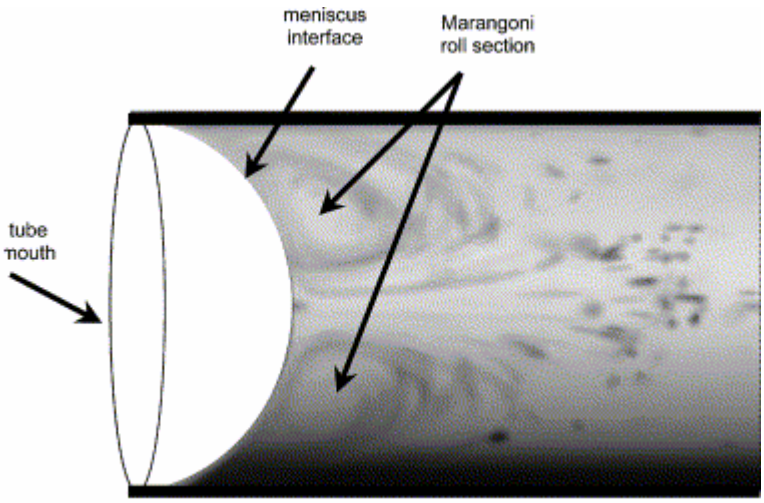

Figure 53: Visualization of the liquid flow pattern using seeding tracers as reported by Buffone et al [69].

A Numerical approach similar to the one presented in this work is already ongoing. The new numerical model take into account the Marangoni effect derived from the temperature gradient, this work has been already approached for single fluid by Wang [70] who obtained a numerical model implemented in Fluent and its results are similar to the experimental results of Buffone et al [69].

UNIVERSITAT ROVIRA I VIRGILI
NUMERICAL AND EXPERIMENTAL STUDY OF FLOW AND WALL MASS TRANSFER RATES IN CAPILLARY DRIVEN FLOWS IN MICROFLUIDIC CHANNELS
Salvatore Cito
ISBN:978-84-693-0720-5/DL: T-425-2010

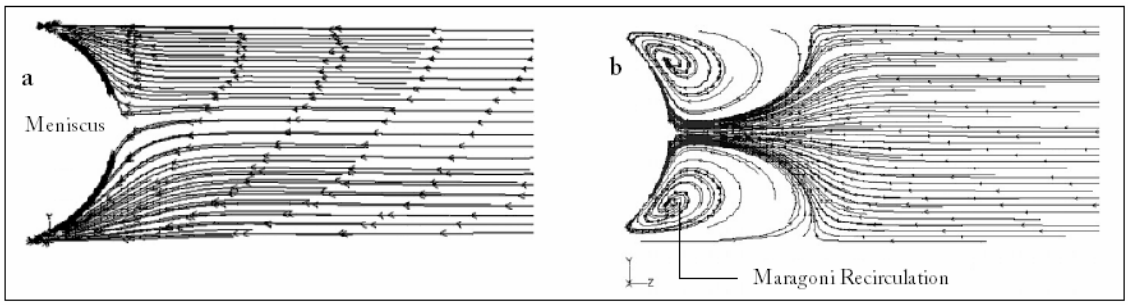

Figure 54: Numerical simulation of evaporation driven flow as reported by wang et all [70] a) without considering Marangoni effect b) considering Marangoni effect.

In the new CFD model, fuel oxidation and oxygen reduction are as well consider using a first order model.

The prospect of using screen printed micro-channel as potential microfabrication technology for mass production of the new generation of microfluidics should be exploited.

UNIVERSITAT ROVIRA I VIRGILI
NUMERICAL AND EXPERIMENTAL STUDY OF FLOW AND WALL MASS TRANSFER RATES IN CAPILLARY DRIVEN FLOWS IN MICROFLUIDIC CHANNELS
Salvatore Cito
ISBN:978-84-693-0720-5/DL: T-425-2010

NOMENCLATURE

A……Area [m^2]

a_m……Acceleration of the meniscus [m/s^2]

C……..Concentration [M]

C_o……...Initial concentration [M]

C_w……..Concentration in the wall [M]

d……...Diameter of circular cross section micro-channel [m]

D……..Diffusion coefficient (Diffusivity) [m^2/s]

F……Force [N]

f……Face [m^2]

g……Gravity [m/s^2]

h……...Height of rectangular cross section micro-channel [h]

K……...Convective mass transfer coefficient [s/m]

k……Consistency index [Pa·s]

k_1……Minimum curvature [1/m]

k_2 ……...Maximum curvature [1/m]

L……Length of micro-channel [m]

L1……..Length of entry zone [m]

L2……..Length of Poiseuille zone [m]

L3……Length of surface traction regime zone [m]

M ……Mean curvature

$\hat{n}$ ……Unit normal

$N|_w^{''}$ ……...Diffusion flux in the wall [mol/(m^2·s)]

t……Time [s]

r ……Radius of meniscus curvature [m]

UNIVERSITAT ROVIRA I VIRGILI
NUMERICAL AND EXPERIMENTAL STUDY OF FLOW AND WALL MASS TRANSFER RATES IN CAPILLARY DRIVEN FLOWS IN MICROFLUIDIC CHANNELS
Salvatore Cito
ISBN:978-84-693-0720-5/DL: T-425-2010

r_1 ……...Radius of minimum principal osculating curvature [m]

r_2 ……..Radius of maximum principal osculating curvature [m]

S……Surface [m^2]

S_m……...Source term [$kg/m^3 \cdot s$]

V_m……....Velocity of the meniscus [m/s]

V_Ω ……...Volume of control [m^3]

u……Velocity [m/s]

W…….Width of rectangular cross section micro-channel [m]

Greek Letters

α ……..Beams intersection angle

δ ……..Spacing of interference fringes [m]

ΔP ……...Capillary driving pressure [Pa]

Δf ……..Doppler shifted frequency [1/s]

Δt ……Time step [s]

ϕ ……Scalar

η ……Apparent viscosity

μ……Dynamic viscosity [Pa·s]

λ …….Wavelength [m]

ν……Kinematics viscosity [m^2/s]

θ……..Contact angle

σ……Surface tension [N/m]

ρ……..Density [kg/m^3]

τ……Sear stress [Pa]

UNIVERSITAT ROVIRA I VIRGILI
NUMERICAL AND EXPERIMENTAL STUDY OF FLOW AND WALL MASS TRANSFER RATES IN CAPILLARY DRIVEN FLOWS IN MICROFLUIDIC CHANNELS
Salvatore Cito
ISBN:978-84-693-0720-5/DL: T-425-2010

Dimensionless numbers

$$Bo = \frac{\rho g h^2}{\sigma}$$ ……Bond number

$$\mathrm{Re} = \frac{\rho V h}{\mu}$$ ……Reynolds number

$$Ca = \frac{\mu V}{\sigma}$$ ……..Capillary number

$$We = \frac{\rho V^2 h}{\sigma}$$ ……..Weber number

$$W_c = \frac{< Sh >}{\sqrt{\mathrm{Re}}}$$ ……..Wall mass transfer rate coefficient

$$Sc = \frac{\mu}{\rho D}$$ ……Schmidt number

$$Sh = \frac{Kh}{2D}$$ ……..Sherwood number

$$T = \frac{t \cdot Vm}{L}$$ ……Non-dimensional time

UNIVERSITAT ROVIRA I VIRGILI
NUMERICAL AND EXPERIMENTAL STUDY OF FLOW AND WALL MASS TRANSFER RATES IN CAPILLARY DRIVEN FLOWS IN MICROFLUIDIC CHANNELS
Salvatore Cito
ISBN:978-84-693-0720-5/DL: T-425-2010

ACRONYMS

CFD	Computational Fluid Dynamics
CD	Capillary Driven
C-MEMS	Carbon Micro-Electro-Mechanical Systems
ESEM	Environmental Scanning Electron Microscope
FVM	Finite Volume Method
LDV	Laser Doppler Velocimetry
PDMS	PolyDiMethylSiloxane
PIV	Particle Image Velocimetry
SDDOCT	Spectral-Domain Doppler Optical Coherence Tomography
ODT	Optical Doppler Tomography

UNIVERSITAT ROVIRA I VIRGILI
NUMERICAL AND EXPERIMENTAL STUDY OF FLOW AND WALL MASS TRANSFER RATES IN CAPILLARY DRIVEN FLOWS IN MICROFLUIDIC CHANNELS
Salvatore Cito
ISBN:978-84-693-0720-5/DL: T-425-2010

AUTHOR PUBLICATIONS

Journal Papers

1. *Fluid-dynamic and Electromagnetic Characterization of 3D Carbon Dielectrophoresis with Finite Element Analysis.* R. Martinez-Duarte, S. Cito, E. Collado-Arredondo, S. O. Martinez and M. Madou. *Sensor & Transducers Journal (ISSN 1726-5479) December 2008.*

2. *Screen-printing as a holistic manufacturing method for multifunctional Microsystems and microreactors.* Pablo Lozano, Diego Bejarano, Salvatore Cito, Daniel Mata, Magdalena Constantí and Ioanis Katakis. 2009 *J. Micromech. Microeng. 19 115007 (8pp) doi: 10.1088/0960-1317/19/11/115007.*

3. *Analysis of capillary-driven flow in micro-channels: Part 1. Visualization and measurement of blood flow using spectral domain optical coherence tomography*. Salvatore Cito, Jordi Pallares, Yeh-Chan Ahn, Zhongping Chen, Ioanis Katakis. In redaction.

4. *Analysis of capillary-driven flow in micro-channels: Part 2*. Numerical simulation of wall mass transfer rates. Salvatore Cito, Jordi Pallares, Ioanis Katakis. In redaction.

Proceeding papers

5. *Analysis of surface-tension-driven blood flow using spectral domain optical coherence tomography.* Yeh-Chan Ahn, Salvatore Cito, Ioanis Katakis, Jordi Pallares, Zhongping Chen. *Proc. SPIE, Vol. 6886, 68860S (2008).*

Oral presentations in International congresses

6. *Wall mass transfer rates in capillary-driven flow in micro-channels*. Cito S., Pallares J., Katakis I. *IUTAM Symposium on Advances in Micro- and Nanofluidics, Dresden, Germany 6-8 September 2007.*

7. *Modelling of transient electrochemical response of in vitro miniaturized diagnostic devices and biofuel cells*. Salvatore Cito, Jordi Pallares, Pablo Lozano, Ioanis Katakis. *XI Trobada Transfronterera sobre Sensors I Biosensors 2006 Girona Spain.*

UNIVERSITAT ROVIRA I VIRGILI
NUMERICAL AND EXPERIMENTAL STUDY OF FLOW AND WALL MASS TRANSFER RATES IN CAPILLARY DRIVEN FLOWS IN MICROFLUIDIC CHANNELS
Salvatore Cito
ISBN:978-84-693-0720-5/DL: T-425-2010

Poster presentation in national congresses

8. *Performance analysis of Screen Printed direct glucose fuel cell*. Chalaris Christos, Salvatore Cito, Diego Bejarano, Pablo Lozano, Ioanis Katakis. *59th Annual Meeting of the International Society of Electrochemistry 2008.*

UNIVERSITAT ROVIRA I VIRGILI
NUMERICAL AND EXPERIMENTAL STUDY OF FLOW AND WALL MASS TRANSFER RATES IN CAPILLARY DRIVEN FLOWS IN MICROFLUIDIC CHANNELS
Salvatore Cito
ISBN:978-84-693-0720-5/DL: T-425-2010

BIBLIOGRAPHY

1. Whitesides, G.M., *The origins and the future of microfluidics.* Nature, 2006. **442**(7101): p. 368-373.

2. Haeberle, S., et al., *Microfluidic for Lab-on-a-Chip*, in *Comprehensive Microsystems*. 2008, Elsevier: Oxford. p. 463-516.

3. Larkin, B.K., *Thermocapillary flow around hemispherical bubble.* AIChE Journal, 1970. **16**(1): p. 101-107.

4. Zeng, S., et al., *Fabrication and characterization of electroosmotic micropumps.* Sensors and Actuators B: Chemical, 2001. **79**(2-3): p. 107-114.

5. Roques-Carmes, T., et al., *The effect of the oil/water interfacial tension on electrowetting driven fluid motion.* Colloids and Surfaces A: Physicochemical and Engineering Aspects, 2005. **267**(1-3): p. 56-63.

6. Kung, C., et al., *Blood flow driven by surface tension in a microchannel.* Microfluidics and Nanofluidics, 2009. **6**(5): p. 693-697.

7. Li, F.-C., et al., *Creation of very-low-Reynolds-number chaotic fluid motions in microchannels using viscoelastic surfactant solution.* Experimental Thermal and Fluid Science. Experimental Thermal and Fluid Science, 2010. **34**(1): p. 20-27.

8. Nguyen, N.-T., X. Huang, and T.K. Chuan, *MEMS-Micropumps: A Review.* Journal of Fluids Engineering, 2002. **124**(2): p. 384-392.

9. Naoki Ichikawaa, C.A.C.I., Kazuo Hosokawab and Ryutaro Maedaa, *Interface motion of capillary-driven flow in rectangular microchannel.* Journal of Colloid ad Interface Science, 2004. **280**.

10. Gervais, T. and K. Jensen, *Mass transport and surface reactions in microfluidic systems.* Chemical Engineering Science, 2006. **61**(4): p. 1102-1121.

11. Jakeway, S.C., A.J. de Mello, and E.L. Russell, *Miniaturized total analysis systems for biological analysis.* Fresenius' Journal of Analytical Chemistry, 2000. **366**(6): p. 525-539.

12. Albareda-Sirvent, M., A. Merkoçi, and S. Alegret, *Configurations used in the design of screen-printed enzymatic biosensors. A review.* Sensors and Actuators B: Chemical, 2000. **69**(1-2): p. 153-163.

13. Viricelle, J.P., et al., Compatibility of screen-printing technology with micro-hotplate for gas sensor and solid oxide micro fuel cell development. Sensors and Actuators B: Chemical, 2006. **118**(1-2): p. 263-268.

14. Krebs, F.C., et al., *Large area plastic solar cell modules.* Materials Science and Engineering: B, 2007. **138**(2): p. 106-111.

15. Dong, H., et al., Screen-printed microfluidic device for electrochemical immunoassay. Lab on a chip, 2007. **7**(12): p. 1752-1758.

16. Washburn, E.W., *The Dynamics of Capillary Flow.* Physical Review, 1921. **17**(3): p. 273.

17. P. Joos, P.V.R., And M. Bracke, *The kinetics of wetting in a capillary.* Journal of Colloids and interface Science, 1989. **136**(1).

18. van Remoortere, P. and P. Joos, *The kinetics of wetting: The motion of a three phase contactline in a capillary.* Journal of Colloid and Interface Science, 1991. **141**(2): p. 348-359.

19. Fahraus, R. and T. Lindqvist, *The viscosity of the blood in narrow capillary tubes* Am J Physiol, 1931. **96**(3): p. 562-568.

20. Karnis, A. and S.G. Mason, *The flow of suspensions through tubes VI. Meniscus effects.* Journal of Colloid and Interface Science, 1967. **23**(1): p. 120-133.

21. Sheng, P. and M. Zhou, Immiscible-fluid displacement: Contact-line dynamics and the velocity-dependent capillary pressure. Physical Review A, 1992. **45**(8): p. 5694.

22. Zhou, M.-Y. and P. Sheng, *Dynamics of immiscible-fluid displacement in a capillary tube.* Physical Review Letters, 1990. **64**(8): p. 882.

23. Fan, H., Y.X. Gao, and X.Y. Huang, Thermodynamics modeling for moving contact line in gas/liquid/solid system: Capillary rise problem revisited. Physics of Fluids, 2001. **13**(6): p. 1615-1623.

24. Martic, G., et al., *A Molecular Dynamics Simulation of Capillary Imbibition.* Langmuir, 2002. **18**(21): p. 7971-7976.

25. Somalinga, S. and A. Bose, Numerical investigation of boundary conditions for moving contact line problems. Physics of Fluids, 2000. **12**(3): p. 499-510.

26. Schönfeld, F. and S. Hardt, *Dynamic contact angles in CFD simulations.* Computers & Fluids, 2009. **38**(4): p. 757-764.

27. Huang, W., R.S. Bhullar, and Y.C. Fung, *The Surface-Tension-Driven Flow of Blood From a Droplet Into a Capillary Tube.* Journal of Biomechanical Engineering, 2001. **123**(5): p. 446-454.

28. Middleman, S., An Introduction to Fluid Dynamics : Principles of Analysis and Design. 1997.

29. Adrian, R.J., *Twenty years of particle image velocimetry.* Experiments in Fluids, 2005. **39**(2): p. 159-169.

30. Otis, L.L., et al., *Quantifying labial blood flow using optical Doppler tomography.* Oral Surgery, Oral Medicine, Oral Pathology, Oral Radiology, and Endodontology, 2004. **98**(2): p. 189-194.

31. R. Martinez-Duarte, et al., Fluido-dynamic and Electromagnetic Characterization of 3D Carbon Dielectrophoresis with Finite Element Analysis. Sensors & Transducers Journal,, 2008. **3,**(Special Issue): p. 25-36.

32. Bejarano, D., et al., Screen printing as a holistic manufacturing method for multifunctional microsystems and microreactors. Journal of Micromechanics and Microengineering, 2009(11): p. 115007.

33. Chakraborty, S., Dynamics of capillary flow of blood into a microfluidic channel. Lab Chip, 2005. **5**(4): p. 421-430.

34. Mazumdar, J.N., *BIOFLUID MECHANICS.* World Scientific Publishing, 1992.

35. ANSYS FLUENT 12.0 Theory Guide. 2009.

36. Buchhave, P., *Particle image velocimetry--status and trends.* Experimental Thermal and Fluid Science, 1992. **5**(5): p. 586-604.

37. Melling, A., *Tracer particles and seeding for particle image velocimetry.* Measurement Science and Technology, 1997. **8**(12): p. 1406-1416.

38. Chen, Z., *TOMOGRAPHY | Tomography and Optical Imaging*, in *Encyclopedia of Modern Optics*, B.D. Guenther, Editor. 2005, Elsevier: Oxford. p. 206-217.

39. Chen, Z., et al., Optical Doppler tomographic imaging of fluid flow velocity in highly scattering media. Optics letters, 1997. **22**(1): p. 64-66.

40. Yeh, Y. and H.Z. Cummins, Localized fluid flow measurements with an He[Single Bond]Ne laser spectrometer. . Applied Physics Letters, 1964. **4**(10): p. 176-178.

41. Chen, Z., et al., Phase-resolved optical coherence tomography and optical doppler tomography for imaging fluid flow in tissue with fast scanning speed and high velocity sensitivity. 2003. US Pat

42. Zhao, Y., et al., Phase-resolved optical coherence tomography and optical Doppler tomography for imaging blood flow in human skin with fast scanning speed and high velocity sensitivity. Optics letters, 2000. **25**(2): p. 114-116.

43. Ahn, Y.-C., W. Jung, and Z. Chen, Optical sectioning for microfluidics: secondary flow and mixing in a meandering microchannel. Lab on a chip, 2008. **8**(1): p. 125-133.

44. McDonald, J.C., et al., *Fabrication of microfluidic systems in poly(dimethylsiloxane).* Electrophoresis, 2000. **21**(1): p. 27-40.

45. Hillborg, H., et al., Crosslinked polydimethylsiloxane exposed to oxygen plasma studied by neutron reflectometry and other surface specific techniques. Polymer, 2000. **41**(18): p. 6851-6863.

46. US. Pat., 0 204 939, 2005.

47. US Pat., 0 046 811, 2003.

48. US Pat., 6 440 645, 2002

49. US Pat., 6 939 451, 2005.

50. D. Filippini, L.F., S. Gwirc, *Thick Film Microchannels: Design and Fabrication.* Microelectronics International, 1996. **13**(2).

51. Iwuoha, E.I., et al., Reactivities of organic phase biosensors. 2. The amperometric behaviour of horseradish peroxidase immobilised on a platinum electrode modified with an electrosynthetic polyaniline film. Biosensors and Bioelectronics, 1997. **12**(8): p. 749-761.

52. Killard, A.J., et al., Development of an electrochemical flow injection immunoassay (FIIA) for the real-time monitoring of biospecific interactions. Analytica Chimica Acta, 1999. **400**(1-3): p. 109-119.

53. Campàs, M. and I. Katakis, *Strategy for the development of sensor platforms for multi-analysis.* International Journal of Environmental Analytical Chemistry, 2004. **84**(11): p. 799 - 807.

54. Kanamura, K. and J.-i. Hamagami, Innovation of novel functional material processing technique by using electrophoretic deposition process. Solid State Ionics, 2004. **172**(1-4): p. 303-308.

55. D.R. Kobs and D.R. Voigt, Parametric dependencies in thick film screening. Proc. ISHM. **18**.

56. Jeong, J.-T., Kim, Moon-Uhn, *Slow Viscous Flow Due to Sliding of a Semi-Infinite Plate over a Plane.* Journal of the Physical Society of Japan 1989. **54** (5): p. JOUR.

57. Riemer, D.E., Analytical model of the screen printing process part 1. Solid State Technol, 1988. **8**.

58. Riemer, D.E., Analytical model of the screen printing process: part 2. Solid State Technol, 1988. **9**.

59. Riemer, D.E., The theoretical fundamentals of the screen printing process Hybrid Circuits, 1989(18): p. 8.

60. Hunter, B., *An analysis of a screen printing system equipped with a trailing blade squeegee.* The International Journal of Microcircuits and Electronic Packaging, 1993. **16**(1): p. 6.

61. Owczarek, J.A. and F.L. Howland, *A study of the off-contact screen printing process. II. Analysis of the model of the printing process* IEEE Trans. Compon. Hybrids Manuf. Technol., 1990. **13**(2): p. 368-375.

62. Anderson, J.T., et al., *Hydrodynamic interactions in the screen printing process.* J. Prepress & Printing Technology,, 2000.

63. White, G., et al., *A model for the screen-printing of Newtonian fluids.* Journal of Engineering Mathematics, 2006. **54**(1): p. 49-70.

UNIVERSITAT ROVIRA I VIRGILI
NUMERICAL AND EXPERIMENTAL STUDY OF FLOW AND WALL MASS TRANSFER RATES IN CAPILLARY DRIVEN FLOWS IN MICROFLUIDIC CHANNELS
Salvatore Cito
ISBN:978-84-693-0720-5/DL: T-425-2010

64. Glinski, G.P., C. Bailey, and K.A. Pericleous, *A non-Newtonian computational fluid dynamics study of the stencil printing process.* Proc. Instn. Mech. Engrs., 2001. **215**: p. 427.

65. Fox, I., et al., *Film thickness prediction in halftone screen-printing.* Proc. of the Institution of Mechanical Engineers, Part E: Journal of Process Mechanical Engineering, 2003. **217**(4): p. 345-359.

66. Choban, E.R., et al., *Microfluidic fuel cell based on laminar flow.* Journal of Power Sources, 2004. **128**(1): p. 54-60.

67. Buffone, C. and K. Sefiane, Investigation of thermocapillary convective patterns and their role in the enhancement of evaporation from pores. International Journal of Multiphase Flow, 2004. **30**(9): p. 1071-1091.

68. Buffone, C., K. Sefiane, and J.R.E. Christy, Experimental investigation of the hydrodynamics and stability of an evaporating wetting film placed in a temperature gradient. Applied Thermal Engineering, 2004. **24**(8-9): p. 1157-1170.

69. Bessette, R.R., et al., *A study of cathode catalysis for the aluminium/hydrogen peroxide semi-fuel cell.* Journal of Power Sources, 1999. **80**(1-2): p. 248-253.

70. Wang, H., J.Y. Murthy, and S.V. Garimella, *Transport from a volatile meniscus inside an open microtube.* International Journal of Heat and Mass Transfer, 2008. **51**(11-12): p. 3007-3017.